Satellite Communications Network of Excellence

IST Network of Excellence No 507052

Chapter "Clear Sky Optics"

of the

e-Book "*Influence of the variability of the propagation channel on mobile, fixed multimedia and optical satellite communications*"

E. Leitgeb, S. Sheikh Muhammad, Ch. Chlestil, M. Gebhart, U. Birnbacher
TU Graz, Inffeldgasse 12, 8010 Graz, Austria

N. Perlot, H. Henniger, D. Giggenbach, J. Horwath
DLR, Oberpfaffenhofen, Germany

E. Duca, V. Carrozzo, S. Betti
UToV, Rome, Italy

The E-book "*Influence of the variability of the propagation channel on mobile, fixed multimedia and optical satellite communications*" is constituted into three parts: Mobile / indoor multipath, atmospheric effects and clear sky optics

Book Chapter 4 for SJA-2413 “Clear Sky Optics”

E. Leitgeb, S. Sheikh Muhammad, Ch. Chlestil, M. Gebhart, U. Birnbacher
TU Graz, Inffeldgasse 12, 8010 Graz, Austria

N. Perlot, H. Henniger, D. Giggenbach, J. Horwath
DLR, Oberpfaffenhofen, Germany

E. Duca, V. Carrozzo, S. Betti
UToV, Rome, Italy

Abstract

Free Space Optical (FSO) links can be used to setup FSO communication networks or to supplement radio and optical fibre networks. Hence, it is the broadband wireless solution for closing the “last mile” connectivity gap throughout metropolitan networks. This chapter gives an overview of free-space laser communications in principles and applications. Investigations of the SatNEx partner (TU Graz, DLR, UToV Rome) and improvements for the future systems are discussed.

4 Clear Sky Optics

Clear Sky Optics also known as “Optical Wireless” or “Free Space Optics” is being considered as a growing and emerging technology with its applications spreading over many areas of telecommunications. Deep-space communications, Inter-satellite links, terrestrial long and short distance links and optical links between HAPs and UAVs are just a few examples of the many possibilities.

4.1 State-of-the-art - review in Clear Sky Optics (TUG, UToV, DLR)

We try to provide an elaborative, but not extensive review of the current state of the art in Clear Sky Optics in terms of its applications as a ”last mile” bottleneck solution for the access network and in space missions.

4.1.1 Introduction in FSO (TUG, Le. Sh.)

In Europe and in USA, about 20 distributors offer optical free space links. The SatNEx-partner are investigating and developing Free Space Optical Communication Systems as well as evaluating existing systems in co-operation with distributors, telephone companies and providers. Optical links in regard to range, bandwidth, traffic and weather (link budget, margin) are projected and calculated. The main emphasis of our research work is to increase the channel capacity, reliability and availability of Optical Free Space Links.

After having explained the advantages and principles of FSO we will show in the first main section Free Space Optical applications in different networking topologies. Terrestrial FSO for short ranges cover the links between buildings on campus or different buildings of a company, which can be established with low-cost technology. For using FSO for long range applications, more sophisticated systems have to be used. Hence, different techniques regarding emitted optical power, beam divergence, number of beams and tracking will be examined. Space applications have to be divided into Free Space Optics-links through the troposphere, for example up- and downlinks between the Earth and satellites, and FSO-links above the troposphere (e.g. optical inter-satellite links). The difference is that links through

the troposphere are mainly influenced by weather conditions similar but not equal to terrestrial Free Space Optics-links. Satellite orbits are above the atmosphere and therefore, optical inter-satellite links are not influenced by weather conditions.
The use of Optical Wireless for the “last mile” access will also be described in more detail and will illustrate the range of applications for FSO last mile networks. Therefore line of sight, reliability and availability, different Free Space Optics-techniques are described. Results of various studies and measurements regarding the reliability of Free Space Optics-links will complete these investigations. In this case also a state of the art review in channel models is necessary.
In the second main part we will show our results in SatNEx on different Optical Wireless Systems. Additionally, we will discuss our measurement results concerning the reliability in case of fog and atmospheric turbulences.
In the following part we will show some improvements for increasing the bit rates and the reliability in future Free Space Optics. That will be described on developed FSO-systems for Gigabit and by using special modulation and channel-coding techniques.
Free Space Optics-links can be used to setup a complete FSO-network or as a supplement to conventional radio links and fibre optics. Most FSO-links are point-to-point links between one transmitting and one receiving station. However, current research [1, 6, 9] is also investigating point-to-multipoint configurations. By using light sources like LEDs with a wide beam angle and / or multiple transmitter optics, the output power within the same laser class can be increased multiple times, and several terminal stations can be connected to central station.

4.1.2 Free Space Optics-Applications **(TUG, Le. Ge. Bi.; UToV, Ca. Du. Lo.; DLR, Gi.)**

This chapter covers terrestrial applications for short and long ranges and space applications. Terrestrial applications and FSO-links through the troposphere are mainly influenced by weather conditions. Therefore, some important characteristics of the atmosphere have to be discussed before describing the FSO-applications in more detail.
The lowest part of the atmosphere up to 10 km above the Earth’s surface is called the troposphere or the weather sphere. It has a varying refraction index which is dependent on the height above the Earth’s surface. Normally the refraction index decrease with the height, but at inversion situations there is different relationship.
Atmospheric conditions degrade laser communications through the atmosphere in two ways. First, the atmosphere acts as a variable attenuator between the transmitting and receiving terminals. Second, a free space laser link is subjected to scintillations.
Attenuation is caused by the weather conditions along the transmission path. Generally, there is low atmospheric attenuation during clear days and high attenuation during foggy days. Rain does not influence optical transmissions heavily, because raindrops have the size of a few millimetres and are large compared to laser wavelengths (1.5 microns) and thus cause minimal scattering of the laser energy. Furthermore, water has minimal absorption at a 1550 nm laser wavelength. Therefore, it is not surprising that the optical transmission is not heavily impacted by rain (only about 3 dB/km). Similarly it is not surprising to find out that optical transmission is impacted dramatically by heavy fog (30 dB/km). This is because the fog aerosols have a comparable size as the used wavelengths, causing much scattering of the laser energy as the fog gets thicker. Absorption effects can be subdivided into absorption and scattering effects. Absorption is caused by many different species of gas in the atmosphere, the dominant one being water vapour, which is in the wavelength region used for wireless optical links. There are two types of scattering, Rayleigh and Mie scattering (see chapter 4.1.3). The amount of scattering depends on the particle size distribution and the density of particles. Generally, any optical wavelength could be used for FSO, but because of the atmospheric conditions and due to the laser safety regulations, 1550 nm is the best suitable

wavelength. The losses due to Mie-scattering in haze or light fog are smaller at longer wavelengths (1550 nm) than at shorter ones (850 nm).
The second major influence on FSO-transmission is scintillation, which is caused by small-scale fluctuations in the refraction index of the atmosphere. Its primary effect is signal fading due to phase changes in the wave front arriving at the receiver. Unless the receiver has a very high dynamic range or the aperture is large enough to average out the scintillation spots, this can have an extremely detrimental effect on the signal. As described above, a foggy day is very bad for free space communication due to the high attenuation. On the other hand it can be observed that scintillations are very low on a foggy day, because of low fluctuations in the atmosphere.

4.1.2.1 Types of FSO-systems for different network architectures

Different FSO-systems for various applications have been developed by research groups and industry. In order to describe the different technologies implemented in available systems, we simplify the concepts to some important elements. Such a simplified scheme for a typical FSO unit for data transmission is shown in figure 1. On the basis of this concept, three types of system design can be distinguished, each as a compromise regarding reliable operation and installation costs for certain applications and distances.

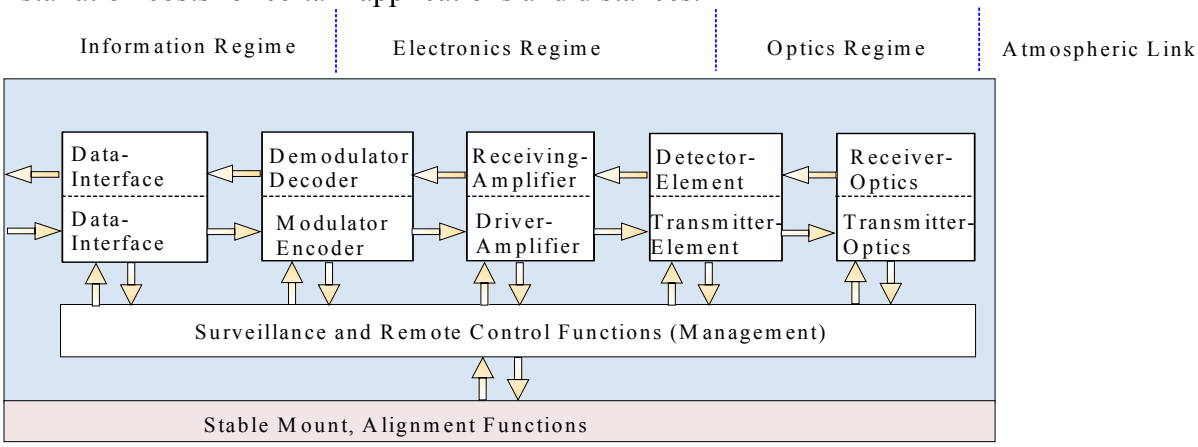

Figure 1: Simplified scheme of the elements of a FSO unit

For the first type of systems, available standard components are combined to build cost-effective solutions. Generally, the value of the beam divergence is high (up to 60 mrad) and allows an easy alignment for the user without the need for a telescope. All elements including the optics do not require as high precision as compared to the other two approaches, allowing higher tolerances at fabrication, and allowing the use of simple mounts at installation. Due to large divergence the requirements for a stable underground are not very high, allowing a quick installation. Suitable distances for high availability operation are limited up to 300 meters because of the wide beam angle (and depending on local climate). Due to Laser Safety Regulations the use of light sources with higher beam divergence allow more output power in the same safety class, which improves the link budget for short distance applications.
Systems of the second type take advantage of a collimated beam as much as possible without active alignment, which leads to a beam divergence of about 2 to 6 mrad. The implementation of fibre-optic technology for coupling directly from fibre to Free Space Optics is a suitable concept. To achieve the same intensity at the receiver in longer distance, the concept requires precise optical components being carefully adjusted, and telescopes or adjustment procedures are needed for the installation. A stable mount on stable ground is required. These first two types of FSO-systems are mainly used for short range terrestrial applications and especially for Last-mile Access. For increasing the intensity at the receiver and to overcome atmospheric turbulences (scintillation) caused by variation of the refraction index, more than one

transmitter- and / or receiver-units are used in one housing. Systems with multiple transmitter/receiver units are called Multibeam- or Multilink-Free Space Optics-systems and are found in both system types.
The third category contains the sophisticated solutions, including strategies to extend the distance for reliable operation as much as possible. The beam divergence reaches values less than 1 mrad leading to low geometrical losses, concentrating all incoming light on a small area around the receiver. To compensate building sway and deviation, automatic tracking of the beam is implemented, adaptive optics may help to compensate atmospheric fluctuations or allow higher optical output over a large area. These systems are in use for long distances and the most accurate solutions with acquisition and tracking for Space Applications. For Space Applications not only direct detection for the receiver is used, but also coherent detection.
Using Free Space Optics-systems from all three categories, various communication links or networks can be realised, including terrestrial FSO (between buildings, hospitals, campus), horizontal and slant paths, air-borne and space communications (between aircraft, unmanned aerial vehicles (UAV), high altitude platforms (HAP) and satellites. By connecting FSO-links and networks to the “Backbone” realised with optical fibres, the FSO-networks and -links can be seen as parts of a global all optical network around the world (figure 2).

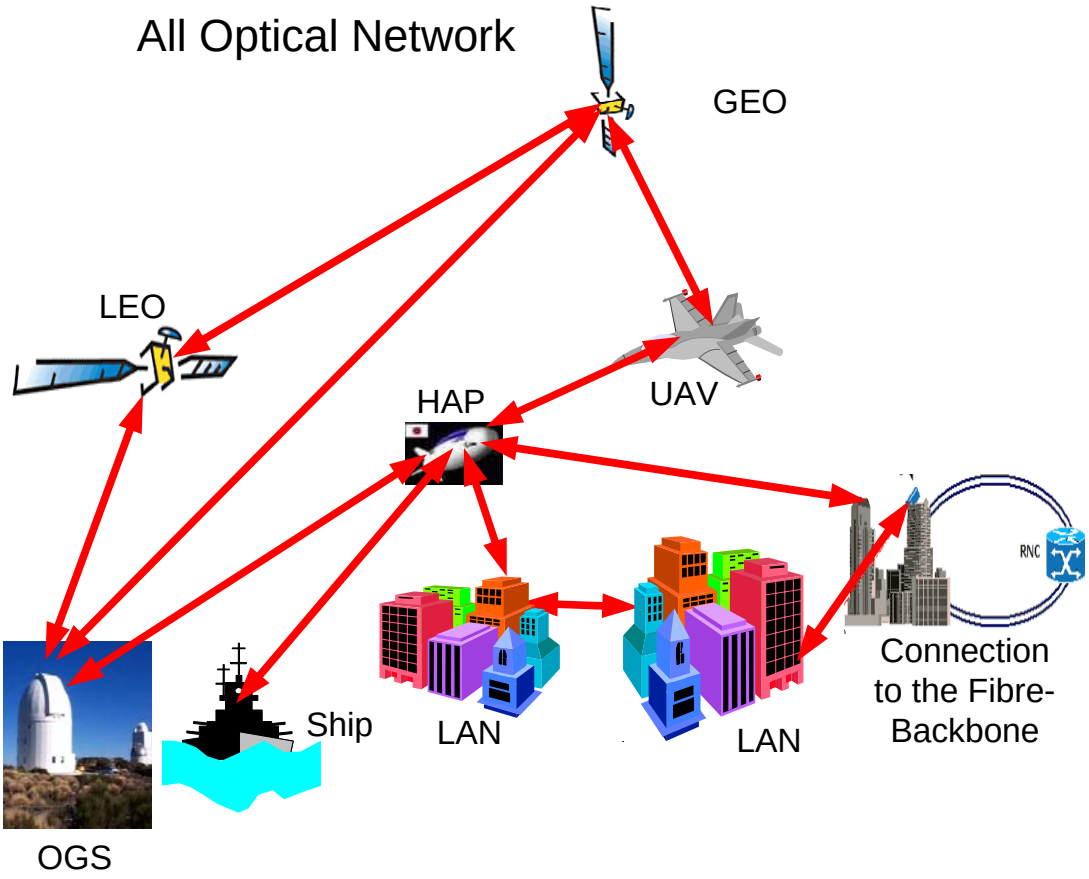

Figure 2: All Optical Network

A very important issue is the reliability and the availability of FSO-links and FSO-networks. In order to estimate the reliability of a network, the reliability of each single component has to be taken into account. For example, the reliability of one FSO-terminal depends on the reliability of all electrical and optical components built into the terminal, including the connection and interface to the network (figure 12).

4.1.2.2 Short range applications

FSO short range applications will be used up to 1 km (maximum 2 km) for connecting buildings or establishing a connection to the backbone.
Within the range of up to 2 km distance, it makes sense to use FSO-systems of type 1 or type 2. These systems will be cost-efficient and they have a high availability and reliability. For short ranges, “Auto tracking” is not necessary. In [1] the ranges for developed type 1 FSO-systems are 100 m, 300 m and 800 m (figure 3a and 3b). In figure 22 an example for a type 2 system is shown.

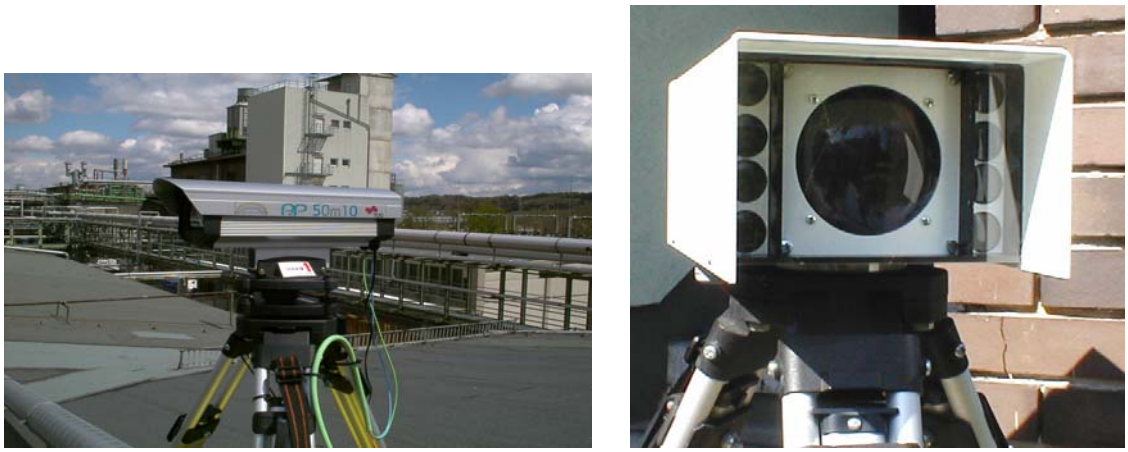

Figure 3: Point-to-Point-System of type 1 for ranges of A) 100 m and B) 800 m (with 8 transmitter units)

In [2, 6] various FSO-systems have been evaluated in regard to different weather conditions. For terrestrial applications it is important to know the influence of the path through the atmosphere, which can be either simulated and modelled or measured over long time periods. The atmospheric path for transmission of a collimated beam of light may be seen as an information channel, to which information is added and on which information gets lost (figure 4). A variety of effects can be described and several theoretical models are known, but not all of them are relevant to this technology. Once more it is a question of technology used, distance and application to find out relevant impacts on Free Space Optics data transmission. Before coming to quantitative results from experiments, a qualitative introduction to some relevant problems is given in this chapter.

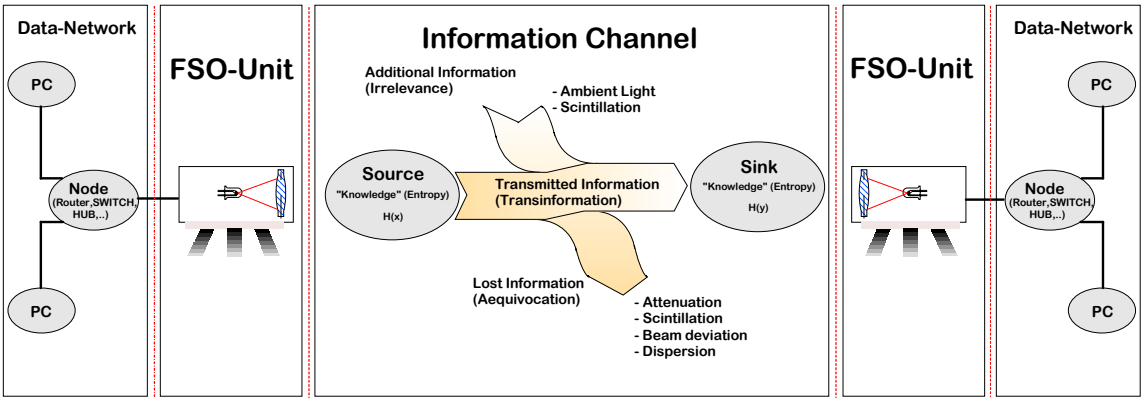

Figure 4: Scheme of data transmission and impacts on the channel

Ambient light that passes the optics and reaches the detector element, which usually is a PIN-photodiode or an avalanche-photodiode (APD), causes additional current that leads to additional white Gaussian noise in the receiver. Depending on the semiconductor materials

and construction principle of the detector there are additional effects coming up. Flicker noise produces irregular disturbances which, if we consider data transmission, affects throughput of longer data packets most. At the same time the noise level raises, the impedance of the detector element decreases, which in most receiver principles leads to a level reduction of the received information signal, sometimes also referred as “burn out”-effect. The dominant source of ambient light for outdoor FSO-Systems is the sun. Therefore the sunlight and the possible positions of the sun have to be considered for practical applications.

An intensity of about 1340 W/m² reaches the Earth, also known as the solar constant, which is reduced to about 1000 W/m² global radiation on ground under clear sky conditions due to wavelength dependent absorption in the atmosphere. Over 90 % comes as direct sunlight, the rest looses directivity and is scattered over the sky contributing to background illumination. The sun is seen from the Earth under an angle of about 9.31 mrad (diameter) with a relative movement of 0.0728 mrad/s. The so called windows of transmittance of the atmosphere include the two most important wavelength regions, leading to specific intensities of about 0.5 to 0.9 watts per square meter and per nanometre (W/m²nm) in the 850 nm spectral region and about 0.17 W/m²nm in the 1550 nm region for direct sunlight on ground. All these figures are estimations for clear sky conditions being subject to atmospheric influences, leading to variations. In general, the impact of sunlight on FSO depends on the angular and the spectral sensitivity of the receiver and the possibility of direct sunlight at the receiver, referring to orientation and mount of the installed system.

Attenuation is the most critical factor for longer FSO-links. The contribution of the free atmosphere is comparatively small at the most commonly used wavelengths around 850 and 1550 nanometres. Values for specific attenuation between 0.2 dB/km under very clear atmospheric conditions up to about 10 dB/km due to dust in urban regions are reasonable.

Far more critical is the impact of the weather situation. It has been reported, that specific attenuation may temporarily raise to more than 300 dB/km in heavy fog, even though these are very rare occasions depending on local climate (and within 3 years of measurement have never been observed in Graz). The situation can be explained by a theory describing the interaction of electromagnetic waves and particles, which can be simplified depending on the ratio of particle size and wavelength, to geometrical optics for interaction with comparatively large particles causing wavelength-independent absorption, and to Rayleigh-scattering for comparatively small particles. The most critical condition appears when both are approximately in the same order, such as optical wavelengths in the order of 1 µm and haze or fog that consists of water droplets at diameters from about 1 to 15 µm. This can be characterized by Mie´s theory of scattering.

However, many factors depending on the properties of the particles are not known, therefore a different approach leads to a well known deterministic formula (1) based on visibility, which can be used in practice. Attenuation caused by scattering can be estimated by

$$a_S \cong \frac{17}{S} \cdot \left(\frac{555}{\lambda}\right)^{0.195 \cdot S} \qquad (1)$$

In this equation a_S is the specific attenuation in decibel per kilometre, S is the visibility for human eyes (sight) in kilometres and λ is the wavelength of transmitted light in nanometres. Usually, the range of visibility is defined as a path of 2% transmission in air (corresponding to about 17 dB attenuation at 555 nm wavelength), the contrast resolution of the human eye. Records of visibility are available at airports or meteorological stations and may be used as one reference to estimate the probability of fog for the local climate of a certain location. The impact of rain is less critical because of the larger particle size in the order of 0.1 to about 5 mm diameter, which has more effect on longer wavelengths such as millimetre waves at several tens of GHz. Falling snow simply absorbs the light by the irregular shapes of particles in the size of about 2 up to 25 mm, leading to a varying attenuation depending on the relation

of particle and receiver optics area. For the same visibility range the conditions for FSO are worse than fog, although site diversity realized by using multiple transmitter optics can improve the quality of the link.
Light transmission in media follows the principle of Fermat, according to which the way of light from one point to another follows the shortest optical path length, which depends on geometrical distance and optical properties of the medium, given by the fraction index *n*. Consequently the fraction index has an impact on light propagation. For free air at sea level n is in the order of 1.0003, but depends on many factors e.g. the wavelength used for transmission, the temperature, the atmospheric pressure and the humidity of the air.
Different sheets of air being crossed by light lead to beam deviation (refraction of light) due to a temperature or pressure gradient, an effect which leads to results similar to misalignment or building sway, causing a reduction of received power which can get critical for very small divergence.
Short-time fluctuations of *n*, so called turbulence cells, lead to irregular changing intensity in the beam, wave-front distortion (changing the angle of received light and causing a spot of light dancing around the focal point) and changing deviation, causing a varying input power at the receiver, also known as scintillation. The largest gradients and therefore strongest effects are observed near hot surfaces like streets, rooftops or side-walls, or over outlets of air conditions or in winter heaters.
The influence of the turbulence cells is not interesting for short ranges, but very important for long distances. Type 1 and type 2-systems will be cost-effective and they will have a high availability and reliability at the last mile area.
As an example for short range applications, the use of Free Space Optics for connecting a Satellite-Earth-Station to the „Backbone“ or to a local area network is described. This is a example for a temporary installation and shows the flexibility of FSO systems.

Figure 5: Mobile Satellite-Earth-station with FSO-Connection demonstrated at the UNO-City Vienna

The Satellite-Videoconferencing-system was used at a Tele-medicine conference in Vienna (figure 5), but it is also well suited for any conference, for Tele-teaching and for military issues. The mobile Satellite Earth station is equipped with Free Space Optics and WLAN

instead of cabeling, so a video-presentation of a doctor in Graz and experts at the conference in Vienna was realised. In the lecture room in Vienna Wireless LAN was available. In order to connect the Wireless LAN with the mobile Satellite-Earth-station outside the UNO-City building, the FSO-link was used.

4.1.2.3 Long range applications

For communication links, which run over distances above 2 km, it is important to use systems of type 3 technology. An example of a commercially available system is shown in figure 6.

Figure 6: DT-50 / DT-IF156 CanoBeam

Another important installation is the Wallberg Experiment [4] in Germany at the German Aerospace Centre (DLR). DLR has performed an Optical Free-space Data Transmission Experiment along with the European Aeronautic Defence and Space Company (EADS), Germany and Contraves Space AG, Switzerland. The scope of this experiment is to verify the tracking capabilities of the OPTEL 02, a space-qualified optical terminal, and to demonstrate optical high data rate transmission through the atmosphere. Two laser diode transmitters at 980 nm, each mounted on a tripod for static pointing and laterally separated by about 4 meters, were placed on a mountain top in the German Alps at a height of 1620 m. Either a pseudo-noise pattern or video data can be transmitted. The OPTEL 02, performing acquisition and tracking, is situated at the DLR site in Oberpfaffenhofen near Munich at 620 m. An APD receiver front-end is connected to an additional 75 mm-telescope in order to receive data up to 270 Mbps. The optical path length between both terminals is 61 km.
At Wallberg a building with two rooms with one window each, physically separated by a distance of four meters, is at the disposal. Despite facing towards a popular foot path, there are no problems with laser safety. The two separated windows allow the use of a two-transmitter concept to reduce scintillation effects. Figure 7 shows a map of the southern Munich area showing Wallberg and Oberpfaffenhofen including an altitude profile for the optical link.
As can easily be seen in the profile, there is a steep slope from the Wallberg mountain top to Lake Tegernsee on the plain. This gives a good reason to place the transmitter on top of the mountain, as little atmospheric disturbance can be expected there. The last few kilometres of the link are close to ground. North of Starnberger lake, there is a marshland, which might cause severe beam disturbance.
The described link is a terrestrial Free Space Optics-path for very long distance. Hence, the beam divergence must be smaller than 1 mrad, resulting in low geometrical losses and concentrating all incoming light on a small area around the receiver. To compensate building sway and deviation, automatic tracking of the beam is necessary. Adaptive optic helps to compensate atmospheric fluctuations. The path characteristic of the Wallberg experiment is similar to Space applications (chapter 4.1.2.4).

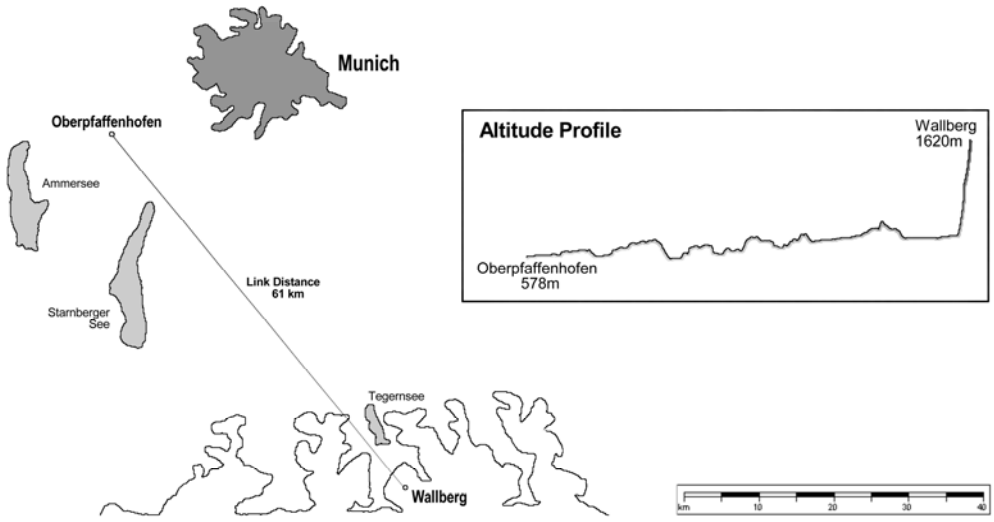

Figure 7: Location and scenario of the Wallberg experiment

4.1.2.4 Space applications (aircrafts and satellites)

The main advantages of FSO links compared to microwave links are small gain antennas (telescope), light terminals, the highest possible data rates at low signal power, no interference with other transmission systems and tap-proof operation using coherent methods. Possible applications for Optical Free-Space Links are inter-satellite links (ISLs) in satellite networks, links for deep space missions, links between unmanned aerial vehicles (UAV), high altitude platforms (HAP) and data links from geostationary satellites (GEO) to Earth ground stations.
Space Applications are divided into Free Space Optics-links in the troposphere (for example, up- and downlinks between the Earth and satellite) and FSO-links above the troposphere (e.g. optical inter-satellite links). Links through the troposphere are mainly influenced by the weather condition similar but not equal to terrestrial FSO-links. Optical inter-satellite links are not influenced by weather conditions, because satellite orbits are above the atmosphere.

Optical vs. RF in free space links: In order to define the most important factors for dimensioning a Free-Space link, we can observe that for a given gain, optical frequencies provide a smaller size of the antenna or, for a given diameter, the gain of the antenna at optical frequencies is extremely higher. This property leads to use lower power and then lower mass and compact terminals. Another advantage in using optical free space links for space application is larger bandwidth and narrower beam-width. Actually, the narrow beam divergence (proper of OISL) has its positive and negative side: if in one hand interferences and background noise are reduced, on the other hand the pointing acquisition and tracking system becomes more complex. It must be noticed that for tropospheric uplink beam, the diameter becomes noticeably wider because of the quickly variation of the refractive index with the height, which makes the optical beam bend from the normal. A similar but lighter effect is suffered by tropospheric downlink beam in the last 10 to 15 km of its path. In conclusion using optical frequencies instead of RF can offer advantages such as smaller mass, wider bandwidth and more dense orbit population. On the other, hand these features pay the cost of a more complex system and a still young technology [8].

Missions and experiments: From the very beginning of the introduction of ISL in satellite communications, the idea of using optical links was present. For example, the IRIDIUM constellation at one time had laser links for its inter-satellite cross-links. TELEDESIC also considered seriously the possibility of providing inter-satellite connectivity at data rates above 1 Gbps. However, due to the costs of the optical terminals and the associated risks due to the lack of experience and maturity of the technology, these two projects boarded finally only RF terminals. The feasibility and all the advantages that OISLs offered started a race between several public and private institutions from the most powerful countries in the researching field. In Europe and Japan, the main source of funding was public (ESA and NASDA) but in the USA the research was carried out both by public (NASA) and private companies (Bell Aerospace, Raytheon).

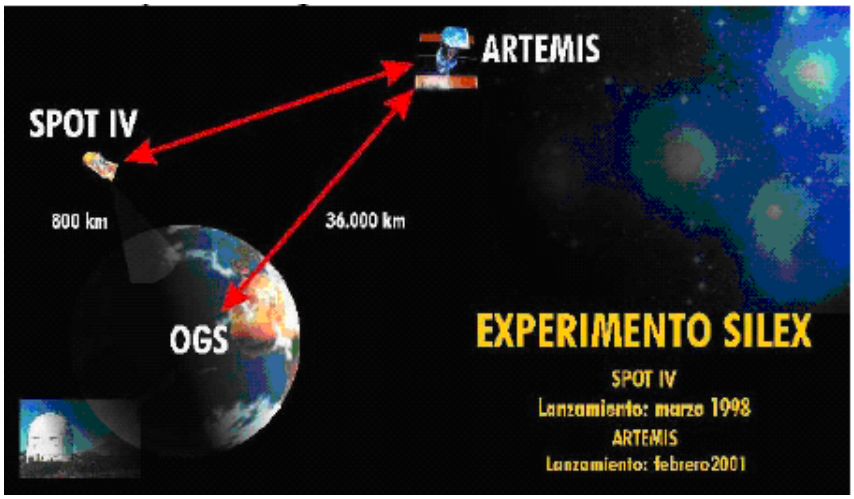

Figure 8: SILEX Experiment

The most important experiment carried out by ESA is shown in figure 8, the world first data transmission between satellites using laser light which took place at 22nd November 2001. A data link between satellites was established using a laser beam as signal carrier. On board ESA's Artemis satellite is the SILEX [W1, W2] system. This system provides an optical data transmission link with the CNES Earth observation satellite SPOT 4, which is orbiting the Earth at an altitude of 832 km, while Artemis was temporarily in a parking orbit at 31 000 km. The SILEX system comprises two optical terminals: PASTEL, on board SPOT 4, and OPALE embarked on ARTEMIS, both identical terminals to save on overall programme cost. The main characteristics of this program are summarised in Figure 11 [22, 23].

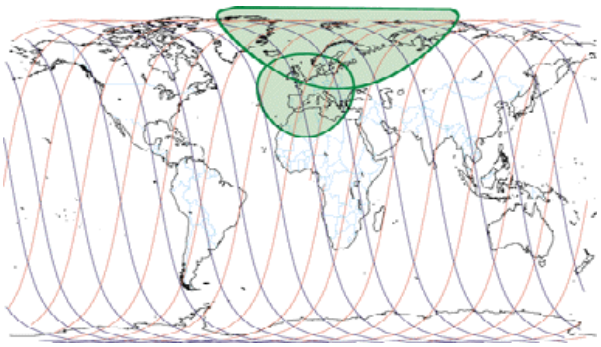

Figure 9: SPOT 4 terrestrial coverage

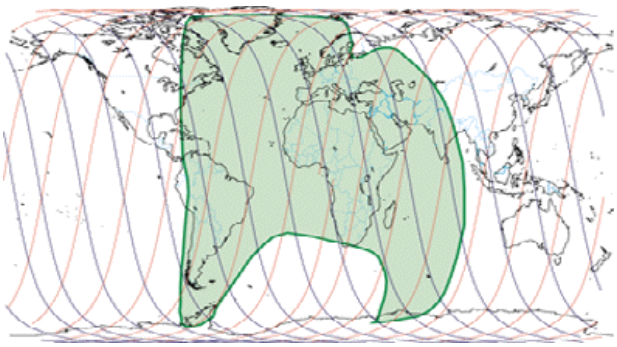

Figure 10: Terrestrial coverage relaying information via ARTEMIS

SPOT 4 takes images from the Earth, but these scenes can only be relayed to the ground immediately after acquisition if the satellite is within the range of a receiving station. Through the laser data link, images taken by SPOT 4 can be transmitted in real-time to the image processing centre in Toulouse, France, via Artemis, thus drastically reducing the time between taking the picture and its delivery to the Earth. This is possible when two satellites are in line of sight, and because the Artemis satellite has a wide Earth coverage that is a much larger area than the acquisition circles of the SPOT 4 system station (as it can be seen in Figures 9, 10). Without the Artemis relay the images are stored on board in SPOT 4's memory and dumped to the ground stations at a later time.

Transmission system	*GaAlAs* Laser Diode: 120mW(peak) Laser Diode Wavelength: 847nm Viterbi encoding Data rate:Approx.50Mbps
Receiver subsystem	Detector: APD (Avalanche Photo Diode) Data rate : Approx.2Mbps Direct detection Wavelenght : 819nm-847nm
Optical Antenna	Diameter : 25cm Wave front error : $\lambda/10(rms)$ Field of view: 75μrad Reflecting Telescope

Figure 11: Main features of SILEX

Another important experiment, carried out by the Japanese government (NASDA and CRL) in collaboration with NEC, is the Optical Inter-Orbit Communications Engineering Test Satellite (OICETS). It is compatible with the GEO satellite ARTEMIS and has on board the Laser Utilization Communications Equipment (LUCE), an optical system working at 0.847 μm, 50 Mbps IM/DD (Intensity Modulation / Direct Detection) and 200 mW laser diode link to ARTEMIS and a 2.048 Mbps IM/DD link at 0.819 μm from ARTEMIS. In 2003, an experimental test was carried out successfully between the engineering model of LUCE and ARTEMIS in the Canary Islands. The OICETS is planned to be launched into the LEO orbit by this year. The last optical system launched by the USA was GeoLite, in 2001. The details of this mission are secret and classified. However, Lincoln Labs are the responsible of this project and is supposed that this satellite had on board a 1550 nm DPSK terminal. This terminal would be based upon erbium doped fiber amplifier technology.

Wavelength choice: The optical carrier wavelength can be chosen in a set of three options.

- **850 nm**. In this band, reliable, inexpensive, high-performance transmitter and receiver components are readily available and commonly used in network and transmission equipment. Nevertheless, these lasers present problems in the sense of lifetime, asymmetric beam and poor output power. The problem of the power can be easily solved by the use of phase arrays. At these wavelengths, the antenna gain is very high, this means that the power requirements are lower and the antenna size can be smaller for a given gain. However, the use of a smaller telescope reaches to more complicated PAT (Pointing Acquisition and Tracking) procedure. Besides, this band of frequencies is the most affected by Doppler phenomenon [24].
- **1064 nm**. At this wavelength it can be used a Nd:Yag laser. These lasers are capable to transmit high amount of power. The problem of this band is a poor efficiency and the quite

hard modulation of Nd:Yag lasers. Single channel systems working in this band, have been proposed with both direct detection and coherent detection [12].

- **1550 nm.** These wavelengths are well suited for space transmission. The high components availability makes the development of WDM (Wavelength Division Multiplexing) FSO systems feasible. However, components are generally more expensive, and detectors are typically less sensitive and have a smaller receive surface area when compared with Si-APD detectors that operate at 850 nm. In addition, these wavelengths are compatible with EDFA (Erbium Doped Amplifiers) technology, which is important for high power and high data rate systems. Finally, the doppler shift at this frequency is lower than at other. It is possible to say that at 1550nm both direct detection and coherent receiver are possible, even if coherent receivers seem to perform higher efficiency, the lower cost of direct detection receivers makes them very competitive. At these frequencies it is possible to carry out multilevel phase keying with high band efficiency (PSK, QAM), and with high power efficiency (multilevel FSK) and hybrid keying as well [14].

Receiver types: In order to define the connection quality of an optical free space link, it is important to introduce the *sensitivity*, a parameter that defines the average power required at the receiver end to achieve a fixed BEP (Bit Error Probability). To reach a receiver best performance in terms of sensitivity, it is necessary to overcome the thermal noise by signal amplification. This increase of performance can be implemented in direct detection receivers and in coherent receivers, as well [14].

- **Coherent detection receivers** (homodyne or heterodyne) require a mixing process which will allow the systems to work at a frequency different from the optical carrier. If the mixing process downs the signal to base-band, the detection process receives the name of *homodyne detection*, otherwise if the process shifts the carrier to an Intermediate Frequency (IF) the process receives the name of *heterodyne detection*. The beating of input signal with a local oscillator (LO) at high power, leads to the amplification of the signal itself at the IF, the sensitivity is lower bounded by the shot noise of the local oscillator. Generally, coherent systems allow a 10-15 dB gain in sensitivity with a consequent reduction of power consumption and/or antenna diameter, at the expense of added complication due to the need of a local oscillator, which supplies a very steady carrier for mixing operation. Apart from the advantage of reaching a sensitivity near to quantum limit, coherent detection in FSO system presents also the important advantage of being immune to background noise [15], since only one spatial mode beats with the LO laser field. On the other, hand taking into account the mobility of one or both terminals of the link, the Doppler affects noticeably the detection performance.
- **Direct Detection receivers** present a very simple structure. Introducing a preamplifier in the receiver scheme leads the system to work effectively at lower level of sensitivity. Anyway, they can perform a very good connection in terms of BEP, with not so wide efficiency gap if compared with a coherent receiver. This can be possible by developing high performing EDFA, used as preamplifier, in particular working in 1550nm band. Another factor that can improve the performance of direct detection receivers is the choice of the best fitting modulation format, for example it has been proved that DPSK signalling performs better with pre-amplified DD receivers.

4.1.3 Reliability of Free Space Optics-links **(TUG Le. Ge. Sh. Bi.; UtoV, Ca. Du. Be; DLR, Gi.)**

A very important issue is the reliability and the availability of FSO-links and FSO-networks. In order to estimate the reliability of a network, the reliability of each single component has to be taken into account. For exampled, the reliability of one FSO-terminal depends on the

reliability of all electrical and optical components built into the terminal, including the connection and interface to the network (figure 3). The reliability of the FSO-link is determined by the reliability of the transmitting FSO-terminal (unit 1 at location A) and the receiving FSO-terminal (unit 2 at location B) and the quality of the optical path in-between. The reliability and availability of the optical path is mainly influenced by the local weather conditions, with fog being the most limiting factor. If not only a single Free Space Optics-link but a network of optical wireless connections is used, the overall reliability is calculated by taking into account all the links in the network and their specific arrangement to each other (parallel or serial). Hence, different network architectures have different availabilities and reliabilities.

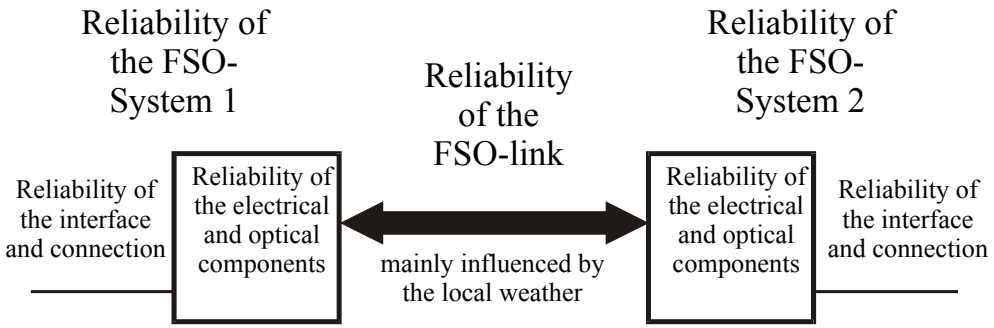

Figure 12: Reliability of Free Space Optics-links

4.1.3.1 Reliability in relevance to the used FSO-network-Architecture

In the following section different architectures are described and compared regarding the overall reliability.

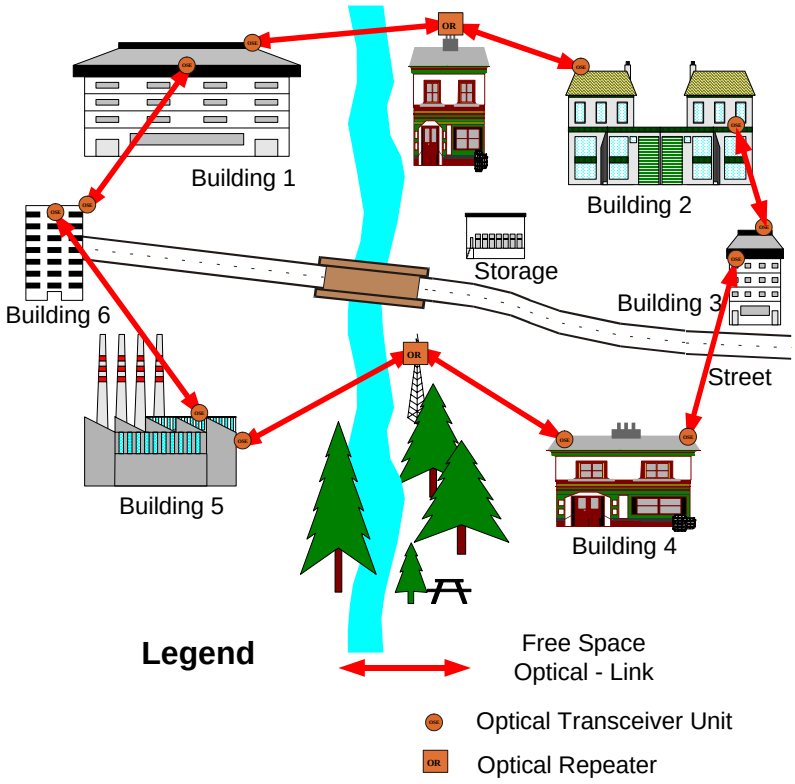

Figure 13: FSO network with ring architecture

Optical Wireless in Ring Architecture: In figure 13 a FSO-network in ring architecture is shown. In the given example, the distances between the buildings are up to 500 m. In the minimum configuration two Optical Receiver / Transmitter Units are installed on the top of each building. Optical Repeaters have to be used, if there is no line of sight between transmitter and receiver.
In the event of a broken link or for example a link failure between building 1 and building 2, the indirect connection can be used. Thereby, the information is sent in the other direction of the ring network passing building 1, building 6, building 5, building 4, building 3, and building 2. Hence, using a ring architecture, a partial security against failure can be achieved. The installation of additional, redundant links increases the availability and the security against failure.

Optical Wireless in Star Architecture: In figure 14 a test installation at the University of Technology Graz (TU Graz) in Austria is shown, using a star architecture. The coverage area of this FSO-network is about 300 m in diameter. An Optical Multipoint Unit is mounted at the roof of a building. Five user terminals are permanently connected by their optical transceiver units to the Optical Multipoint hub station. The five user-terminals are located at the surrounding buildings and offer a connection via the FSO-link to the Optical Multipoint Unit. In this configuration the Optical Multipoint Unit is realised with five Free Space Optics-Point-to-Point units, each of them directed to one user FSO-terminal. The Optical Multipoint Unit is interconnected by switches with the backbone network of TU Graz.

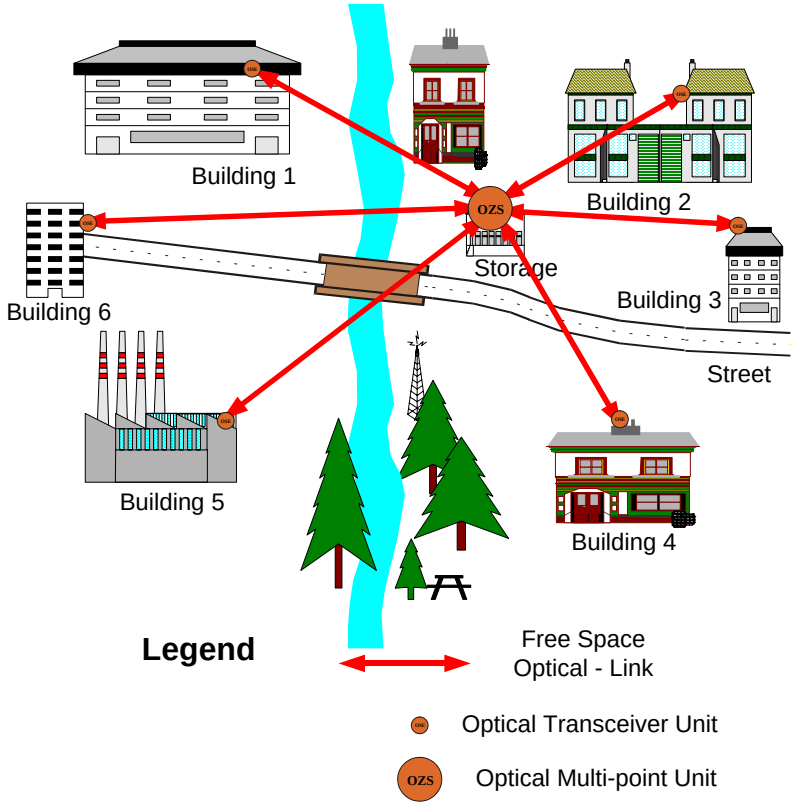

Figure 14: FSO network with star architecture

The advantage of this configuration is the shorter distance between any two FSO-units. In general, the Optical Multipoint Unit is located in the centre of the area, mounted on the tallest building. But this architecture has the disadvantage of a single point of failure. If the Optical Multipoint Unit fails, a system breakdown of the whole installation is caused. To improve the reliability of this architecture, a redundant Multipoint Unit would have to be installed. The

second Optical Multipoint Unit can also be mounted on moveable platforms, e.g. a van, for increasing the flexibility and decreasing the setup time. However, for the installation of Multipoint Units on cars, Free Space Optics-systems with “auto tracking” are preferable.

Optical Wireless in meshed architecture: For high reliability, the optimum network architecture is a meshed network. Meshed networks combine the benefits of the above described architectures, because different connections are possible. An example of a meshed FSO-network is given in figure 15 and 16.

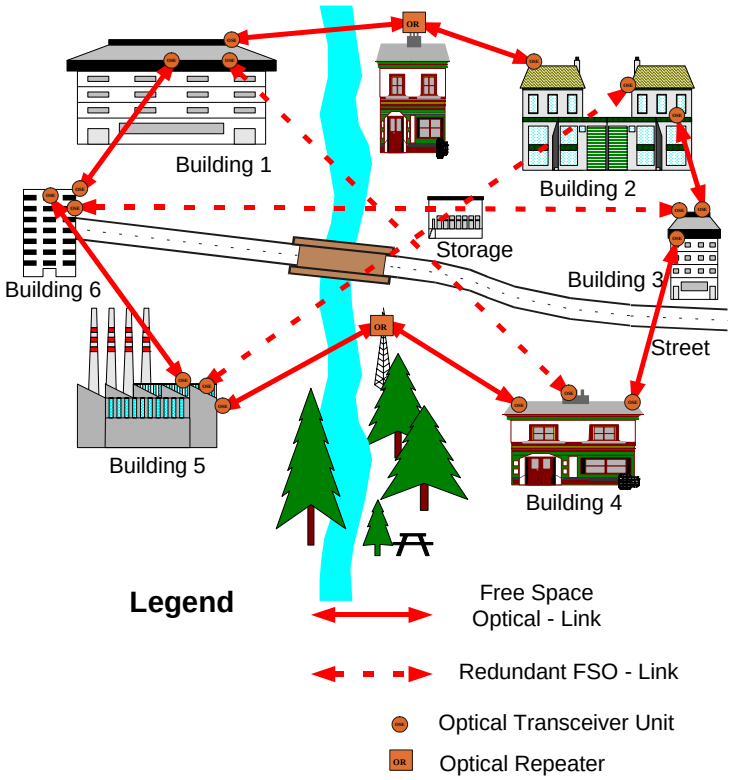

Figure 15: Optical Wireless (meshed architecture, solution A)

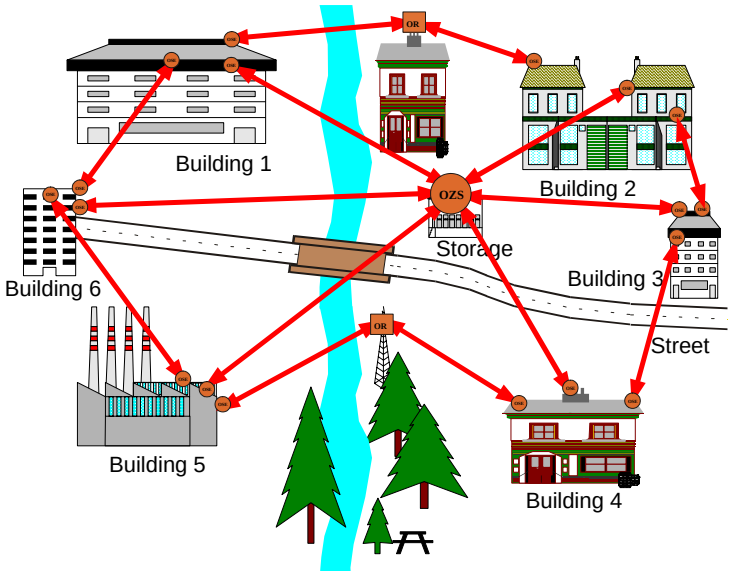

Figure 16: Optical Wireless (meshed architecture, solution B)

Connecting to the Backbone: The access network resides between the individual subscribers and the network operator’s backbone network. Fibre often does not reach paying customers. Only 3% of world-wide Businesses are on fibre, and 75% are within a mile from fibre. Nowadays the backbone is realised with fibre and so the connection with Free Space Optics offers many advantages. The FSO-systems work protocol transparent like a fibre link. Hence, the same networking technologies used in fibres can be used over Free Space Optics. It is possible to couple from FSO-systems directly into the optical domain or with optical / electrical conversion and regeneration to the network-fibre. Also coupling into a Wavelength Division Multiplex (WDM) is possible, by connecting different Optical Wireless Systems with a Wavelength Division Multiplexing unit to the WDM-fibre network.

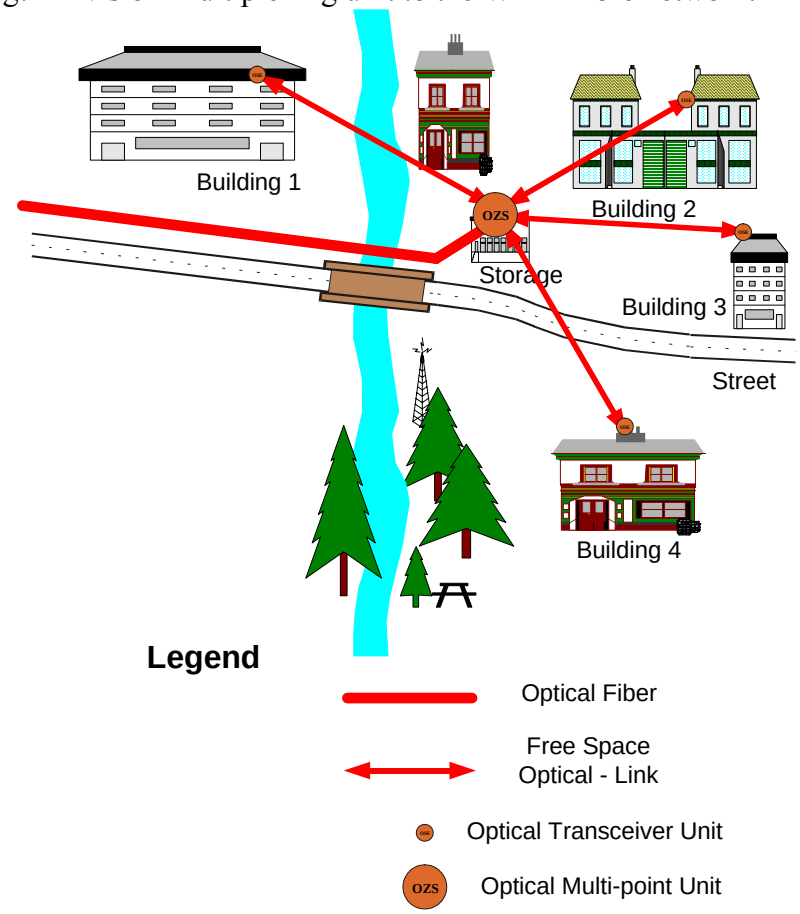

Figure 17: Optical Wireless Access with Point-to-Multipoint Architecture

In different architectures and configurations, the FSO-unit can be connected to satellites, directional radio links, (mobile) telephone networks, or fibre optics. In figure 17 a connection to a fibre based backbone realised with a Point-to-Multipoint architecture is shown. The Optical Multipoint Unit is connected with a switch or router to the backbone network (thick solid line in figure 17). The users in the buildings 1, 2, 3 and 4 are linked with their FSO-terminal units to the central optical multipoint unit.

4.1.3.2 Reliability in relevance to Visibility

Optical wave propagation through the atmosphere requires a free line of sight from the location of the transmitting terminal to the receiving terminal. Even though receivers for infrared transmission are more sensitive compared to the human eye in the visible light region, the influence on the radiation is very similar. Especially for networking applications, where high availability is essential, the weather influence is a key factor. Visibility data,

collected over several years either by free eye estimation or, more accurately, with a transmissiometer instrument at meteorological stations or at airports as runway visibility range (RVR) can be used to calculate availability in free-space optic network planning. Atmospheric transmission can be described by the BEER-LAMBERT law.

$$\tau = \frac{P_d}{P_0} = e^{-\gamma d} \tag{2}$$

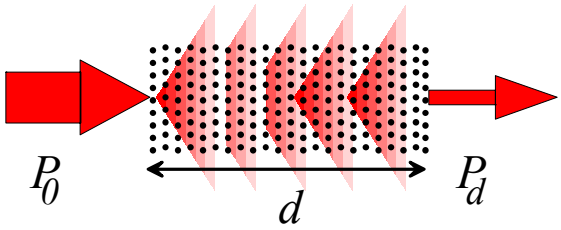

Figure 18: Transmission according to the BEER-LAMBERT law

The transmission τ for an optical wavelength means the relation of the optical power P_d at the end of an atmospheric path of distance d to the optical power P_0 which was originally sent (figure 18). According to the BEER-LAMBERT law transmission can be expressed by the extinction coefficient γ and the atmospheric path distance d. The extinction coefficient γ is constituted by processes of absorption α and scattering β by particles in the atmosphere. In detail, these particles can be the molecules of the atmospheric gas constituents and the larger aerosol particles.

$$\gamma(\lambda) = \alpha(\lambda) + \beta(\lambda) = \alpha_m(\lambda) + \alpha_a(\lambda) + \beta_m(\lambda) + \beta_a(\lambda) \tag{3}$$

For the wavelengths used in Free Space Optics, especially 850 nm and 1550 nm, atmospheric absorption can be neglected. Scattering by molecules $\beta_m(\lambda)$, which can be described by the Rayleigh scattering model, only get important for optical wavelengths smaller than 400 nm. The main important process that remains is the scattering of light by aerosol particles $\beta_a(\lambda)$ in fog. It can be described by the Mie scattering model for single interactions between particles and waves.
By definition the visibility range V is the atmospheric path distance for a transmission of 2 %. This is expressed in the Koschmieder equation:

$$V = \frac{\ln\left(\frac{1}{\tau}\right)}{\gamma_{550\,nm}} = \frac{\ln\left(\frac{1}{0.02}\right)}{\gamma_{550\,nm}} = \frac{3.912}{\gamma_{550\,nm}} \tag{4}$$

Sometimes a slightly different definition is used in the literature, defining the visibility range at 5 % transmission. This leads to a factor of 2.996 instead of 3.912. Reforming this equation allows to calculate the extinction coefficient for 550 nm, at the centre of the visible light range.
To adapt visibility data for infrared wavelength transmission, the wavelength dependency of the scattering process has to be taken into account. A first relation based on empirical measurement data was proposed by Kruse [5]:

$$\gamma(\lambda) \cong \beta_a(\lambda) \cong \frac{3.912}{V} \cdot \left(\frac{\lambda}{550\,nm}\right)^{-q} \tag{5}$$

The exponent q in equation (5) depends on the visibility distance range. To include also low visibilities in dense fog, the original Kruse equation was modified by Kim [3, 5] to

$$q = \begin{cases} 1.6 & for\ V > 50\ km \\ 1.3 & for\ 6\ km < V < 50\ km \\ 0.16\,V + 0.34 & for\ 1\ km < V < 6\ km \\ V - 0.5 & for\ 0.5\ km < V < 1\ km \\ 0 & for\ V < 0.5\ km \end{cases} \quad (6)$$

In general it is problematic to find a relation which allows the recalculation of visibility data from 550 nm to longer wavelengths. Different types of fog can cause different attenuation for longer wavelengths at the same visibility range, actually depending on the particle size distribution and the particle density according to the Mie scattering model. But visibility data does not include information about the particles, even rain and snow are included. Measurement data indicates that longer wavelengths are less attenuated in haze and light fog, while there is no wavelength dependency in dense fog. New theoretical calculations from Alnaboulsi for advection fog and convection fog indicate that shorter wavelengths are less attenuated at very short visibilities, which is the most critical case for high available Free Space Optics.
Hence, even if visibility data should not be over-interpreted, it is a useful information for availability prediction. Probably the best compromise is to assume no wavelength dependency. Especially for short-range high availability applications this seems to be the best approach, except for 10µ-technology. It is convenient for technical applications to calculate in decibels, so the extinction coefficient γ can be recalculated to attenuation due to scattering

$$a_{SCAT} = \frac{10}{\ln(10)} \cdot \gamma(\lambda) \cdot d \quad (7)$$

Equation (7) considers attenuation α_{SCAT} (in dB) over the full atmospheric path distance d, while equation (8) considers the specific attenuation $\alpha_{SCAT,\ SPEC}$ (in dB/km) for a transmission threshold of 2 %.

$$a_{SCAT,\ SPEC} = \frac{10}{\ln(10)} \cdot \gamma(\lambda) = \frac{10 \log\left(\frac{1}{\tau}\right)}{V} \cong \frac{17\ dB}{V} \quad (8)$$

4.1.3.3 Reliability and availability of the installed FSO-link

To introduce this topic, which is of high relevance for the practical use of Free Space Optics-systems in communication networks, the meaning of the expressions shall be explained.

- **System reliability** *R(T)* is the probability that the system works correctly during the time period *T* under defined environmental conditions.
- **System availability** *A(t)* is the probability that the system works correctly at the time *t*.

Because the Free Space Optics-link just offers the physical layer for data transmission, the conditions for correct operation of the system usually are defined by a maximum tolerable bit error rate (BER) for the specified data rate (e.g. BER = 10^{-9} for 100 Mbps). The bit error rate increases, if too much or not enough optical power is received. In this sense, Free Space Optics-systems usually are very secure by construction, if they can avoid overload and if they simply switch off the connection to the network, when the received optical power gets too low because of atmospheric attenuation, before too many bit errors are produced. This threshold is also referred as the receiver sensitivity limit P_{RS}. Especially short range systems can be described in this way and behave like a wired connection, offering the specified performance over the full distance. For long distance FSO connections using more collimated and more coherent light, fluctuations in the received power get increasingly important. This makes it

difficult to set the right sensitivity limit and could also cause performance degradation by burst errors, which can be avoided by channel coding and error correction techniques.
Related are safety issues, which do not actually refer to data transmission, but in general to conditions for operation. To satisfy laser safety regulations according to IEC / EN 60 825, especially to meet laser class 1 which certifies safety under all possible conditions over long time, or the classes 1M, 2 (visible light) or 3A is important to allow the operation without further restrictions. The main concern of laser safety is the human eye, which focuses light coming through the Iris aperture of max. 7 mm diameter to the retina, so light intensity is actually measured. In the same eye safety laser class, more power is allowed for longer wavelengths up to 1400 nm because of transmittance and focus characteristics of the eye. Hence, 1550 nm technology has an advantage against 850 nm here. More power is also allowed for light sources with a higher divergence angle compared to point sources, because only point sources can be concentrated in a very small spot on the retina. For this reason, light sources like LEDs, optics using diffusers, or multiple transmitter optics have an advantage. In addition to laser safety also the regulations for mounting the systems must be met, too.
The availability of an installed Free Space Optics-link mainly depends on the power link budget and the local climate conditions, causing increased attenuation over periods of time. The properties of an FSO system excluding the effects of the atmospheric path and distance can be summarized in the system power factor P_{SYS} (in dBm) to

$$\begin{aligned} P_{SYS} &= P_{TX} + G_{TX} + A_{RX} - \sum\left(a_{TX} + a_{RX}\right) = \\ &= P_{TX} + 10\log\left(\frac{4\pi}{2\pi\cdot\left(1-\cos\alpha/2\right)}\right) + 20\log\left(R_A\right) - \sum\left(a_{TX} + a_{RX}\right) \end{aligned} \tag{9}$$

In (9) the optical output power in decibels over one mill watts (dBm) is represented by P_{TX}, the geometrical transmitter gain in decibels is G_{TX} (depending on the full beam divergence angle α), the geometrical gain at the receiver due to optics aperture radius R_A is A_{RX} and losses in the optics of transmitter and receiver are represented as a_{TX} and a_{RX} (dB). This allows calculating the power received P_{RX} in distance d by

$$P_{RX} = P_{SYS} - D_L = P_{SYS} - 20\log\left(\frac{2d}{1m}\right) \tag{10}$$

Equation (10) includes the decibel value D_L of the geometrical distance d in meters and gives the received power P_{RX} without any atmospheric influence or pointing losses.
The specific link margin M_{SPEC} for an installation can be found with the receiver sensitivity limit P_{RS} for proper operation

$$M_{SPEC} = \frac{1000m}{d}\cdot M = \frac{1000m}{d}\cdot\left[P_{SYS} - D_L - P_{RS}\right] \tag{11}$$

The basic condition for system availability A is that the specific link margin exceeds the specific attenuation, which can be expressed by

$$A = \begin{cases} 1 & for \quad M_{SPEC} \geq \sum a_{SCAT,SPEC} \\ 0 & for \quad M_{SPEC} < \sum a_{SCAT,SPEC} \end{cases} \tag{12}$$

at the time t.
The appearance of fog can only be statistically described, usually as the steady-state availability, which is approximated by measurements over long periods of time.
As an example, a one year runway visibility range data set from Graz, Austria, is shown in figure 19. In this data, point 3 represents the probability for a visibility of less than 1500 m,

equal to a specific attenuation of 11.4 dB/km, which was approximately 5 % of one year´s time. The probability for visibilities less than 200 m indicated in point 1 was 0.01 %, which means that a FSO installation would reach 99.99 % average availability during this year if it has more than 85 dB/km specific margin. Such link availabilities and even more are possible if only the link distance does not exaggerate a certain value.

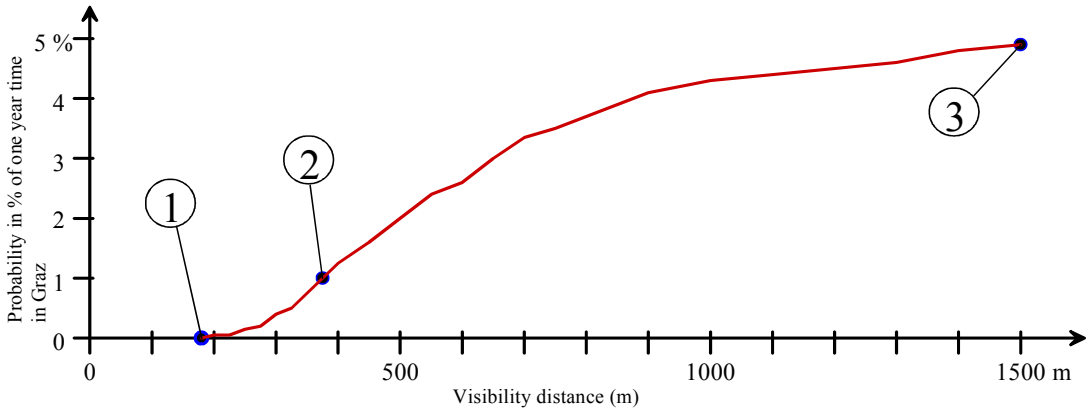

Figure 19: Full year visibility data profile for the city of Graz, Austria

Based upon this climate example, it is possible to calculate availability contours for specific Free Space Optics-systems characterised by their system power factor. Figure 20 shows this for two types of systems. Type one is a cost efficient general purpose type with a comparatively large beam divergence and receiver acceptance angle, allowing quick installation and easy mount. Type three is a sophisticated system with small beam divergence and automatic beam tracking specialised for longer distances. Typical system properties may be between these two cases.

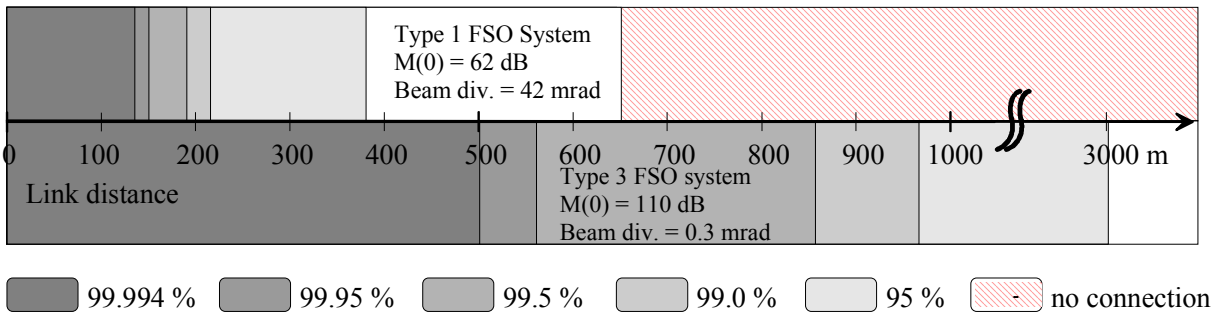

Figure 20: Calculated availability contours for two FSO-systems for the visibility data set of figure 19

A practical measurement with a commercial FSO system was performed in [2, 6] over the same period of time as used in figure 19. The system used 850 nm wavelength and a beam divergence of 2 mrad for an installed link distance of 2.7 km. Multiple beam technology was implemented to reduce scintillation effects in the optical domain and to increase system reliability. The system power figure was 96 dBm and the specific link margin approximately 7 dB/km. Figure 21 shows the seasonal and diurnal dependencies of the unavailability of the link.

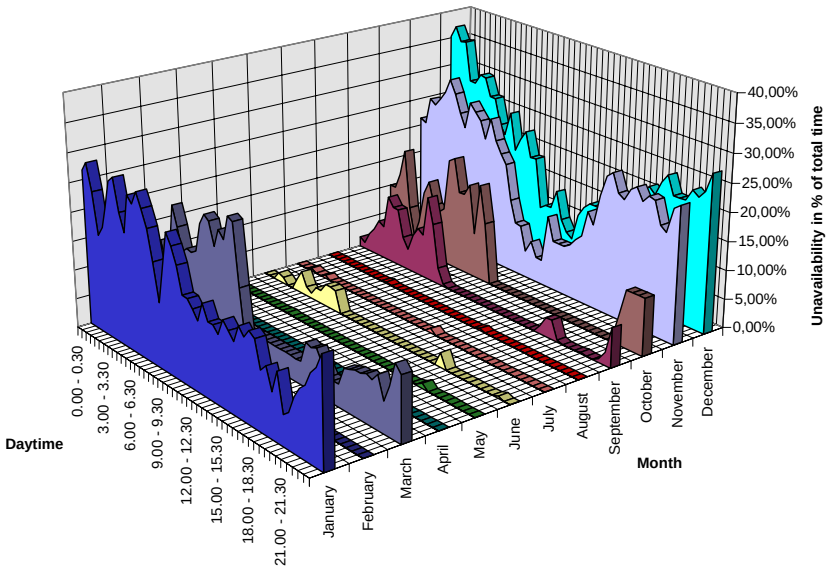

Figure 21: Seasonal and diurnal dependency of measured unavailability of a 850 nm FSO system at 7 dB/km specific margin in Graz, Austria

A clear dependence on the season can be seen, as it is typical for Central Europe and North America, for example. The major cause of unavailability was fog, especially convection or radiation fog, which appears at the end of the day and during night, caused by ground cooling due to radiation, and is resolved by sunlight during the day. This is the cause for the daytime dependency.

The performance of the system was very good; at 155 Mbps data rate the monthly averaged bit error rates (BER) reached values between 10^{-11} and 10^{-13}. A one year follow up trial [11] of the same optical link combined with 40 GHz technology with approximately 2.5 dB/km specific margin did result in 99.926 % reliability for the combination of optical and millimetre wave, a so-called hybrid wireless link, while the availability of the millimetre wave link was 97.989 % and for the Free Space Optics-system 96.813 % during this year. A short range FSO-system with 70 dB/km specific margin did show an availability higher than 99.96 % in the winter season during this time.

For practical applications this means that broadband and high available wireless links can either be reached over short distances with optical links only, or over longer distances by the combination of very high frequency and optical links. If the application is not time critical or does not require high availability (like for example remote data storage), additional Free Space Optics-links over several kilometre distances can increase the network throughput dramatically.

Reliability refers to the inner properties of the system in first place, which can be expressed by the mean time-to-failure (MTTF), or the FIT rate actually. 1 FIT means the probability for a device to fail in 10^9 hours of operation. In Free Space Optics-systems especially the transmitting elements have a limits of lifetime, depending on the conditions under which they are operated. In general, the output power reduces gradually, and finally the device will fail. Major manufacturers qualify their products and provide statistical data for the performance over time. VCSELs and LEDs have a typical lifetime of 10^5 to 10^8 hours of operation. Providers of fibre optic networks state that typically 1-2 of 1000 media converters can fail within a year. Operating the devices below the output power limit and avoiding extreme temperature variations can improve the lifetime a lot.

In the sections above we have seen the different types of Free Space Optics-systems, their characteristics and their advantages. For the Last Mile FSO-systems with Light Emitting

Diodes (LED) as source are a well suited solution, because they are cheap and data rates in the range of tens of Mbps are sufficient. Using LEDs has the advantage that problems with Laser- and Eye Safety are minimised. Low cost Free Space Optics-systems using LEDs instead of laser diodes have been developed by [1, 9] for data rates of 10 and 100 Mbps.
The developed systems combine available standard components to realise cost-effective solutions. The beam divergence usually covers values from about 8 to 60 mrad, allowing an easy alignment for the user without the need of a telescope. All elements including the optics do not require a precision as high as needed for other approaches, allowing higher tolerances at production, and the use of simple mounts. Due to large divergence, the requirements for a stable underground are not very high allowing a quick installation. Suitable distances for high availability operation are limited by the wide beam angle and depending on local climate to up to 300 meters. Due to Laser Safety Regulations the use of sources with larger emitting area allows more output power in the same safety class, which improves the link budget.

4.1.3.4 High Availability with Hybrid Wireless Networks (combined Optical and RF-links)

The availability of FSO-links is limited by weather patterns like fog and heavy snowfall. Microwave based communication links operating at high frequencies (40 – 43 GHz) offer comparable data rates and need line-of-sight as well. Link availability for microwave systems is limited by heavy rain. Combining Free Space Optics-links with microwave links within a hybrid FSO/microwave communication network has the advantage of added redundancy and higher link availability. Measurements over a period of one year show a combined availability of 99,93% for the climatic region of Graz (Austria) which proves that the combination of both technologies leads to a highly available wireless connection offering high bandwidth [11].

Figure 22: Installation of a GoC Multilink 155F in combination with LMDS

Discussing the individual advantages and disadvantages of FSO and radio communication technologies, the idea was born to combine optical and microwave links for introducing redundancy and to achieve higher availability. Therefore a measurement scenario has been set up in Graz, Austria to compare the link availability of a microwave and a free space optical link between the same locations influenced by the same weather conditions. The distance of this redundant link is 2.7 km and the two locations are in line of sight. Graz is located in an area where various weather conditions appear and the climatic zone is very problematic for optical and microwave communication systems. Microwave and FSO communication links (figure 22) have roughly the same properties regarding offered data rates and flexibility of setup, but operate under different conditions, with their benefits and challenges.

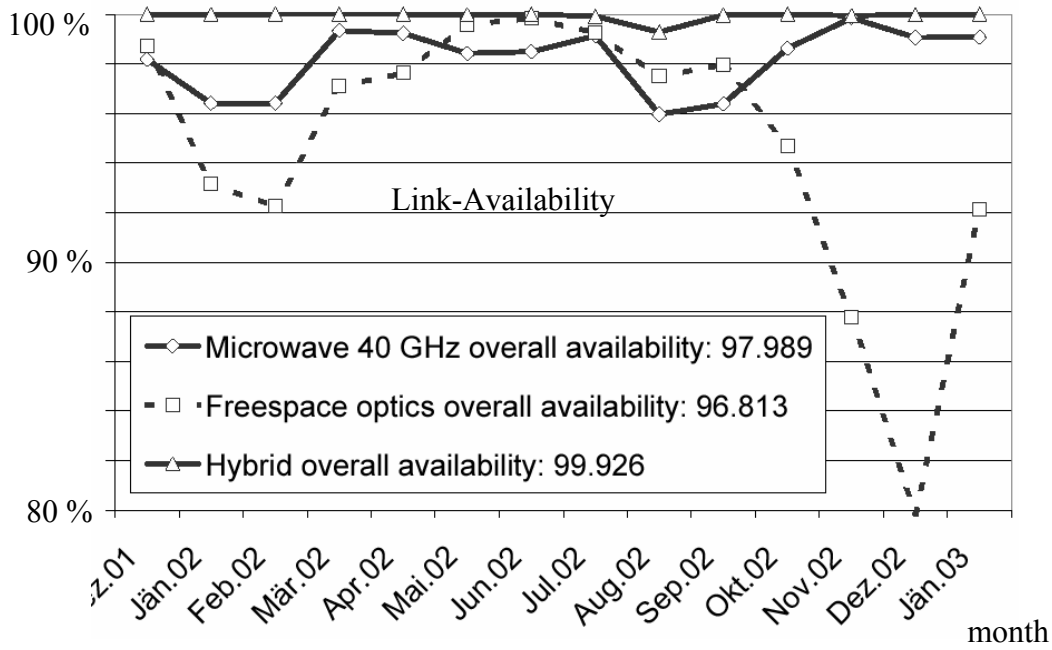

Figure 23: Availability of the separated links and the hybrid

The measurement result is drawn in Figure 23 for each month. The dotted line indicates the optical link. Obviously the optics is highly influenced by fog and snow fall, which can be seen in December. In contrast the microwave link does not have excessive losses during this period, and the hybrid reaches nearly 100%. A similar situation appears in January and February. During this time snow fall, fog and rain occur, which can be seen in the low availability of both links. Nevertheless, the hybrid has very high availability. This can be seen as proof, that the systems have nearly orthogonal behaviour. From March to July both systems have approximately the average availability. The next interesting section is the summer with heavy thunderstorms. In the observed year this happened in August, where both systems do not have excessive bad availability, but the hybrids availability decreases to 99.28%. The reason for this behaviour is the loss of the optical link during heavy thunderstorms. A month later nearly the same single availability is obtained, but the hybrid has again a high availability.
The big advantage of the hybrid is the fact, that systems with a single system availability of 97% can be improved to 99.926%, which is identical with a gain enlargement of transmitting power of 12 dB in the microwave link case.

4.1.3.5 Influences on OISLs

At the time to design a communication system to board it into a satellite, there are some important factors to have into account such as mass, size, data rate and power consumption. For a given diameter, an antenna at optical frequencies exhibits an extremely high gain. That allows to use a compact transmitter of low power and mass. Another factor to consider is that the optical system will have a narrower bandwidth than a RF system. The far-field 3-dB beam divergence and the far-field beam width at a distance L from the telescope are approximately:

$$\theta_{-3dB} = A \cdot \frac{\lambda}{D} \quad (13) \qquad W = A \cdot \frac{\lambda}{D} \cdot L \quad (14)$$

where λ is the wavelength, D is antenna diameter and A depends on the aperture properties. For the worst case (GEO-GEO link), the beam width is over 360 m for a 20 cm telescope and

a wavelength of 850 nm. Working with such narrow beam, leads to a more complex Pointing Acquisition and Tracking (PAT) system to board on satellites. This complexity derives from the necessity to point from one satellite to another over a distance of tens of thousands kilometres with a beam divergence angle of microradians as the satellite moves and vibrates. Such vibrations decrease the received signal and, therefore, increase the bit error probability of the system [16].

Pointing, Acquisition and Tracking: Acquisition is generally considered to be the most difficult stage, because laser beams are typically much smaller than the area of uncertainty [17]. To precisely point its beam, each terminal must be able to know the exact position of its counterpart. A rough estimate of this information will be derived from the orbit parameters of the satellite. The terminal points towards the assumed position of its partner either by employing a pointing unit moving the whole telescope with a two-axis gimbal or applying a coarse pointing mirror. Then a beacon is activated by one or both of the terminals, providing the direction to point to before the communication signal is active. Tracking the beacon or the communication laser allows the fast steering mirror to follow the exact position of the other terminal.

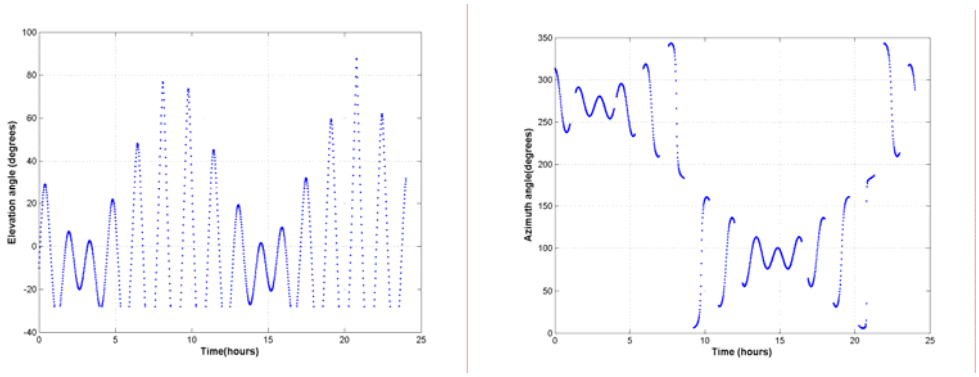

Figure 24: Azimuth and elevation angles between ARTEMIS and SPOT-4 satellites

The problem of acquisition is that usually the diameter of the beacon laser beam at the receiving terminal is much smaller than the uncertainty area of coarse pointing. This uncertainty is caused by several effects, e.g. atmospheric disturbances, attitude control errors, mechanical resonances from servos, momentum wheel movements, control jet firing, etc. In figure 25 it is shown an acquisition protocol suitable for LEO-GEO systems [18]. A beacon laser source carried on one of the terminals scans the uncertainty area. At the same time, the other terminal has a wide field-of-view sensor which stares over its cone of uncertainty. This sensor can be based on a CCD array, for example, and is read out at ≤ 50 Hz frame rate so that incoming light is integrated over a relatively long period giving high detection sensitivity. The beacon source requires a large angular divergence to minimize the acquisition time and high power (on the order of 1 to 20W). Typical acquisition periods for an O-ISL are desired to be ≤ 60sec.

To initiate optical inter-orbit communications, each satellite continuously transmits the communication beam toward the other to enable the counter satellite to improve its pointing accuracy. Generally, one or more separate lasers, operating at wavelengths differing from that of the communication laser, are used to generate the beacon. It is even possible to use the communication signal as beacon. Once the acquisition sequence is completed successfully, the terminal will make a transition into coarse tracking and finally into fine tracking mode. Coarse tracking is performed by a control loop (bandwidth ~10 Hz) driving the coarse pointing mirror. The fine tracking loop controlling the fine steering mirror should have a bandwidth of ~ 1kHz. The tracking function measures the angular error between the direction of the incoming and outgoing beams. The difference is used as feedback for mirror pointing.

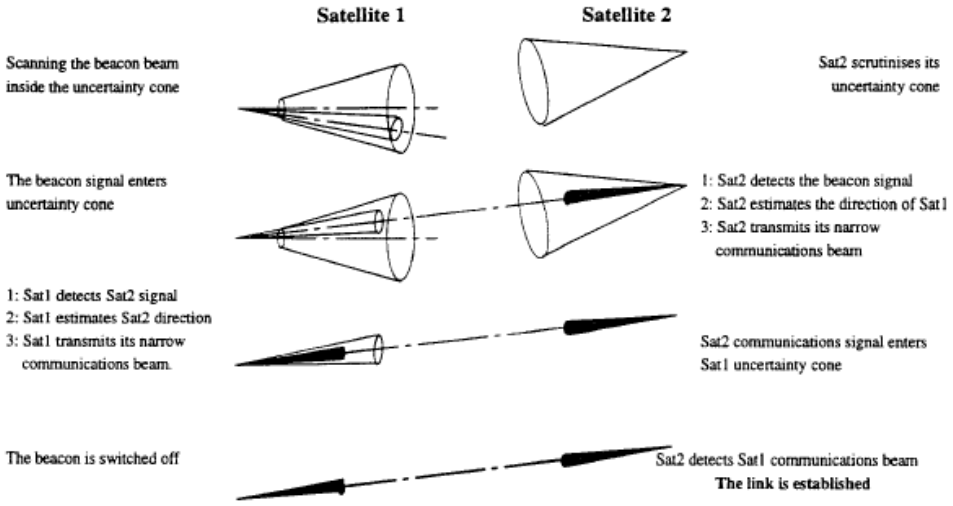

Figure 25: Example of the acquisition procedure

Mainly two forms of angle error sensors are considered: CCD-arrays and quadrant photo diodes (QPD). Depending on the scenario, the relative velocity of the terminals can reach high values. One critical issue is the maximum angular speed the tracking subsystem is capable to follow. This problem mainly concerns the coarse pointing mirror since the fast steering mirror only compensates for minor pointing errors (e.g., vibrations of the platform).
Even when the link is established, satellites suffer vibrations and misalignments can occur. This involves a degradation of the link in term of a reduction of SNR. Elevation and azimuth pointing error are both normally distributed with the same variance, so the radial pointing error is the root square of the sum of the azimuth and elevation angle and can be described by a Rayleigh distribution. In [16] the pointing losses are modelled by a factor that corrects the instantaneous received power, for a Gaussian beam it is:

$$L_T(\theta) = e^{-G_T\theta^2} . \tag{15}$$

The variance of the pointing losses is calculated as a function of SNR in the tracking bandwidth and a slope factor (SF) that converts the angular offset in linear voltage:

$$\sigma = \frac{1}{SF \cdot \sqrt{SNR_{trk}}} \tag{16}$$

Assuming an SF=25000 rad^{-1} and a transmitter aperture of 0.3 m, the impact of pointing losses on SNR is shown in Figure 26.

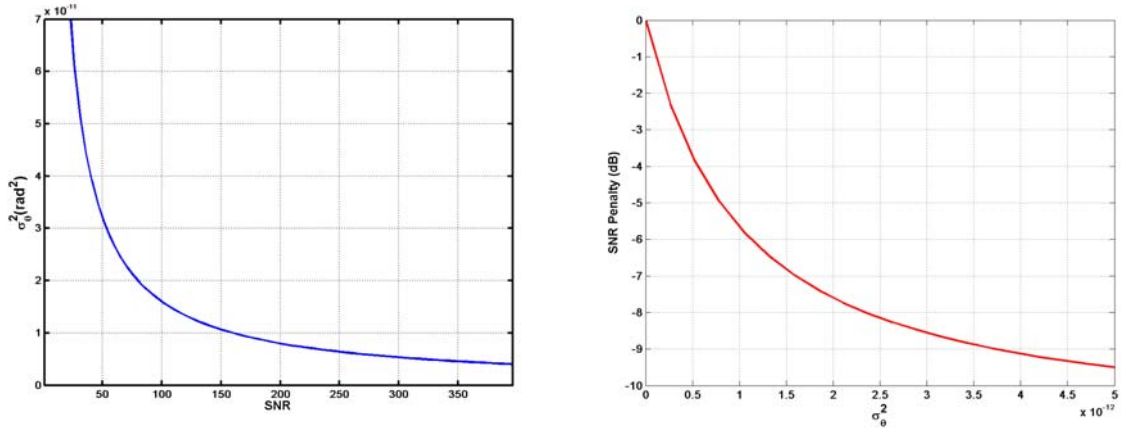

Figure 26: a) Pointing variance as function of tracking SNR and b) SNR degradation

Doppler Effect: Doppler effect is due to relative motion between source and receiver. In the case of an intra-orbit inter-satellite link, satellites move at the same speed, which means that the relative speed between the two satellites is zero and, consequently, this effect does not affect. However, in the case of inter-orbit inter-satellite links, the satellite in the lower orbit travels at higher speed than the satellite at the higher one. This non-zero relative speed is translated into a shift of the received frequency. The Doppler shift has to be estimated in order to enable reliable communications and its compensation can significantly enhance the performance for frequency shift keying, amplitude shift keying coherent communications and even on-off keying direct detection communications, mainly if the Doppler shift is greater than the data rate. If Doppler effect is neglected, it can cause the failure of packet detection, carrier frequency synchronization, serious degradation of demodulation performance and frequent failure. In few words, the probability of outage for the link could not be satisfactory.
A link between two satellites moving at relative velocity $\upsilon(t)$, the received frequency is given by:

$$\nu(t) = \nu_c + \nu_c \frac{\upsilon(t)}{c} \cos(\alpha(t)) \tag{17}$$

where ν_c is the optical frequency of the signal, $\alpha(t)$ is the angle between the relative velocity and the signal propagation direction and c is the light speed. The Doppler shift reaches a maximum value when the radial component of the relative velocity is at a maximum too. By simulation, it is possible to face a realistic problem: Doppler shift evaluation on ARTEMIS-SPOT-4 link. As it can be seen from Figure 27, Doppler shift is a function of relative speed. In a LEO-LEO link, the relative speed is between 14.4 and 15 km/s. In a GEO-LEO link, as ARTEMIS and SPOT-4, the motion is almost due to the LEO satellite, so the relative speed is more or less the half, that is, around 7.5 km/s. By calculation it can be found that the maximum Doppler shift is between [-4.838, 4.838] GHz.

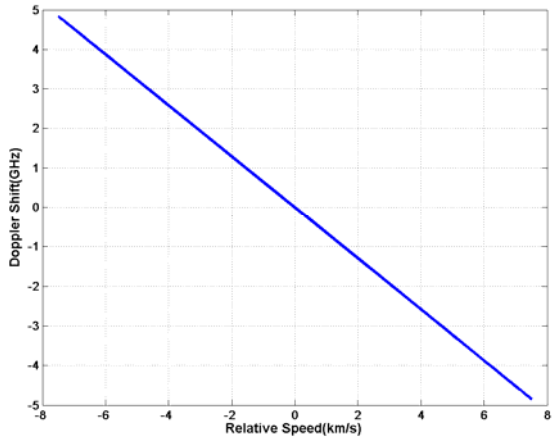

Figure 27: Doppler shift as function of the relative speed

The receiver end must be able to accommodate the signal in this range of frequencies around the central carrier. The maximum shift occurs in the shortest access, where the relative speed between satellites is higher. In the same time, the minimum shift occurs in the longest access (figure 28, 29). Doppler treatment is usually done in coherent systems, where the recovery of the carrier is critical. In direct detection systems there is no carrier to lock to. So it is important to develop a receiver that is able to manage Doppler effect with no need of a carrier recovery subsystem. There are two possible ways to follow in order to reduce Doppler shift. On one hand, it is possible to board on satellites an OPLL [7]. In this case the receiver end will be able to follow frequency variations in the range of Doppler shift. Of course this solution does not fit with direct detection, since it could be a waste of payload. On the other

hand, it is possible to compensate the Doppler shift in optical domain. The insertion of a preamplifier in the DD receiver scheme leads the system to perform efficiently a good level of sensitivity, and they can perform a very good connection in terms of BEP, with not so wide efficiency gap if compared with a coherent receiver. This can be possible by developing high performing EDFA preamplifier in L-C band. Another factor that can improve the performance of direct detection receivers is to choice the best fitting modulation format, for example it has been proved that DPSK signalling perform best with pre-amplified DD receivers.

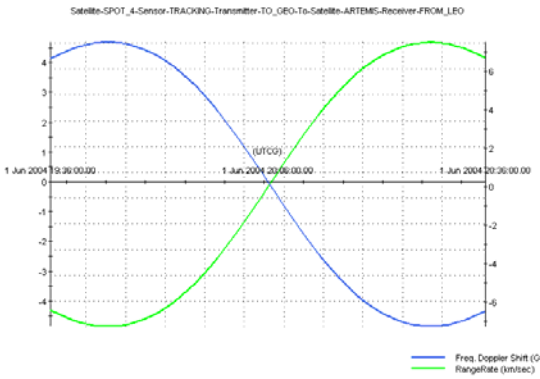

Figure 28: Maximum doppler shift

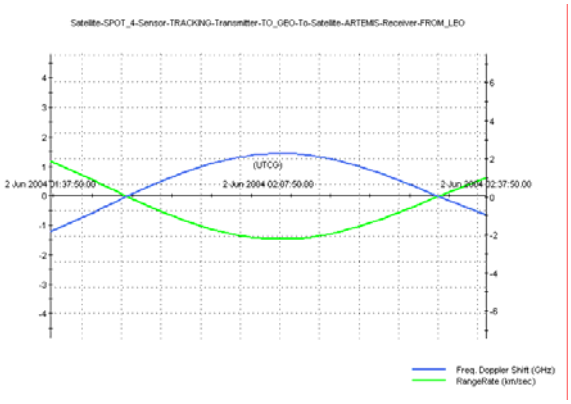

Figure 29: Minimum doppler shift

In Figure 30 it is shown a receiver scheme for a direct detection 2.5 Gbit/s optically preamplified system, signal recovery it is ensured by a simple filtering in the right band. In order to manage the correct detection, the system must be able to follow all frequency shifts induced by Doppler effect.

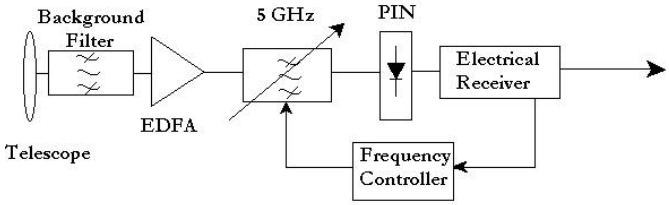

Figure 30: 2.5 Gbit/s Direct Detection optically pre-amplified receiver scheme

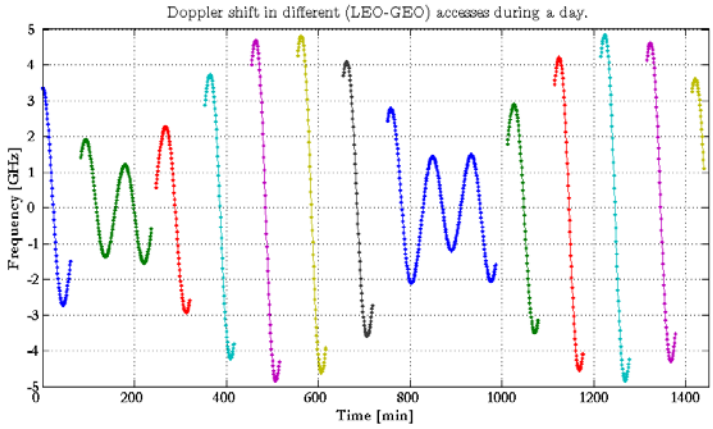

Figure 31: Doppler shift in different accesses

At the beginning of each new access, LEO reaches the GEO range of visibility, then PAT procedure starts. In this first stage Doppler shift is always positive, since LEO approaches GEO (as shown in figure 31). To ensure the correct filtering, it is possible to use an optical

filter with a bandwidth of 5 GHz, centered at f_0+2.5GHz, where f_0 is the signal carrier. By this filtering the receiver end will be able to follow the signal through its frequency variations. The maximum shift occurs during the shortest access, where the relative speed between satellites is higher. When one access ends the Doppler shift is negative, by the next access beginning the filter must be tuned at the starting frequency of f_0+2.5GHz again. By simulation it can be proved that the minimum time delay from the end of one access to the beginning of the next one, is 600 sec, that is a very long time for tuneable optical filter in 1550nm band. In direct detection system, there is no carrier to lock to, besides the presence of an optical preamplifier can improve the performance of this system also with respect to Doppler effect. By the use of a DD pre-amplified receiver scheme, a sensitivity reduction can be evaluated as a function of the filter bandwidth related to the signal bit-rate [19], as shown in Figure 32:

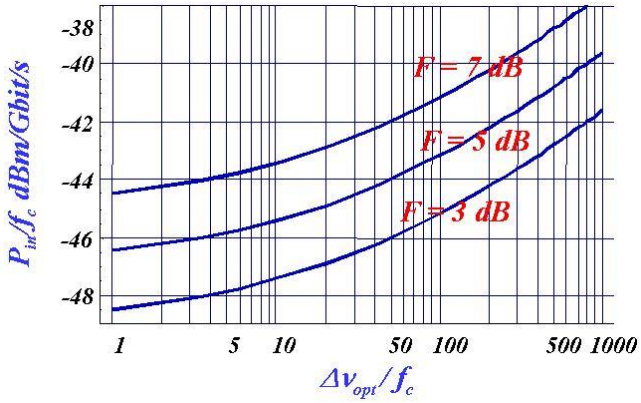

Figure 32: Sensitivity penalty, due to optical filter bandwidth increasing, related to signal Bitrate

Receiver sensitivity penalty can be calculated by the following relationship:

$$P_{in} = f_c \cdot h\nu \cdot F\left[\gamma^2 + \gamma\sqrt{\frac{\Delta\nu_{opt}}{f_c}}\right] \tag{18}$$

where f_c is the signal bit rate, F is the preamplifier noise figure, γ is the optical signal to noise ratio, $\Delta\nu_{opt}$ is the bandwidth of optical filter. In a system with f_c =2.5Gbit/s, F=3dB, $\Delta\nu_{opt}$=5GHz and ν=1550nm, it can be calculated the sensitivity penalty that is around 2dB, with respect to the case of optimum filtering, which is a neglectable reduction of performance [20].

Noise Sources: The number of noise sources affecting an inter-satellite system depends on the detection technique (direct detection or coherent detection) and if the system is optically pre-amplified or not. A detailed demonstration can be found in [21]. These noise sources can contribute to the overall noise process, depending on the configuration of the system. In function of if the receiver employs an APD detector or a PIN detector with a preamplifier, some of these noise sources will be present or not.

- **Shot Noise** It depends on the statistical nature of photon to electron conversion and also because the photons arrive at the photo-detector at random times described by a Poison distribution.
- **Background Noise** The light incoming from the called star field, arrives to the photo-detector and manifests itself as a noise due to the shot noise process inherent to the photo-detection. The background noise can be defined in terms of a noise current density and is given by the expression:

$$\sigma_{bg}{}^2 = 2 \cdot q \cdot F \cdot B_e \cdot R_d \cdot M^2 \cdot N\pi \frac{D^2{}_r}{4} \cdot \Delta\lambda \tag{19}$$

($\Delta\lambda$ is the optical filter bandwidth, D_r is the diameter of the receiver aperture, N is the optical background irradiance in $W/m^2/\mu m$ [21]). In some circumstances, direct sunlight may cause link outages for periods of several minutes when the Sun is within the receiver's FOV. However, when the receiver is most susceptible to the effects of direct solar illumination can be easily predicted. When direct exposure (i.e., pointing) of the equipment cannot be avoided, narrowing the receiver FOV and/or using a narrow-bandwidth light filter can improve system performance. It is important to remember that interference by sunlight reflected off a glass surface is possible as well. Degradations caused by radiating celestial bodies other than the sun are generally negligible, but a receive telescope pointing directly into the sun can result in a reduction of the SNR at the decision gate by up to 15dB; eventually, the increased noise power will even disrupt communication if a sufficiently strong data signal cannot be provided.

- **Dark Current Noise** It refers to the current that flows in a photo-detector when there is no optical radiation incident on the detector and operating voltages are applied. The dark noise is dependent upon the operating temperature of the photodiode and its physical volume. The noise increases with the temperature and the physical dimensions. Therefore, it can be reduced cooling the detector or reducing the dimensions of it. It can be expressed as follows:

$$\sigma_{dc}^2 = 2 \cdot q \cdot F \cdot M^2 \cdot I_{dc} \cdot B_e \tag{20}$$

  where I_{dc} is the dark noise current, F is the excess noise factor of the photo-detector and M is the avalanche gain (equals to 1 in the PIN photo-detector case). Recall that both the background noise and the dark current noise contribute to the production of shot noise and could be grouped in a single expression.
- **Thermal Noise** Pre-amplification is necessary in order to reach manageable levels for detection. Random thermal motion of the conductors in these electronics systems manifests itself as a fluctuating noise component even in the absence of any incident signal. This noise component, referred to as thermal or Nyquist noise, degrades the detection sensitivity, and in non-pre-amplified PIN photo-detector systems, usually dominates over shot noise. Thermal noise is modelled as a stationary Gaussian random process with a variance of

$$\sigma_{th}^2 = \int_{-\infty}^{\infty} S_{th}(f)df = \frac{4kTB_e}{R_f M^2} \tag{21}$$

  where k is the Boltzmann constant, T is the temperature, R_f is the receiver resistance.

4.1.3.6 Mobile Optical Communications in Aerospace Applications - Overview of Development Status 2005

Long-range optical free space communications today is still in its development. While fixed directive optical near-ground links can be bought of the shelf, the atmospheric and tracking constraints in mobile applications are posing a not fully covered demand on mobile optical links inside the atmosphere. Most mature yet are space applications like optical inter-satellite links. Due to the absence of the perturbing and attenuating atmosphere, the optical technology can benefit ideally from the roughly linear gain improvement with rising carrier frequency in a point-to-point link.

ESA has demonstrated here the first reliable and reproducible inter-satellite link between its geostationary communications test satellite ARTEMIS and the earth reconnaissance low earth orbit satellite SPOT-IV in 2001. This experiment is called SILEX (Semiconductor Inter-Satellite Link). It also was used to demonstrate a GEO-ground link between ARTEMIS and ESA's optical ground stations on Tenerife.

On the military side, the US has been working on optical satellite-ground and air-ground links since at least forty years. This work was also put further through the SDI program in last century's eighties, where high-power laser beams were transmitted through the turbulent atmosphere.
Following is a description of the main developed hardware and experiments which have been carried out in this field or are ongoing.

SILEX (ESA): SILEX (Semiconductor Inter satellite Link EXperiment) was the first reliable optical inter satellite link. The SILEX system comprises two optical terminals: PASTEL on board the French earth observation satellite SPOT-4 and OPALE (Optical PAyload for Inter Satellite Link Experiment) embarked on the European GEO communications satellite Artemis. Due to its long development time and some launch delays, the OPALE-technology is quite outdated compared to current standards (mass of 157 kg and electrical power consumption of 150 W, 50 Mbps uplink and only 2 Mbps downlink with IM/DD-technology). But SILEX successfully demonstrated the first optical data transmission between the two European satellites in November 2001 and hitherto proved very reliable.
Japan is participating in the SILEX programme with its own laser terminal, LUCE (Laser Utilizing Communications Equipment), to be carried onboard the Japanese OICETS LEO-satellite (Optical Inter-orbit Communications engineering Test Satellite).

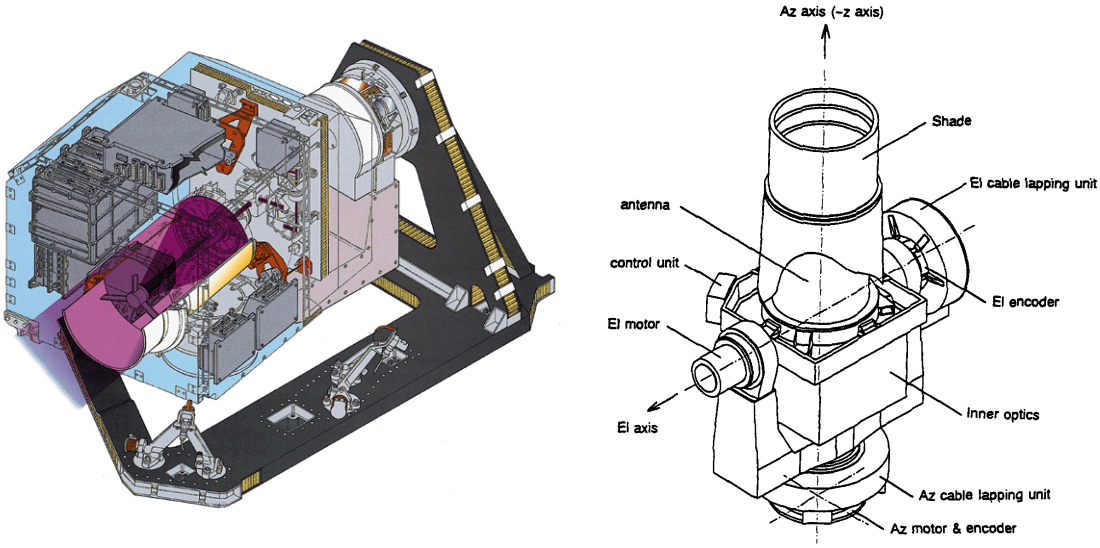

Figure 33: The OPALE Terminal (onboard ARTEMIS) built by Matra Marconi Space (left) and a schematic sketch of LUCE Terminal built by CANON Inc (right)

The SROIL Project (Swiss / ESA): In 1996 ESA awarded Contraves-Space a contract for the development of a "Terminal for Short Range Optical Intersatellite Links (SROIL)". The homodyne detection receiver uses a 1064 nm Nd:YAG laser, high sensitivity homodyne detection with the patented "sync bit" technology developed at DLR-KN. A combined coherent detection and tracking is used. The data rate of SROIL is 1.2 Gbps, the overall mass and power for a flight model 15 kg and 40 W. Size is approximately 30 x 20 x 50 cm. A two-axis pointing assembly in front of the telescope allows the SROIL terminal to achieve almost full hemispherical pointing. A breadboard demonstrator was completed in 1998.

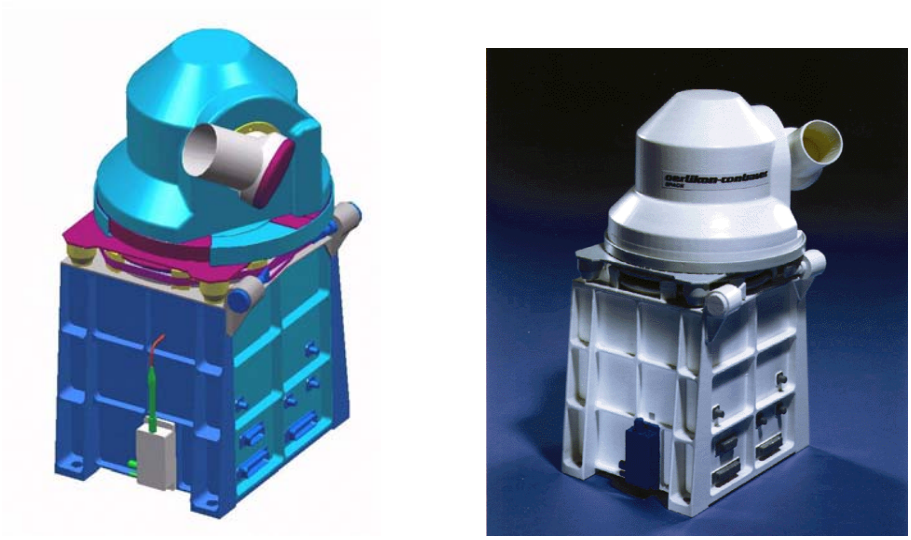

Figure 34: CAD outline and model of the SROIL Terminal

DLR-LCT (Germany): DLR-LCT was a German national funded project with TESAT (former Bosch-Satcom) as prime contractor and Carl-Zeiss-Oberkochen, DLR-KN and other German research-institutions as partners. LCT stands for “Laser Communications Terminal”. A homodyne BPSK Inter-Satellite-Link terminal operating at several Gbps with distances of several thousand km was developed in the frame of this project. The operating wavelength is 1064 nm (Nd-YAG-Lasers). This project is further pursued in the LCT-IOV (In-Orbit Verification) on-board TerraSAR-X …

TSX-LCT-IOV (Germany): A further developed DLR-LCT shall be tested on-board the German SAR radar-satellite TerraSAR-X which will be launched in mid-2006. This LEO has an LCT with 125 mm aperture embarked on its side as secondary payload. Further technical parameters of this terminal are still confidential, but very advanced performance in terms of power consumption and weight can be expected. Tests will be performed first with a downlink to a terrestrial ground station in Spain with 5.5 Gbps and in a second step with another LCT on-board another LEO which is not decided about yet. Aeronautical test scenarios are not foreseen with the TSX-LCT.

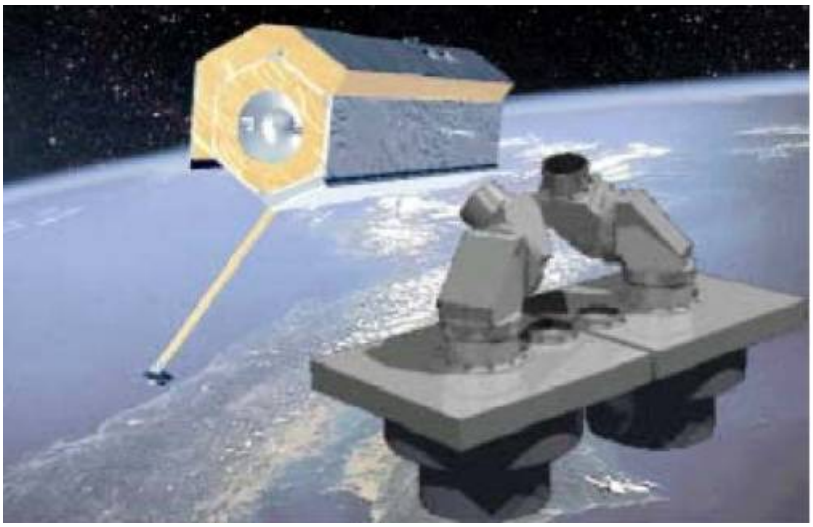

Figure 35: One DLR LCT (front inlay shows two terminals) will be embarked on Germany's TerraSAR-X (seen in the background)

FASOLT (Germany / Swiss): An optical ground-to-ground, direct-detection transmission experiment over 61 km was carried out by the German Aerospace Centre (DLR) in cooperation with the European Aerospace and Defence Systems Company (EADS) and Contraves Space AG, Switzerland.

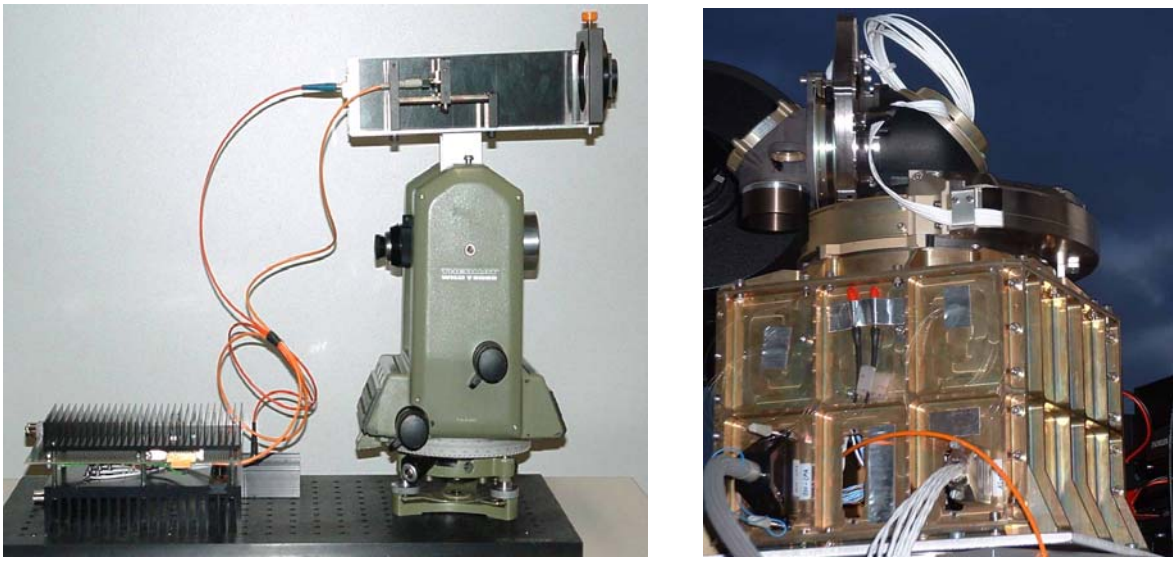

Figure 36: The FASOLT transmission system

In Figure 36 (left) is shown the FASOLT transmission system (including driver electronics for 270 Mbps intensity modulation with 500 mW, output power at 808 nm and fibre coupled telescope on top of a theodolite). The Optel02 demonstration model (by Contraves) during PAT experiments at DLR is illustrated at the right picture.

The FASOLT-project succeeded in demonstrating optical communications in the near-ground, very high optical turbulence layer with 100 Mbps at a mean bit error rate of 10^{-4} and demonstrate the pointing and tracking capabilities of the Contraves Optel02 terminal. Special means (transmitter diversity) were implemented to reduce fading.

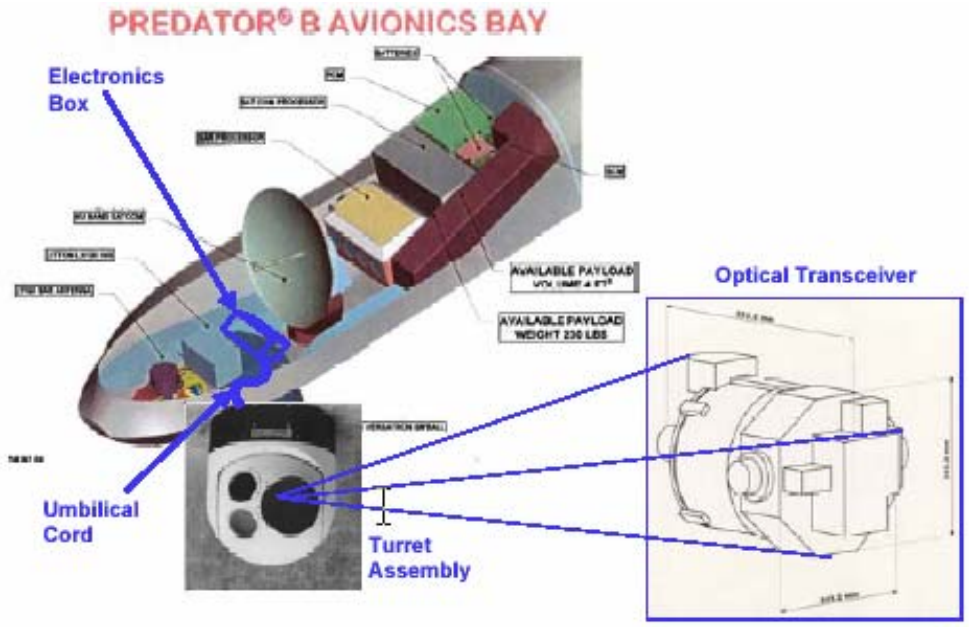

Figure 37: The optical payload and its integration to the UAV

Altair UAV-to-Ground Lasercom Demonstration (USA): One of the current projects of the Optical Communications Group at JPL/NASA is the development of a bi-directional optical communications link from an Altair UAV to ground stations. The optical payload uses a 200 mW downlink laser at 1550 nm. The altitude of the UAV shall be around 18 km.
The mount shown above is a conventional turret positioned at the bottom of the UAV. The turret has been equipped with the optical antenna and additionally serves as housing for the observation systems (cameras).

LOLA (France): The project that comes nearest to directed avionic optical link scenarios is LOLA (Liaison Optic en Laser Aeroporté), a project sponsored by then French ministry of defence. Its aim is to establish an optical link between a mid-altitude aircraft (5 - 6 km altitude) and ESA's geostationary test-satellite ARTEMIS. The parameters for this link are thus given by ARTEMIS's SILEX-performance (50 Mbps uplink, 2 Mbps downlink, IM/DD with wavelengths between 800 and 850 nm). Little is known about the progress of LOLA which started in summer 2003 and shall begin flight-tests in 2006. During the development phase a TBM 700 aircraft will serve as a test platform. The targeted application is the communication with military MALE- or HALE-UAVs. For this purpose, a complete new constellation of GEOs or MEOs with optical communication terminals is anticipated.

CAPANINA-FELT (Germany / EU): In the frame of the EU-FP6-STREP "CAPANINA" (Communications from Aerial Platform Networks delivering Broadband for All) a high-speed optical downlink from a stratospheric platform shall be demonstrated. Long-term aim of this approach is rather the high-speed backbone interconnection of a HAP-network than the data downlink to the ground, though the later type of link could also evolve as an advantageous technology when used in conjunction with site-diversity inside the HAP network to avoid cloud-blockage.
The optical communications terminal that is being build for CAPANINA is named FELT (Free-space optical Link Terminal) and the optical downlink experiment is called STROPEX (Stratospheric Optical link EXperiment). Transmission distance from the HAP will be up to 60km and envisaged data-rates are up to 1.25 Gbps. 1550 nm is used for data-transmission and 986 nm and 808 nm as beacon wavelengths.
In summer 2005 this terminal shall be flown on a stratospheric balloon and one year later it shall be tested on-board NASA's solar powered stratospheric UAV "Pathfinder-Plus".

Other Projects: Japan's CRL has expressed interest in putting an optical terminal on the ISS for performing LEO-Ground link tests at 1550 nm. Also the Russian Energia company is following a similar approach. The Japanese are also operating an optical ground station for optical communications from LEOs near Tokyo which they intend to use with their OICETS satellite. Optical Ground Stations (OGS) also are operated by ESA (at Izana, Tenerife) and JPL (at Table Mountain, California, capable of fast LEO-tracking). DLR-OCG also follows plans to install a highly agile OGS-telescope at DLR-site Oberpfaffenhofen which shall be capable of tracking LEOs, HAPs, and aircrafts.

4.1.4 General description of the atmospheric optical channel (DLR, Pe. He. Gi. Ho.)

Compared to microwave and RF wave propagation, the transmission of an optical wave through the atmosphere suffers from various deleterious effects. As depicted in figure 38, atmospheric effects can be divided in two main groups: attenuation and index-of-refraction effects. The amount of attenuation for a given scenario can be relatively well predicted (see Section 4.2.1) whereas variations of the refractive index due to turbulence are random in

nature. Refractive-index turbulence makes the atmospheric medium a fading channel. In particular, the effects of turbulence on the laser beam are

- **Wave-front distortion:** the successive phase distortions along the path make the beam less and less coherent. Large tilts of the wave-front are referred to as angle-of-arrival fluctuations.
- **Broadening of the beam:** as a consequence of deviated light, the broadening of the beam increases the beam radius and thus reduces the mean intensity.
- **Redistribution of the intensity within the beam:** the propagation of the distorted wave-front leads to destructive and constructive interferences that break up the beam intensity profile.
- **Wander of the beam centroid:** this is caused by turbulent cells bigger than the beam radius. The beam is then redirected and wanders over a "mean" optical axis.

Another atmospheric effect related to the refractive index is the beam-offset caused by the layering of the atmosphere. This is particularly important for up- and Downlinks at large zenith angles.

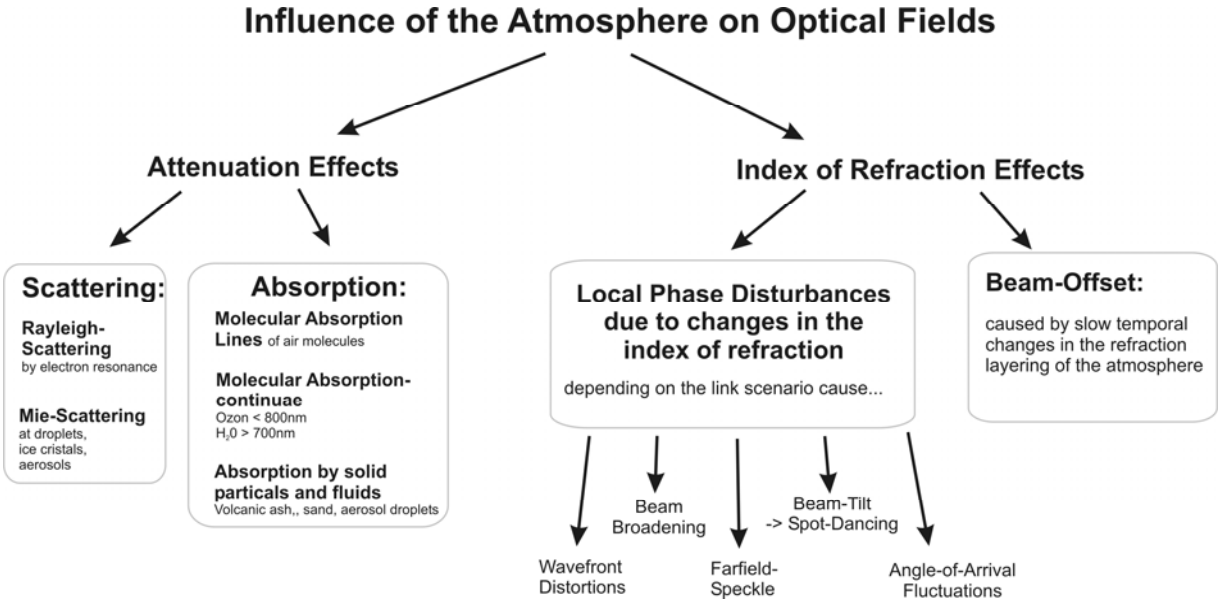

Figure 38: Overview of atmospheric effects

The atmospheric channel is wavelength dependent. In today’s optical communications, one is using laser wavelengths between 750 nm and 1650 nm. This spectrum can be separated into two domains depending on the semiconductors used at the receiver: silicon (Si) photodiodes are sensitive between 500 nm and 1000 nm and cooperating laser diodes (LDs) emit e.g. at 800, 850 or 900 nm. On the other side, Indium-Gallium-Arsenide (InGaAs) or Germanium (Ge) photodiodes show their optimum detection between 1000 nm and 1700 nm. This range matches the LDs for terrestrial fiber communications between 1300 and 1650 nm.
Optical Free Space Communications Terminals can either use incoherent modulation formats like IM/DD (Intensity Modulation / Direct Detection) and PPM (Pulse-Position Modulation), or they can use coherent formats like heterodyne-FSK or homodyne-BPSK. Because the latter are susceptible to wave-front distortions - which are induced by atmospheric index-of-refraction turbulence - coherent modulation formats can only be used in atmospheric and esp. avionic application scenarios with elaborate receiver technologies. As PPM suffers from background noise and is only advantageous in low data rate applications, IM/DD is primarily chosen as modulation format. Though IM/DD also suffers from background noise, its impact

is reduced with increasing data rate because of the improving relation between signal- and background-light.
With Intensity Modulation, the binary data-stream is modulated as on/off pulses on the transmitter laser. The receiver detects this signal by monitoring the photo-current which is produced by the incoming photons on a high-sensitive photo diode. This detection process is not very frequency-selective, meaning that any photons that are in the sensitivity range of the detector-semiconductor (which is typically several hundreds of nanometers) can produce photo-electrons. To reduce background noise and stray-light noise, wavelength filters are introduced into the beam path of the optical terminal. But these filters still have a transmission range of some nanometers, as narrower filters have too low transmission also in their maximum and thus cause too much attenuation.
When adopting terrestrial fiber communications (like the SONET-standard) for FSO, one would transmit the binary data as a continuous uninterrupted stream of bits (synchronous transmission). During experimental work it became clear that the long fades in atmospheric FSO do undermine the applicability of synchronous transmission: These deep fades can cause frame- and even clock-losses which complicate resynchronisation to the data stream extremely. Until complete synchronization on higher protocol-levels is regained, already the next deep fade can interrupt transmission again, causing a very high mean BER.
Instead of synchronous, an asynchronous - packet-oriented - data transmission can be chosen. Each packet has its own clock-synchronization preamble and thus is independent from preceding fades. As long as the packet is shorter in time than the typical fade-duration (DoF), each packet is either completely transmitted or completely lost. Lost packets can be recovered to a certain extent by applying packet-level FEC algorithms. Higher protocol layers have to assure the repeat request for the few packets that could not be recovered.
The channel can be said to be a very slow fading channel. Characterising the optical fading channel with synonyms from the microwave channel behaviour description, the optical channel is also non frequency selective. Furthermore the channel has a very long memory, because the channel state is constant for a very long time. The error probability of each symbol depends on past symbols, because for a very large amount of symbols the expected received power can be assumed as constant. Receiving constant power the signal is only affected by the detector noise.

4.2 Characterization, Simulation and Measurements of the Atmospheric Optical Channel (DLR, UToV, TUG)

To predict the attenuation through the atmosphere, the molecular composition of the atmosphere has to be studied and modelled. In particular, a strong height dependence of the attenuation can be observed.
Regarding the effects of turbulence, several theories have been developed to characterize the distorted beam wave. Depending on the strength of the fluctuations or on the type of propagated wave, these theories are more or less successful. On the other hand, all communication systems are not equally sensitive to wave distortions. For IM/DD systems, the signal is carried solely by the optical power and thus phase distortions are of less importance. For coherent systems, however, phase distortions reduce severely the system performance. As an alternative to classical theory, propagation through turbulence can be assessed by means of numerical simulations. These provide valid results over regimes of both weak and strong fluctuations. The distorted optical fields resulting from simulations can be further transformed to reproduce the receiver processing.
Once the deleterious effects of atmospheric channel are understood and characterized, it is possible to elaborate mitigation techniques that improve the level of the received signal.

4.2.1 Attenuation in the Earth’s Atmosphere (DLR, Pe. He. Gi. Ho.)

The following figure 39 roughly depicts the structure of the lower earth atmosphere. The tropopause is the part between troposphere and stratosphere. Its altitude varies with the geographic latitude between approx. 6 km and lower at the poles and up to 16 km and higher around the equator.

Cloud-top layers are limited to the height of the tropopause, with strongly decreasing abundance over 4 km altitude. Also the optical density of clouds decreases for clouds higher than 5 km (ice-clouds). This cloud-altitude profile strongly increases the availability of aeronautical optical links with both communication partners above 4km altitude.

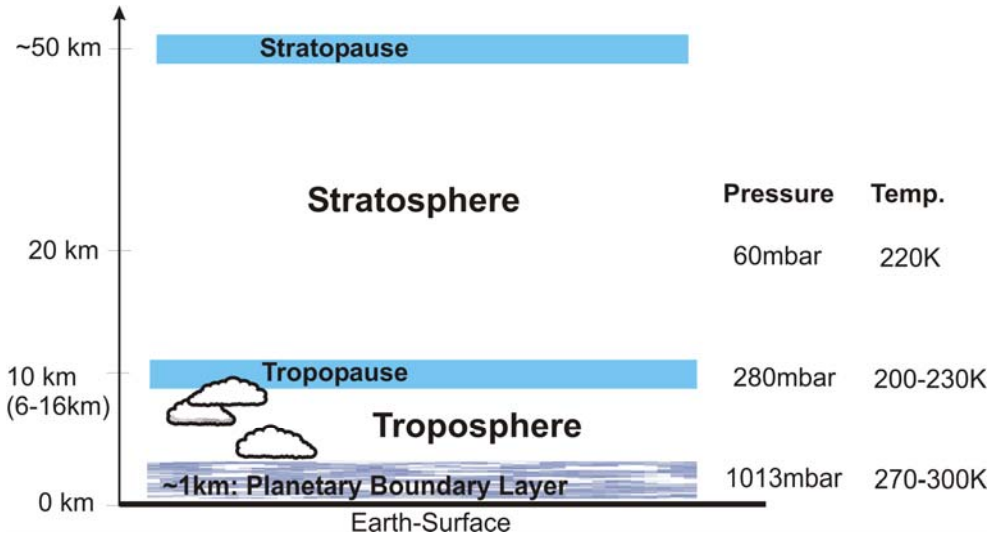

Figure 39: Structure of Earth's atmosphere

4.2.1.1 Clear-Sky Attenuation

As mentioned in Section 4.1.4, atmospheric attenuation can be distinguished in molecular absorption, Rayleigh-scattering, and aerosol-scattering. The free-space attenuation caused by beam broadening is not regarded in the scope of this section. Molecular absorption is an effect of electron- and nucleus-resonance of atmospheric molecules, Rayleigh-scattering is caused by the atmospheric molecules acting as dipole-antennas, and aerosol-scattering is caused by droplets and particles that are larger than the wavelength that is influenced. Other distinguished attenuation effects are the ozone-continuum and the water-vapour-continuum.

The aerosol-scattering above 10 km is governed by the volcanic activity level of the earth's atmosphere, as volcanoes can inject dust particles into altitudes of about 20 km, where they can stay for several weeks. In the here applied atmospheric model, the volcanic activity state is distinguished in four levels: *background* (1), *moderate* (2), *high* (3), and *extreme* (4). Level 4 occurs extremely seldom (a few times each century), thus level 1 can be regarded as best-case, 2 as typical, and level 3 as worst case.

The amount of attenuation per path kilometre is quantified with the absorption coefficient α to the basis e. The fraction p of directed optical power that is transmitted over path-length d with constant attenuation coefficient α is calculated by:

$$p = e^{-d \cdot \alpha} \tag{22}$$

When α varies over path coordinate z the path-integral has to be used:

$$p = e^{-\int_0^d \alpha(z)\, dz} \tag{23}$$

Different atmospheric models take into account the geographic latitude and the season, (e.g. "mid-latitude winter", "tropical" or "polar"). To calculate values for atmospheric attenuation, here the atmospheric constituents data base "mid-latitude summer" according to [27] is used. Clear-skies (no clouds) are presumed in all cases. The next figure (40) compares the wavelength-dependence of the three major optical attenuation effects inside the atmosphere.

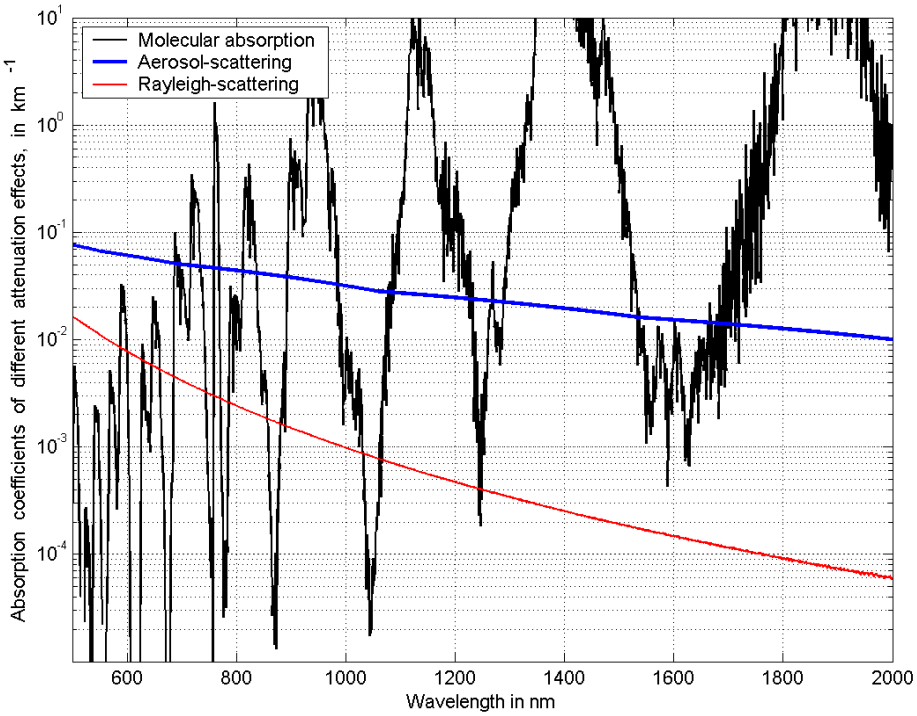

Figure 40: Comparison of the 3 major clear-sky atmospheric attenuation effects, at sea level

Molecular absorption lines: While Rayleigh- and aerosol-scattering show only weak wavelength dependence, molecular absorption develops very narrow but strong lines. Figure 41 shows exemplarily the thin but strong molecular absorption lines caused by water vapour around 1300 nm.

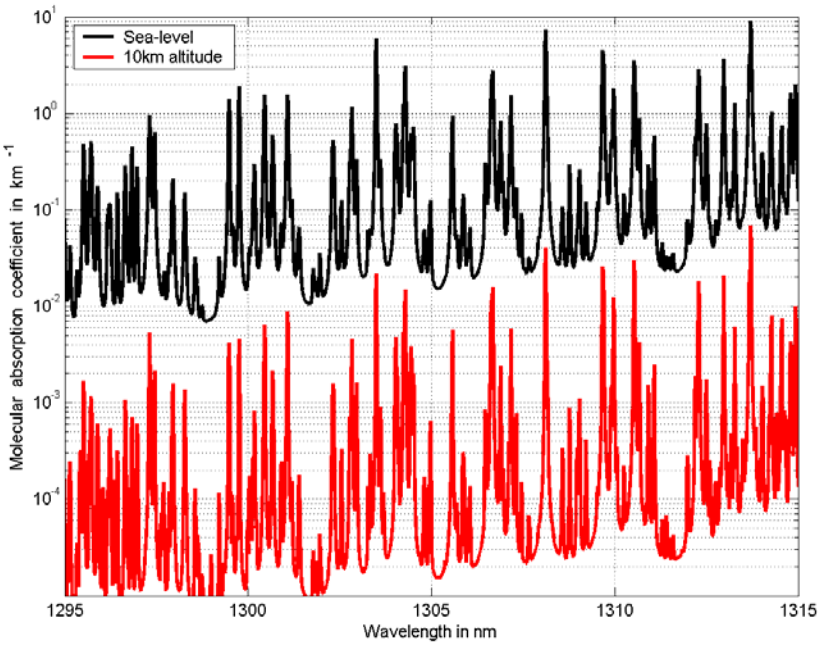

Figure 41: Molecular absorption lines caused by water vapour around 1300 nm at sea level (upper line) and in 10 km altitude

Total attenuation coefficient over wavelength in certain altitudes: By summing up the separate atmospheric attenuation coefficients, one can calculate the total absorption coefficient for a certain wavelength and altitude, as shown in the following figure 42.

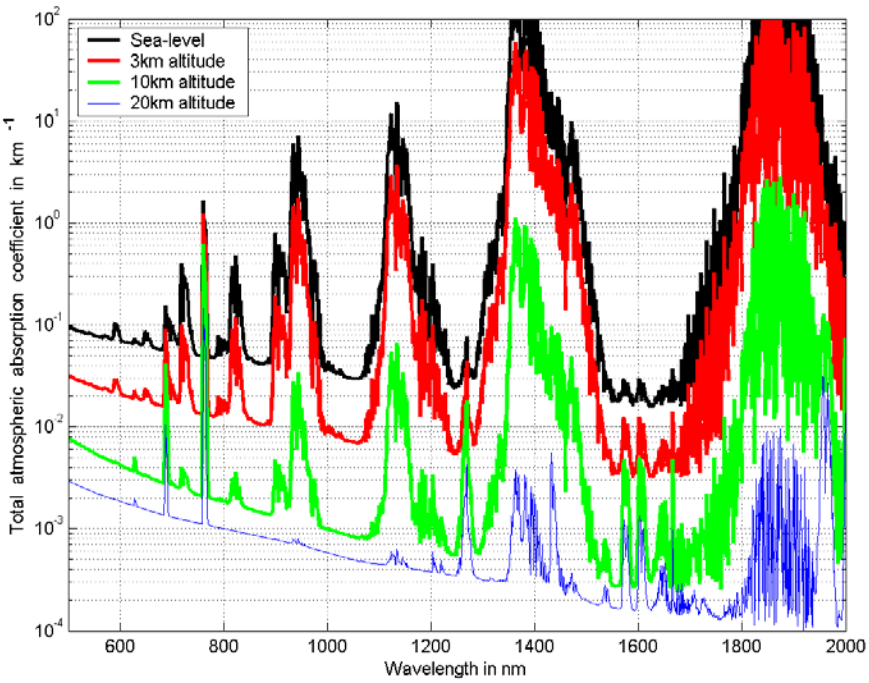

Figure 42: Total atmospheric attenuation coefficient over wavelength (500 nm to 2 µm) in four different altitudes (sea level, 3 km, 10 km, 20 km) for volcanic activity level 2 (values averaged over 1 nm)

Attenuation drops with altitude due to reduced air-density. Also, the change of atmospheric constituents (like water-vapour, ozone) with altitude leads to relative changes in the profile. It is obvious from figure 42 that certain wavelengths with large total attenuation coefficients (like around 970 nm or 1400 nm) are not suitable for signal transmission through the atmosphere. As a very rough limit for typical atmospheric applications (like near-ground optical communications over several km), the coefficient must not exceed 0.1.

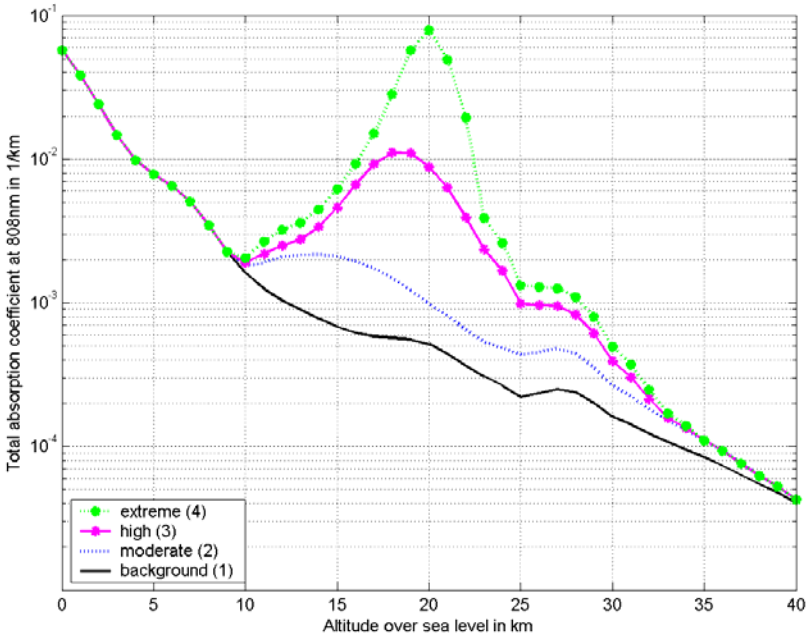

Figure 43: Total atmospheric attenuation coefficient over altitude for 808 nm

Total attenuation coefficient over altitude for three typical laser wavelengths: The plots (figure 43, 44, 45) show the total attenuation height profiles for 808 nm, 1064 nm and 1550 nm for the four different volcanic activity levels. The accumulation of aerosols in 20 km is clearly visible.

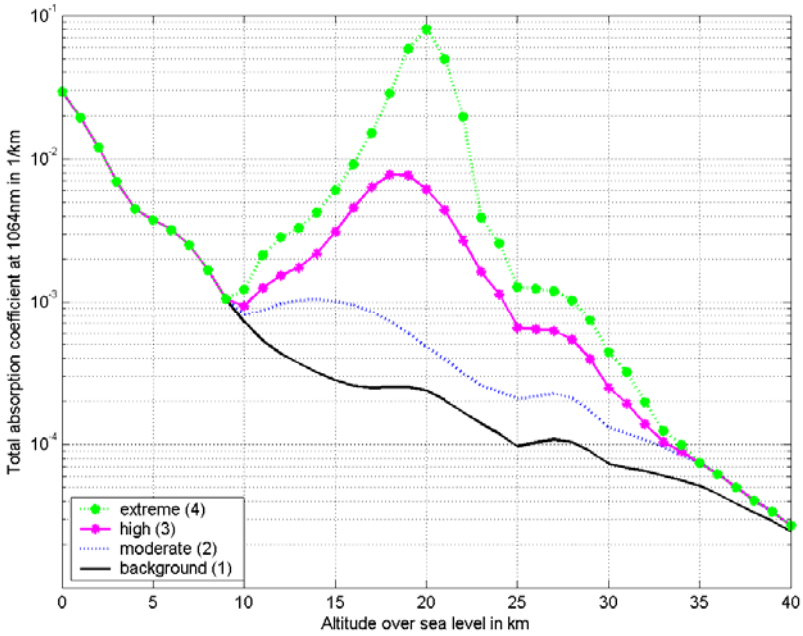

Figure 44: Total atmospheric attenuation coefficient over altitude for 1064 nm

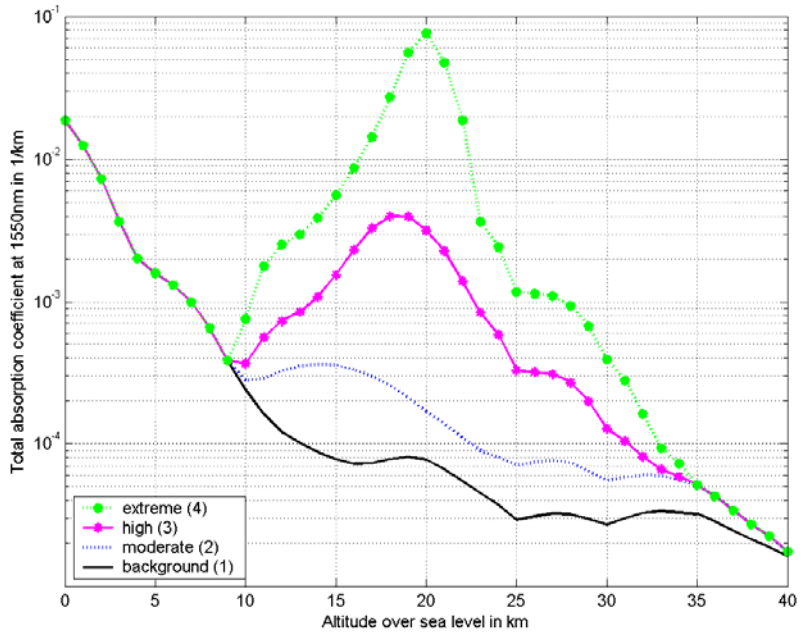

Figure 45: Total atmospheric attenuation coefficient over altitude for 1550 nm

Path attenuation calculations: To estimate the total path attenuation for a certain link scenario, the integrated atmospheric attenuation can be calculated by integrating over distance. Basic parameters for these calculations are wavelength (λ), altitude of partner 1

(A1), altitude of partner 2 (A2), distance between the partners, and volcanic activity level. For downlinks from outside the atmosphere (or uplinks), instead of A2 the link's elevation angle has to be considered. Earth's curvature has to be regarded for long horizontal links.

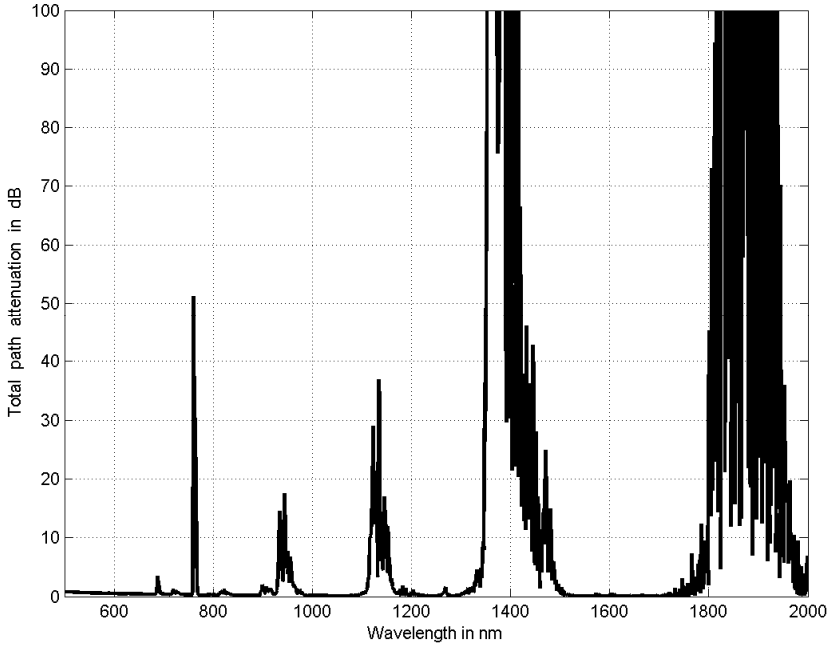

Figure 46: Total atmospheric path attenuation in dB from 500 nm to 2 µm for an optical downlink (or uplink) under 45° elevation angle from outside the atmosphere to a ground station situated in 2 km altitude. Impact of volcanic activity level negligible

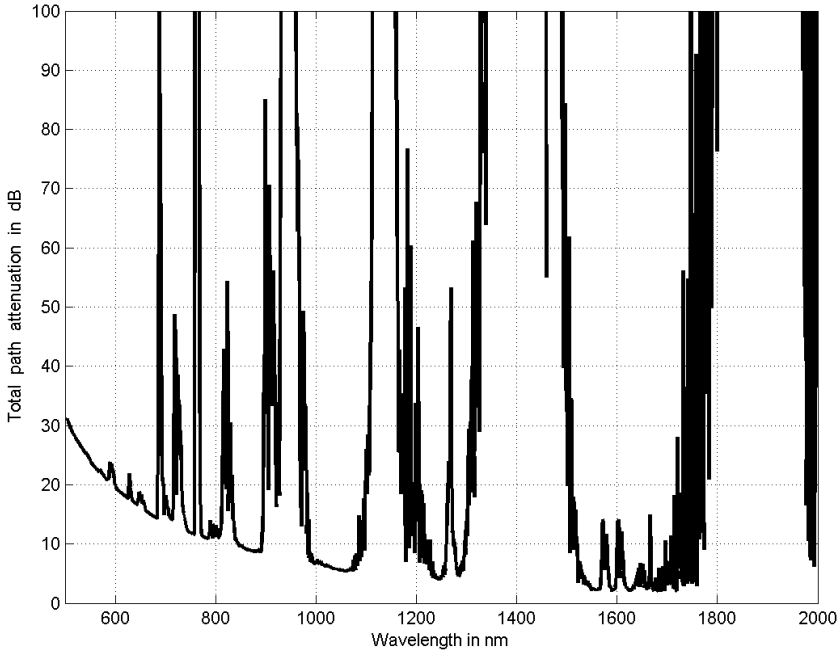

Figure 47: Total atmospheric path attenuation in dB from 500 nm to 2 µm for a link between two aircraft, one in 6 km and the other in 10 km altitude and 400 km apart (not impacted by volcanic activity because the path lays below 10 km altitude

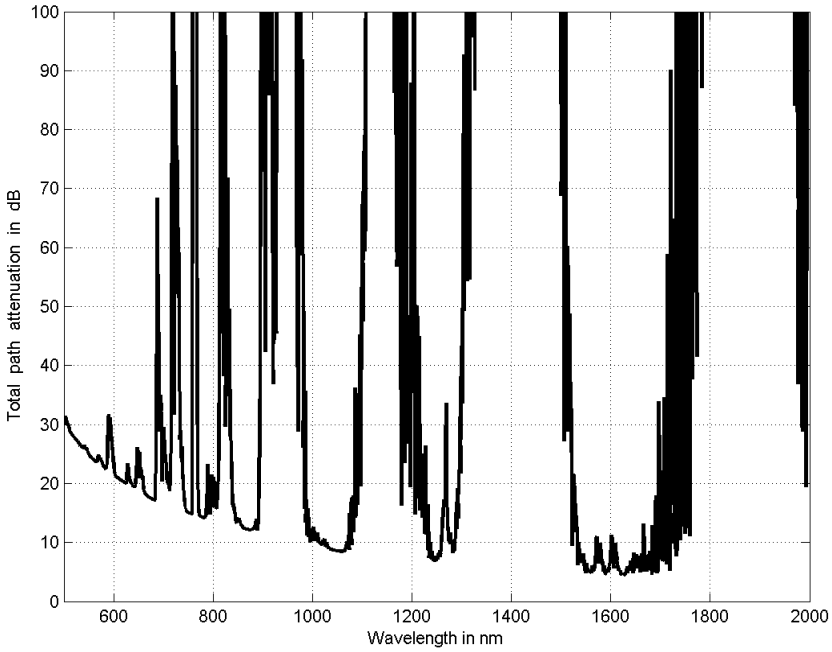

Figure 48: Total atmospheric path attenuation in dB from 500 nm to 2 µm for a horizontal path with both partners in 2 km altitude and 140 km distance (not impacted by volcanic activity because the whole path lies below 10 km altitude

In figure 46 to 48 we see that the optical path attenuation can reach extremely high values far above 100 dB in typical (future) communications links, making accurate wavelength selection essential.

Summary - Atmospheric Attenuation: The foregoing investigations serve for proper selection of laser sources for atmospheric free-space transmission. Depending on the kind of path, small shifts in wavelength can produce several dB of differences in attenuation. The well introduced 1064 nm and 808 nm show acceptable attenuation, while 1300 nm or 850 nm are less preferable. Between 500 nm and 2 µm, wavelengths around 1550 nm are the primary choice in terms of atmospheric attenuation. Of course, other parameters like receiver sensitivity also have to be regarded. The volcanic aerosol concentration in the lower stratosphere has to be regarded especially with long horizontal links inside the stratosphere like e.g. between high altitude platforms positioned between 18 and 25 km altitude.

4.2.1.2 Non-Clear Sky Atmosphere - Effects of Fog, Dust and Clouds

The path attenuation due to clouds, fog and dust (also called hydrometer) is expected to be great many greater than the clear sky attenuation. Clouds occur in altitudes up to *13 km* in the temperate latitudes. The droplet or ice particle sizes rang is from *5* up to *1000 µm* and the size distribution can be described using for example the *Levin* or *Khgian-Mazin* distribution [36, 47]. Dust and fog consists of water droplets with a lesser particle radius in the region of *0.1 µm*. Optical HAP up- and downlinks have to cross the whole cloud layer and near the ground, in the boundary layer, the link is additionally affected by fog and dust. Also the behavior of hydrometer is significant for the optical free space communication. Describing the behavior of spherical droplets influenced by the complex index of refraction could be done using the Mie-theory. This theory fits quite well for water droplets in warm clouds and fog but for ice clouds the assumption of spherical particles is not really true. As a result of the manifoldness of ice crystals and the lack of information about the size distribution for special

ice particles it is very difficult to find exact analytical descriptions of this problem. Therefore the Mie-theory is used to estimate the effects of ice particles at least.
Mie-theory uses efficiencies Q_i [unitless] which characterize the interaction of radiation with a scattering sphere particle. Q_i are cross sections normalized to the particle cross section. E.g. the scattering cross section Q_s can be greater than the shadow (using a geometrical optics view) because of diffraction. With the particle size distribution function *f(r)* and the extinction efficiency Q_e the optical thickness for hydrometers is generally given by:

$$\tau = \int_0^d \int_0^\infty f(r) \cdot Q_e(x,n) \cdot \pi \cdot r^2 \, dr \, dz \tag{24}$$

The path through the scattering medium (width *d*) is described by the integral over *z*. The extinction efficiency Q_e is a function of the complex refractive index *n* of the scattering particle and the Mie-size-parameter *x* which can be expressed as function of wavelength λ and particle radius *r*:

$$x = \frac{2 \cdot \pi \cdot r}{\lambda} \tag{25}$$

n is different for water in warm clouds and ice. The imaginary part of *n* multiplied by $4 \cdot \pi / \lambda$ is equal to the absorption coefficient α. The extinction efficiency Q_e can be split into the scattering efficiency Q_s and the absorption efficiency Q_a,. Q_e describes the attenuation due to scattering into directions which are not the direction of the incident ray and due to absorption effects.

$$Q_e = Q_s + Q_a \tag{26}$$

For typical particle sizes to be found in clouds of *4* to *40 μm* (mean particle radius <*r*> of a warm cloud: *10 μm*; ice cloud: *30 μm*) the absorption can be neglected compared to the scattering, especially for shorter wavelengths. A perspicuous reason for negligible absorption at shorter wavelengths is the almost real refractive index of water and ice. Effects in dust and fog particles (*0.1* to *1 μm*) are more dominated by absorption (see figure 49). Also in fog and dust longer wavelength are favorable due to less extinction. For clouds no significant wavelength dependence is recognizable.

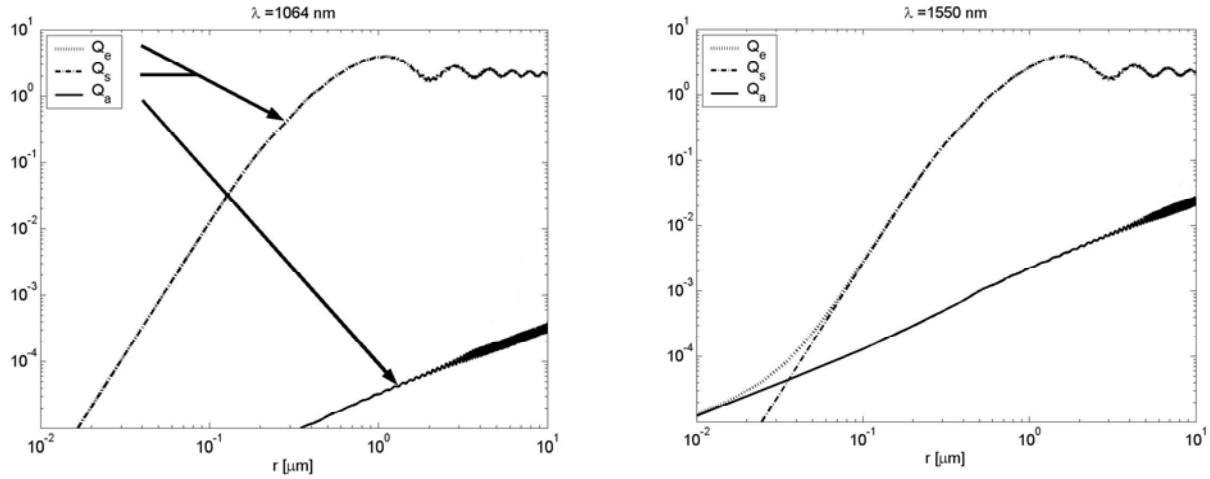

Figure 49: Scattering and absorption efficiencies vs. particle radius for a wavelength of 1064 nm (left) and 1550 nm (right), [34]

Displaying the extinction efficiency for different wavelengths over the particle size shows that for typical particle sizes for clouds *(>4 μm)* the efficiency converges to the constant value of *2* (see figure 49).

With this and the use of the droplet concentration N, the formula for the optical thickness can be simplified to

$$\tau \approx 2\pi N \langle r \rangle^2 d \,. \tag{27}$$

The standardizes *C1 cumulus cloud* model with $N=100\ cm^{-3}$, $\langle r \rangle = 4\ \mu m$ [36] and a typical cumulus cloud depth of about *1000 m* leads to an optical depth of $\tau=10$.

The scalar phase function $P(\theta)$ of a particle gives the energy scattered per unit angle at the angle θ from the direction of incidence divided by the total scattered energy. It is apparent from figure 50 that for larger Mie-parameter (large particles like in clouds, short wavelength) the phase function is stronger in the forward direction.

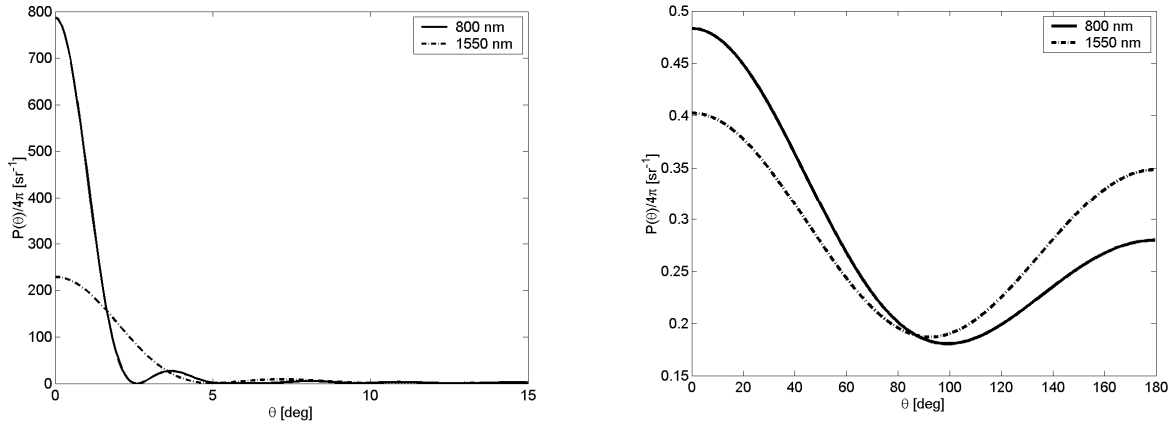

Figure 50: Phase function for r=10 μm water particles vs. scatter angle (left plot, in the not displayed region from θ=15° to 180° P(θ) is already zero); right plot: phase function for dust particles with r=0.1 μm [34]

4.2.2 Effects of Turbulence (DLR, Pe. He. Gi. Ho.)

Optical turbulence in the atmosphere affects both the phase and the intensity of the optical field. Intensity fluctuations represent the scintillation phenomenon. The scintillation of a beam can be separated in two effects: the beam wander and the redistribution of the intensity within the beam

4.2.2.1 Kolmogorov Therory of Turbulence

When the flow of a viscous fluid exceeds a critical Reynolds number, the flow changes from laminar to a more chaotic state called turbulence. In the atmosphere, air turbulence is created by the mixing of warm and cool air caused either by wind shear or by convection. These two phenomena produce eddies of large scales that break up into smaller eddies to form a continuum of eddy sizes. Viewing eddies as cells, figure 51 illustrates the process of energy transfer. The scales of those turbulence eddies range from a lower limit l_0, called inner-scale, to an upper limit L_0, called outer-scale. Eddy sizes lying between those bounds represent the so-called inertial range. Turbulent eddies smaller than the inner scale l_0 belong to the viscous dissipation range, they disappear as the remaining energy in the fluid motion is dissipated as heat.

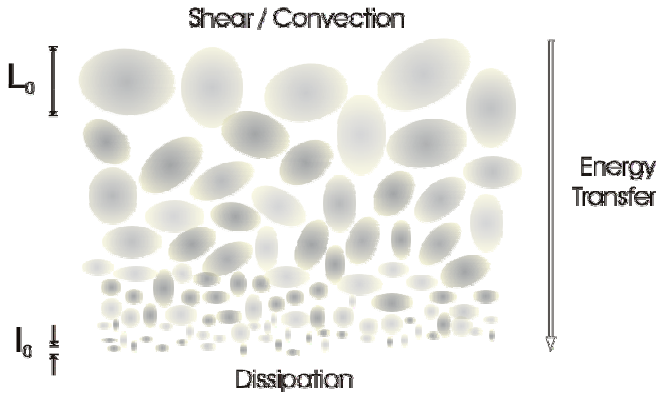

Figure 51: Energy transfer cascade in Kolmogorov theory of turbulence.

The index of refraction n in the atmosphere can be expressed for optical and IR wavelengths in the form [49].

$$\begin{aligned} n(\mathbf{s}) &= 1 + 77.6\times10^{-6}\left(1 + 7.52\times10^{-3}\lambda^{-2}\right)\frac{P_{atm}(\mathbf{s})}{T(\mathbf{s})} \\ &= 1 + 78\times10^{-6}\frac{P_{atm}(\mathbf{s})}{T(\mathbf{s})} \end{aligned} \tag{28}$$

where **s** is a 3-dimensional spatial vector, λ is the wavelength in μm, P_{atm} is the atmospheric pressure in millibars, and T is the temperature in kelvins. The wavelength dependence is small for NIR frequencies and λ was set to 1 in the second expression of Eq. 28. Since pressure fluctuations are normally negligible, we see that the index of refraction follow the fluctuations of the air temperature.
Kolmogorov's theory gives us the 3-dimensional power spectral density $\Phi_n(\kappa)$ for the refractive-index. This takes the following form

$$\Phi_n(\kappa) = 0.033 C_n^2 \kappa^{-11/3} \qquad 1/L_0 < \kappa < 1/l_0 . \tag{29}$$

where the scaling factor C_n^2 is called the refractive-index structure constant. Although valid only in the inertial range, the Kolmogorov spectrum is often extended over all wave numbers by assuming $l_0 = 0$, $L_0 = \infty$. Other spectrum models have been proposed for calculations when inner and outer scales cannot be ignored [48].

4.2.2.2 Theory of Propagation through Random Media

Many theoretical approaches have been tried to characterize the optical wave distorted by turbulence. The most successful approach is the Rytov theory which is limited to the regime of weak fluctuations. Other approaches are the *extended Huygens-Fresnel principle*, the *parabolic equation method* or the *Feymann path integral*. Analytical results from the respective approaches on the statistical wave parameters can be found in [45, 38, 49].

4.2.2.3 Simulations of Propagation through Turbulence

In simulations of optical propagation through turbulent atmosphere, we use the same simplifications to Maxwell's equations as in the classical treatment of turbulent propagation. Absence of depolarization effects allows the consideration of a scalar optical field, which leads to a stochastic Helmholtz equation. Additionally, small-angle scattering yields the parabolic equation:

$$\partial_z u = \frac{j}{2k}\left(\partial_x{}^2 + \partial_y{}^2\right)u + jkn_1 u . \tag{30}$$

The complex quantity u denotes the slowly varying envelope of the scalar electromagnetic field in the (x,y,z) space; k is the wave number and $n_1 = n - \langle n \rangle$ is the local deviation of the refractive index from its ensemble average. Without the second term, which models stochastic phase perturbations due to the atmosphere, Eq. 30 is the parabolic wave equation.

The *split-step* approach to numerically simulating atmospheric propagation amounts to partitioning the propagation distance into "reasonably sized" sub-distances $\Delta z_i = z_i - z_{i-1}$, $i = 1 \ldots N$, $z_0 = 0$ and to alternately simulate the effects of both terms in (30) individually for each Δz_i. "Reasonably sized" here means that Δz_i is, on the one hand, small enough so that the "split-step approximation"

$$u(x,y,z_i) \approx \exp\left(\frac{\Delta z_i}{2}\frac{j}{2k}\left(\partial_x{}^2 + \partial_y{}^2\right)\right)\exp\left(\int_{z_{i-1}}^{z_{i-1}+\Delta z_i} jkn_1 dz\right)\exp\left(\frac{\Delta z_i}{2}\frac{j}{2k}\left(\partial_x{}^2 + \partial_y{}^2\right)\right)u(x,y,z_{i-1}) \quad (31)$$

of the formal solution to (31) is justified and, on the other hand, large enough so that the realizations of the stochastic phase perturbations, or phase screen,

$$\phi_i = \int_{z_{i-1}}^{z_i} k n_1 dz \quad (32)$$

can be generated independently for each Δz_i. The phase screens ϕ_i thus take the form of 2-dimensional random fields. Figure 52 illustrates the partitioning of the turbulent volume and the modeling of each turbulent section by thin phase screens. Note that the characteristics of the phase screens are given by the refractive-index power spectrum, we further assume that the phase perturbations obey Gaussian statistics.

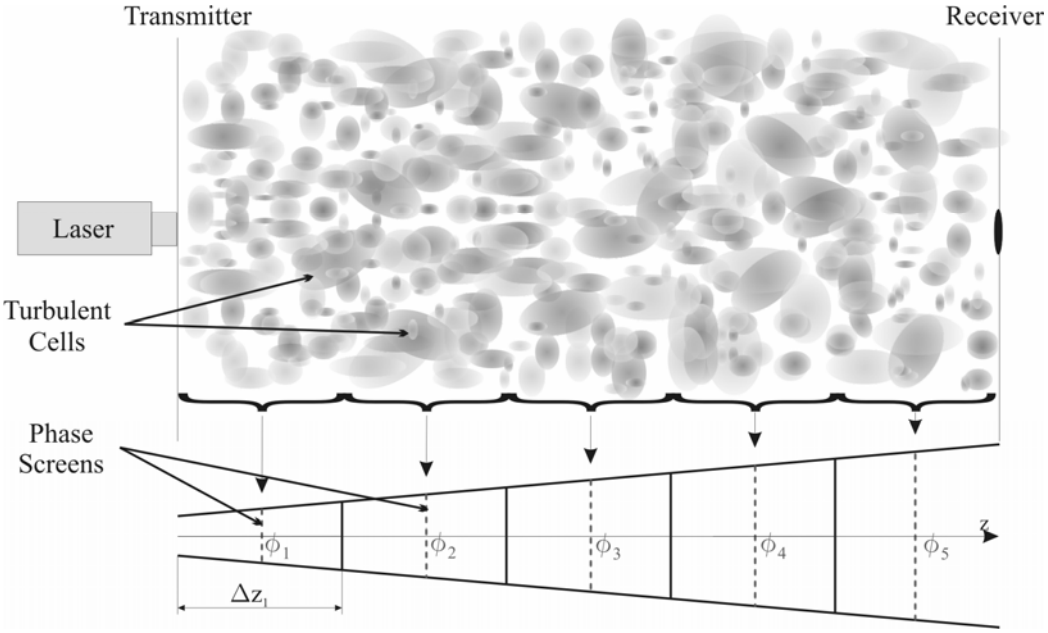

Figure 52: Partitioning of the turbulent volume into thin phase screen that modulate the propagating wave

The complex field $u(x,y,z_i)$ is represented by a finite number of sample values as obtained by a regular sampling in X- and Y-dimension, that is, by a grid of sample values $u(l\Delta x, m\Delta x, z_i)$, $l = 1 \ldots M$, $m = 1 \ldots M$. For z_0 the grid simply bears the sampled transmitter beam profile; the values at z_i, $i \geq 1$, are subsequently obtained from the values at z_{i-1}. The layout of the propagation algorithm is sketched in figure 53. This algorithm has been thoroughly described in the literature [35, 39, 40].

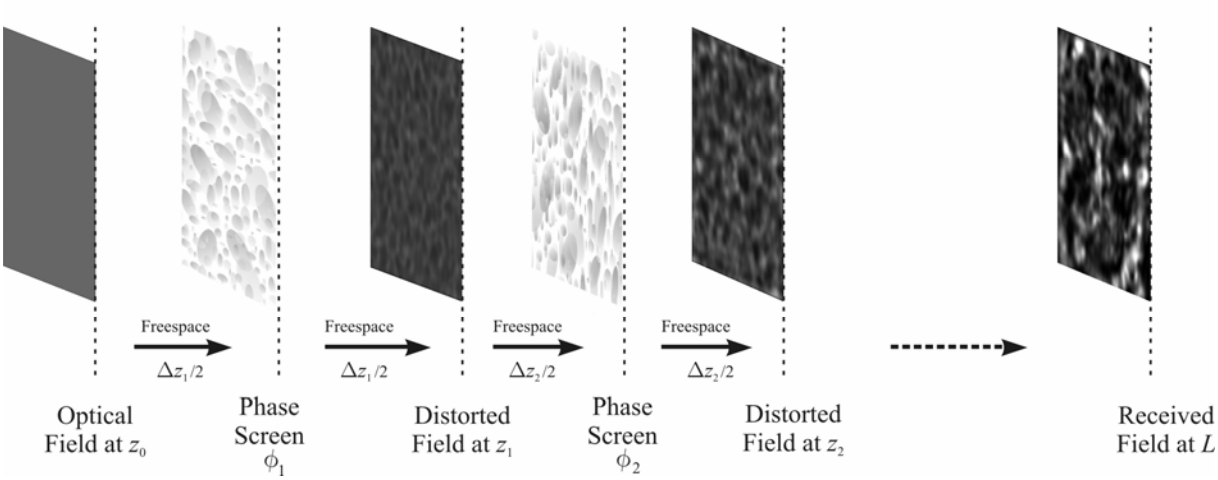

Figure 53: Layout of the propagation algorithm. Here the propagation of a plane wave is illustrated and the transverse intensity is shown at the different stages of the propagation

If computational resources were unlimited, one would always choose a grid size large enough to cover the entire beam profile with a spatial sampling rate appropriate to accurately resolve all small-scale modulations of the field. In long-range beam propagation scenarios, however, this turns out to be infeasible for the beam diameter becomes very large due to diffraction. One solution which has already been proposed by Rubio et al. [42], is to sacrifice coverage of the full beam cross section in favor of maintaining a sampling interval that resolves atmospherically induced modulations of the field on all scales equal and below the receiver aperture diameter. The order of magnitude of an appropriate sampling interval must not become larger than l_0, the lower bound of the inertial sub-range of turbulence. We maintained $\Delta x \leq l_0/3$ in our simulations.

In order to simulate beam propagation effectively, the sampling interval gets adapted according to the diffractive beam spread. Like Rubio et al., we resample the field at those propagation distances z_i where the next propagation step would render the sampling rate insufficient without re-sampling (see figure 54). The grid size stays the same, so the extent of the field represented by the grid gets reduced in a re-sampling step (from some value X_i' to X_i). Since we use an FFT-based propagation algorithm entailing periodic boundary conditions, we finally multiply the re-sampled field with a super-Gaussian damping function to avoid spurious “self-interference”[1] in subsequent propagation steps.

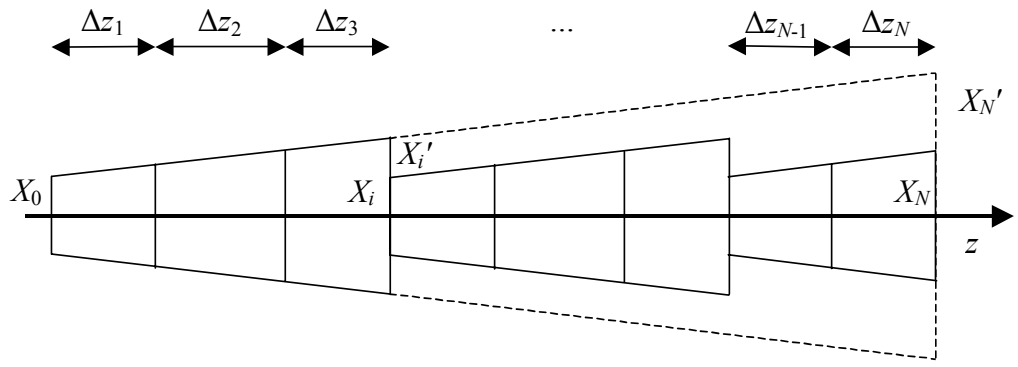

Figure 54: Step-wise simulation with occasional re-sampling of the field

[1] Other authors call the effect “aliasing”; it actually is the analog to aliasing in the spatial domain.

4.2.2.4 Loss due to scintillation

Scintillation can have a severe impact on the communication performance of IM/DD systems. The performance evaluation strongly depends on the receiver model and on its various noise sources. If the receiver had an infinite sensitivity and no noise sources, then scintillation, no matter how strong it is, would not degrade the system performance since it would always be possible to find a detection threshold that keeps the bit error rate (BER) below the maximum authorized BER. Thus, the evaluation of the scintillation loss depends on the receiver and on the photodetection characteristics. David proposed in [26] a procedure to determine the required additional Tx-power to reach a given BER for an IM/DD system.

4.2.3 Mitigation of Turbulence-Induced Fades (DLR, Pe. He. Gi. Ho.)

Turbulence induced fades cause performance degradation in the optical links and in this section we discuss the possible mitigation techniques for such fades.

4.2.3.1 The Concept of Diversity

The idea behind diversity is to dispose of several signals at the receiver that contain the same information and to process these possibly distorted signals in order to recover the correct information with certitude. For the mitigation of turbulent atmosphere, the mostly used techniques make use of spatial diversity (referred to as “small-scale”). Some other diversity techniques can also improve the link quality in some particular cases. For the mitigation of cloud coverage, we resort to spatial diversity on a “large-scale”.
The processing of the different signals carrying the same information usually follows one of the three following techniques:

1. Equal Gain Combining (EGC): Summing up of all signals
2. Maximum-Likelihood Selection (MLS): Selection of only the strongest signal
3. Maximum Ratio Combining (MRC): Proportional scaling of all signals according to the ratio compared with the largest signal

4.2.3.2 Small-Scale Spatial Diversity

The idea of small-scale spatial diversity is to reduce the effects of turbulence by taking advantage of the finite size of the turbulence cells or the finite size of the intensity speckles at the receiver. Although the positions of the transmitter and receiver do not have to be changed, diversity is reached by extending the size (or the structure) of the terminals.

Tx Spatial Diversity: Tx-Spatial Diversity is achieved using several transmitters laterally displaced. All transmitters emit their beams towards the receiver. The respective beams go through different turbulent volumes and thus are affected differently by distortions. By averageing all the signals transmitted by each beam (EGC approach), the receiver reduces the fades that would occur with a single beam.

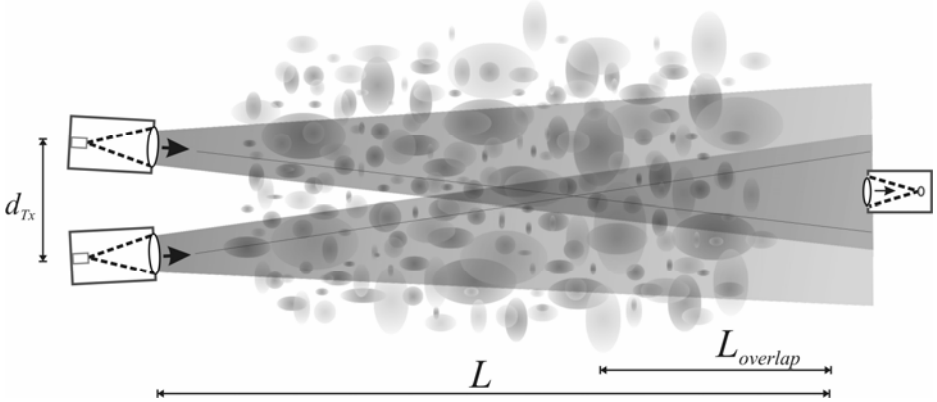

Figure 55: Use of two transmitters to reduce the fluctuations of the received power

As depicted in figure 55, the distance d_{Tx} separating two transmitters should be large enough to keep the overlap distance $L_{overlap}$ small. For most scenarios, a separation d_{Tx} less than one meter is sufficient to significantly reduce the fluctuations.
In the *Wallberg-Experiment* (part of the project *FASOLT*) reported in [30], two transmitters have been used. The distribution of the measured Rx-power is shown in figure 56 when one and two transmitters are switched on, both powers have been scaled to the same mean value to avoid the influence of doubled Tx-power in the distribution functions.

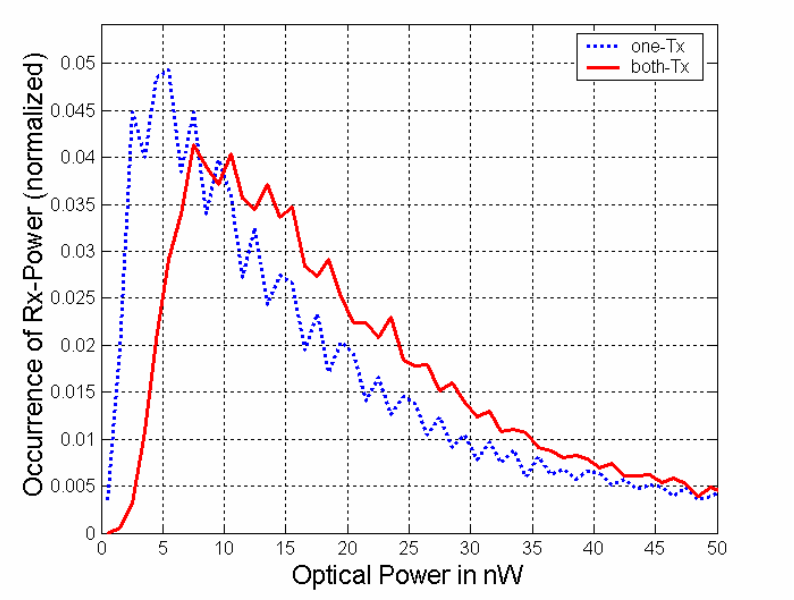

Figure 56: Distribution of the Rx-Power when either one or two Transmitters are used

Rx-Aperture Averaging: Scintillation is characterized by the presence of intensity speckle patterns in the propagated beam. If the receiver has a collecting aperture that is large enough, it can average several intensity speckles over its aperture (EGC approach) and, in this way, reduce the fluctuations of the received signal (in addition to collecting more mean power).
In figure 57, one can see the image of a 20 cm telescope pupil irradiated by a laser beam. This pupil was recorded at DLR Oberpfaffenhofen during a hot summer day where the 810 nm laser and the Rx-telescope were 400 m apart, each being located on a building at about 15 m altitude., the correlation length was found to be about 2 cm which roughly corresponds to the first Fresnel zone $\sqrt{L/k}$.

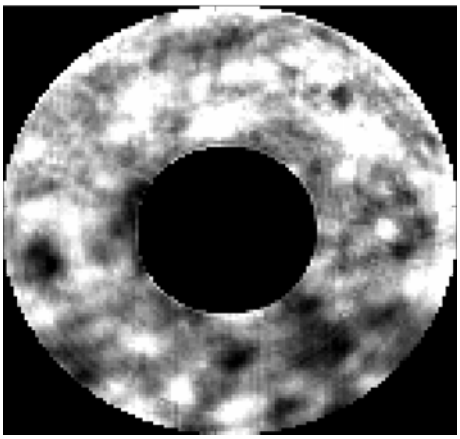

Figure 57: Measured pupil image of a 20 cm telescope. L = 400 m, $C_n^2 = 10^{-13}$ $m^{-2/3}$. A single mode beam was directed horizontally at 15 m above ground

Figure 58 shows plots of the probability density function (PDF) of the collected power (normalized to its mean) for several Rx-aperture diameters. These PDFs were estimated from field measurements at DLR Oberpfaffenhofen [41]. We can see that the variance decreases as the diameter of the Rx-aperture is increased.

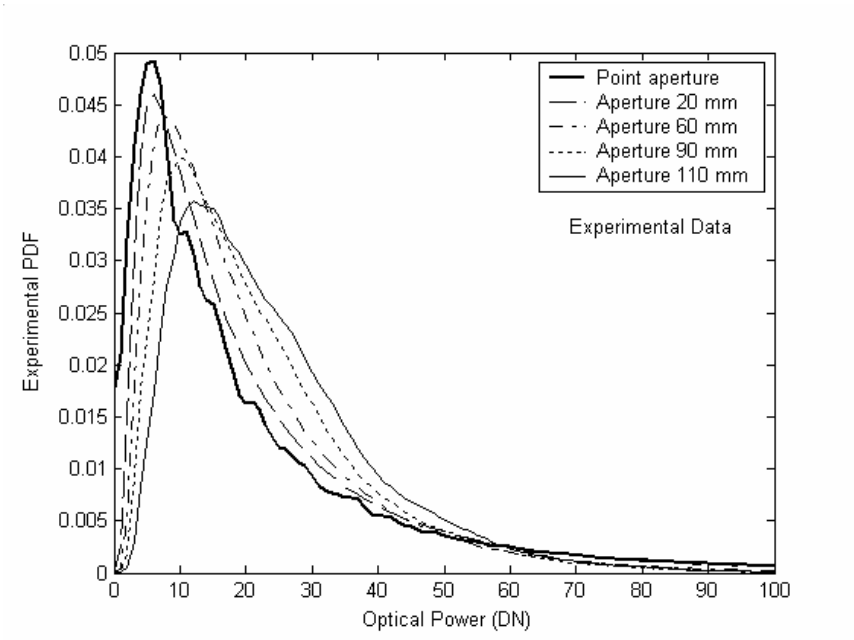

Figure 58: PDFs of the Rx optical power

Focal Array Receiver: Rather than trying to correct the received optical field (as in *adaptive-optics* known from visual astronomy), the idea behind a focal array receiver (FAR) is to detect the focal speckle pattern with an array of reception sensors and then to optimally recombine these signals [32]. The size of the array corresponds to the diameter of the speckle pattern. The spatial extent of the speckle pattern in the focal plane grows with the ratio of receiver aperture diameter to coherence-length of the optical field.
The total short-term SNR is optimized through sensors assessing the different signal strengths. Thus, a focal array receiver is an intelligent focal diversity receiver. Though the concept is also applicable to direct detection receivers, it offers most benefit with coherent detection.

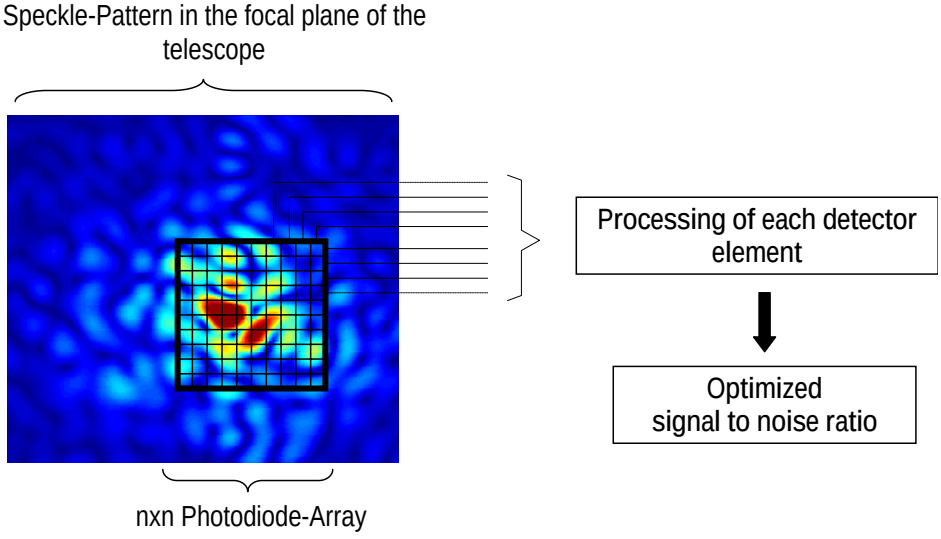

Figure 59: The focal array receiver (FAR) concept

4.2.3.3 Other Diversity Techniques

Among other diversity techniques, we describe wavelength-diversity and time-delay diversity.

Wavelength diversity is based on the fact that different wavelengths suffer from different perturbations. By separating the different wavelengths at the receiver, the signal carried by the different wavelengths can be recovered by means of a soft decision process.

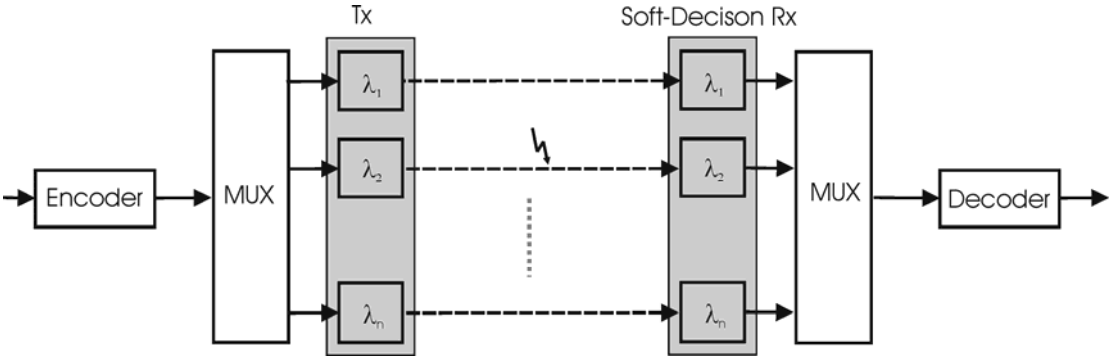

Figure 60: Wavelength diversity and multiplexing

Time-delay diversity consists in resending the information a short time later, hoping the signal will not be affected twice by a fade. To improve the communication performance while using this diversity technique, one should use two different channels: one for the first transmitted signal and another for the repeated signal. This enables the receiver to separate the two signals and, in this way, a continuous data transmission based on MLS-diversity can be achieved.

4.2.3.4 Packet-Layer Forward Error Correction (FEC)

The atmospheric optical channel can be said to be a very slow fading channel [36]. Characterising the optical fading channel with terms from the microwave channel behavior description, the optical channel is also non frequency selective. Furthermore, the channel has a very long memory. This is because the channel state is constant during the transmission of a very large amount of symbols. Receiving constant power, the signal is only affected by the receiver noise.

When adopting terrestrial fiber communications (like the SONET-standard) for FSO, one would transmit the binary data as a continuous uninterrupted stream of bits (synchronous transmission). Slow fading in an FSO atmospheric channel reduces the performance of a synchronous transmission scheme, especially because of losses of synchronization during data transmission. During a fade, a great quantity of data is lost and cannot be recovered by an FEC implemented in the physical-layer transmission [33]. Obviously, in that case, the communication scheme will not work, because at least the decoder and the interleaving devices can not work without a continuously locked synchronization.

Instead of having a synchronous transmission, an asynchronous - packet-oriented - data transmission can be chosen. Each packet has its own clock-synchronization preamble and thus synchronization is independent of preceding fades. Usually, in an asynchronous packet transmission scheme, a cyclic redundancy check (CRC) is used to determine packets with errors. So if a fade occurs when a packet is transmitted, the errors introduced by the fade are detected. The simplest way to handle with these fault packets is to erase them (that’s what Ethernet does, for example).

As fade duration in an atmospheric optical free-space channel is typically much longer than possible physical-layer (bit-wise) code-words, it is suitable to use packet-layer FEC. Packet-

layer coding works in principle the same way as physical-layer coding: Code-words consist of symbols. The difference is that, for physical-layer coding, symbols are typically bits whereas for packet-layer coding whole packets are seen as symbols. Considering for example an Ethernet packet with a length of 1500 bytes as a symbol, the transmission time of a symbol would be 12 μs assuming a 1 Gbit/s channel data rate, and 1.2 ms for 10 Mbit/s. So these time constants, especially for lower data rates, are in the same order of magnitude as atmospheric turbulence (1 ... 10 ms) fluctuations.
The principal steps using packet-layer coding are shown in the following figure. Usually packet coding is used for file-based transmission. So a serial data stream is first buffered and fragmented into files. These files are then divided into packets. The decoder forms code-words by adding parity (redundancy) packets to the source packets. As a next step an inter-leaver could be used to scramble the packet-stream (code-words consisting of source and parity packets). After interleaving, each packet is packed into a physical-layer transport protocol frame (e.g. Ethernet frame) by adding a header with synchronization preamble.

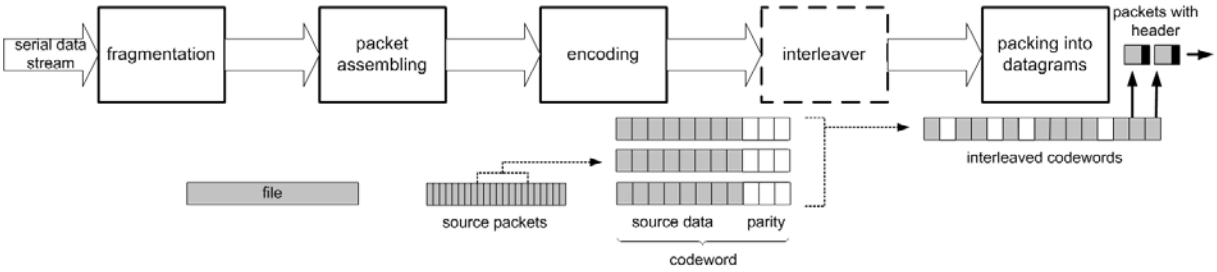

Figure 61: Packet-layer encoding of a serial data stream before transmission

Usually, physical-layer protocol packets (Ethernet) are routed using a network-layer protocol (e.g. IP) and a transport-layer protocol (e.g. UDP). These higher layers bring additional overhead due to their headers and are usually not needed for point-to-point connections.

Performance of Packet Coding: For packet-layer coding scheme, a code-symbol is a packet. The coding performance is usually evaluated in terms of symbol error ratio (SER) rather than in terms of bit error rate (BER) [25]. The SER is defined as the ratio of the number of data packets not recovered after decoding to the number of data packets transmitted. A lost and not recovered parity packet is neglected in the SER. So, SER is 0 for an error free transmission and 1 when no packets are recovered.

$$SER = \frac{\text{data packets not recovered}}{\text{number of data packets transmitted}} \tag{33}$$

(for example: 1 packet is not recovered out of 100 transmitted packets the SER = 0.01; 99 packets are not recovered out of 100, SER = 0.99)

The following plot shows the performance of a *LDGM (Low Density Generating Matrix) staircase* packet-layer code [W4]. The code has 50 % redundancy and a packet size of 1472 bytes. The codeword length n = 5292 packets. Having a probability of packet erasure p_e = 44.5 %, the code can recover almost all data packets (SER = 0).

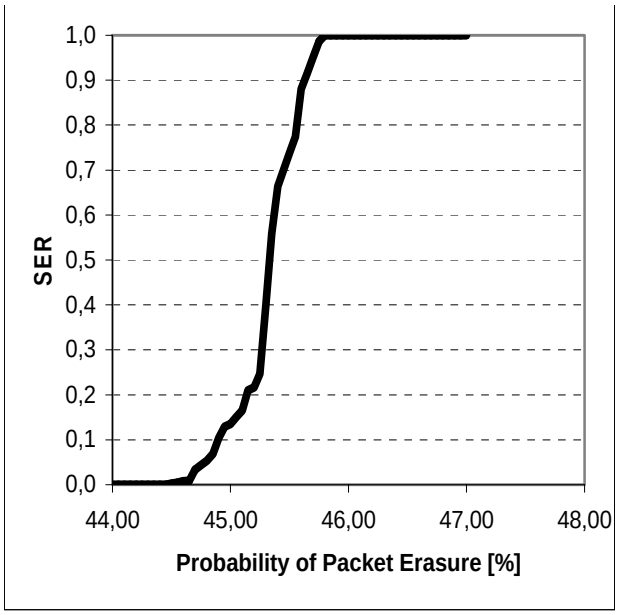

Figure 62: SER vs. probability of erasure packets p_e for a packet-layer code with 50 % redundancy and a code-word length of 5292 packets. The packet size is 1472 bytes. This plot was generated by real file transmission simulations

Estimation of the Redundancy R for Full Recover of Erased Packets: Let n the number of symbols in a codeword, k the number of data symbols in a word, then n-k is the number of parity symbols in a word and the redundancy R is given by:

$$R = \frac{n-k}{n} \tag{34}$$

Considering p_e the probability of packet erasure and assuming a uniform packet erasure process, the following rule of thumb can be made to estimate the coding gain [29, 43]: “*For not losing packets, i.e. for error-free transmission, it can be said that the code needs a redundancy R which is 10% more than the probability p_e of packet erasure”*.

That is,

$$R = p_e + 0.1 \tag{35}$$

One of the conditions for the link feasibility is that the redundancy should not exceed 0.5. Using the maximum allowed redundancy, we have

$$R_{max} = 0.5 \tag{37}$$

and, from Eq. (35), the condition on the probability of packet erasure is

$$\begin{aligned} p_e &= R_{max} - 0.1 \\ &= 0.4 \end{aligned} . \tag{38}$$

Estimation of the Probability P_e of Packet Erasure: Let us first consider the probability $p_{e,ST}$ that a packet is discarded for a given Rx-power level. Because the Rx-power level is constant, $p_{e,ST}$ represents a short-term probability. The probability $p_{e,ST}$ is given by the probability that at least one bit error occurs in the packet:

$$\begin{aligned} p_{e,ST} &= \Pr\left(\text{At least one error in packet}\right) \\ &= 1-\Pr\left(\text{No error in packet}\right) \\ &= 1-\left(1-BER_{ST}\right)^{l_{pkt}} \\ &\approx l_{pkt}BER_{ST} \end{aligned} \tag{39}$$

where BER_{ST} is the short-term BER, i.e. the probability, for a given Rx-power level, that a bit is wrongly detected, and where l_{pkt} id the packet length in bits. The probability of losing a packet when there is no fade is not zero, but this probability is much lower than the probability of losing a packet during a deep fade.

With P_R the power level, we can write the global probability p_e that a packet is discarded as follows

$$\begin{aligned} p_e &= \left\langle p_{e,ST} \right\rangle \\ &= \int_0^\infty p_{e,ST}\left(P_R\right) f_{P_R}\left(P_R\right) dP_R \end{aligned} \tag{40}$$

Influence of the Packet Size l_{pkt}: On the one hand, the larger the packet, the more likely the packet will be discarded and the link performance decreases.

On the other hand, if the packets become too short compared to the correlation time τ_c of the fading channel, interleaving (which we try to avoid) is required. Moreover, for short packets the coding speed is reduced and also the overhead for headers is greater.

When is Packet Interleaving Required? Coding can correct symbol (here packets) errors within a codeword. If the error burst is longer than the codeword the code fails. An interleaver can spread error-bursts over more than one codeword by scrambling the data stream. Therefore the data stream must be buffered for a time longer than the typical fade duration. As a result interleaving leads to a latency which is a little bit longer than the channel correlation time.

Interleaving is required when the codeword-length is much shorter than the duration of fades. A fade much longer than the codeword-length produces a packet burst error affecting a series of code-words. The duration τ_{pkt} of a packet transmission is given by

$$\tau_w = \frac{l_w}{B} \tag{41}$$

where l_w is the codeword-length in bits and B is the bit rate in bit/s. The mean duration of fades is given by the correlation time τ_c of the channel. Let us consider the two following cases:

1) The correlation time is much shorter than the transmission of one code-word:

$$\tau_c << \tau_w \tag{42}$$

In this case, several fades occur within a codeword. In this case, some packets in the codeword may be discarded but can be recovered by the code. Interleaving has no influence if the number of errors is not too high.

2) The correlation time is longer or equal than the transmission of one code-word:

$$\tau_c \geq \tau_w \tag{43}$$

In this case, one fade will affect one or more whole code-words. In this case, interleaving is required to spread the errors over affected and non-affected code-words.

4.2.3.5 Other Mitigation Techniques for Turbulence

Rx Adaptive Optics: The objective of adaptive optics is the correction of the incoming wave-front by deformable mirrors. This is clearly valuable when the transmitted information is located in the coherence of the optical wave. However, adaptive optics usually implies complex and expensive systems.

Rx Tip-Tilt Tracking: The tracking of the tip-tilt (slope) of the incoming wave-front amounts to the tracking of the spot focused on the detector. By tracking and correcting the “dancing” of the focused spot enables to keep the spot (i.e., the full received power) on the detector.

4.2.4 Ground Station Availability (Large-Scale Diversity) (DLR, Pe. He. Gi. Ho.)

Large scale diversity can be provided by having more than one ground station available, this concept and its benefits are discussed in this chapter.

4.2.4.1 Cloud cover statistics

The cloud cover describes the amount of sky (area of a data set) covered or obscured by clouds. Global cloud cover data is available from several satellite missions (e.g. APOLLO, NOAA-11) for some years. Considering the mean cloud cover in the region between latitude *40°N* up to *49°N* and *7°E* up to *13°E* longitude (southern Germany and northern Italy) it can be observed that the cloud cover structure is uniform in winter due to less convection and homogenous weather conditions in a large region in this time of the year. Also for less convection homogenous cloud cover can be seen above the sea. The mean cloud cover reveals a sharp gradient between land and sea. In general it can be observed that cloud cover structure is often inverse for summer- (speckled) and wintertime (smooth) as well as for autumn and spring. Thus, the annual mean cloud cover is not a meaningful quantity to show differences of different regions. Big cities like Munich act like a thermal island and show up to *6 %* more low clouds than the rural countryside [37]. Nevertheless, there are regional effects, e.g. Alpine river valleys have less cloud cover than their surroundings while the forelands it is the opposite. For great importance for free space communication is more the probability of clear sky or the probability of having only thin cirrus-clouds than the mean cloud cover. The probability of having only cirrus-clouds with an optical thickness of less than *1* (attenuation *<4.3 dB*) is given in figure 63.
Beside the clear sky probability the mean optical thickness is of interest. The *International Satellite Cloud Climatology Project* [W3], ISCCP, gives maps with the seasonal mean optical thickness. Again due to inverse effects yearly mean values do not make sense. The mean optical thickness for Germany for example is in summer *4 (17 dB), 9 (39 dB*) in winter and *7 (30 dB)* in autumn and spring. Notable is the Iberian-Island which shows all-the-year a mean optical thickness of about 5 (22 dB). Nevertheless e.g. for Germany the probability for clear

sky *(<30%)* and the mean cloud attenuation *(>17 dB)* is not feasible for a reliable optical up-/down-link to a HAP. So, spatial diversity concepts should be taken into account to achieve a reliable high data rate optical ground-HAP link.

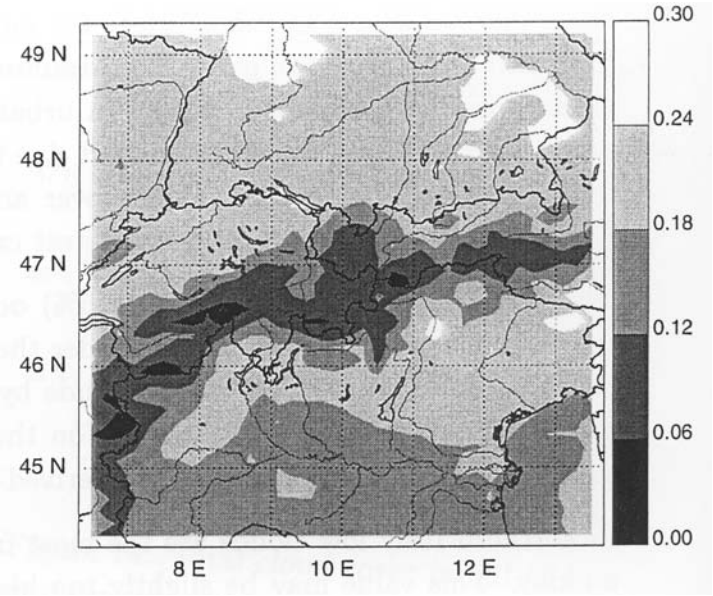

Figure 63: Probability of having only thin clouds with an optical thickness less than one (region: southern Germany to northern Italy, 3-year mean). Data taken from the APOLLO mission [37]

4.2.4.2 Diversity concept

The availability of a single ground station depends on the present cloud cover. As the cloud cover considering a large surface is not homogeneous, sides can be found where the present cloud cover is low. So in a ground station space diversity concept the ground station with the lowest cloud cover is used to advance the availability of the up-/downlink from a HAP network. The HAPs in the network are connected by optical inter-HAP-links and the ground stations are connected by a fiber network. The lower rate services for the users are provided by microwave links so that they are not affected by cloud cover. Only the high data rate network connection of the combined user channels is done optical.

For the placing of the ground stations it is important to know the correlation distance of the cloud structure. In Europe the cloud cover is mainly driven by warm and could fronts traveling with about *37 km/h* in eastward direction. The West-East spread of warm-fronts is greater than the spread of cold-fronts and measures about *300* up to *500 km*. The North-South spread is greater than *1000 km*. As a result of that it is favorably to arrange the ground stations mainly in West-East direction with a distance greater than the spread of the front-cloud-system *(500 km)*. Analyses of satellite cloud data also shows for southern Europe a correlation of cloud systems within a distance of *500 km* [46].
If the HAP is positioned at an altitude of *25 km* in the middle between two ground stations which are separated by *500 km* the elevation angle to the HAP will be *3.5°*. This is not acceptable because the link distance is about *10* times larger than the distance at zenith angle and for low elevation angles the boundary layer effects (e.g. high turbulence, fog, shadowing effects) count very well. Again a solution for that will be the use of a ground station diversity concept: A network with its HAPs positioned next to the ground stations is favorably. The HAPs are connected using high data rate optical inter-HAP-links which are working very well in the stratosphere due to weaker atmospheric effects in the higher altitudes. For the up-/downlink the ground station with the best visibility (in the network) to the HAP is used. If the clouds cover changes by time the station with the best downlink conditions could also change.

Typically these changes occur in the frame of tens of minutes to hours depending mainly driven by the wind speed.

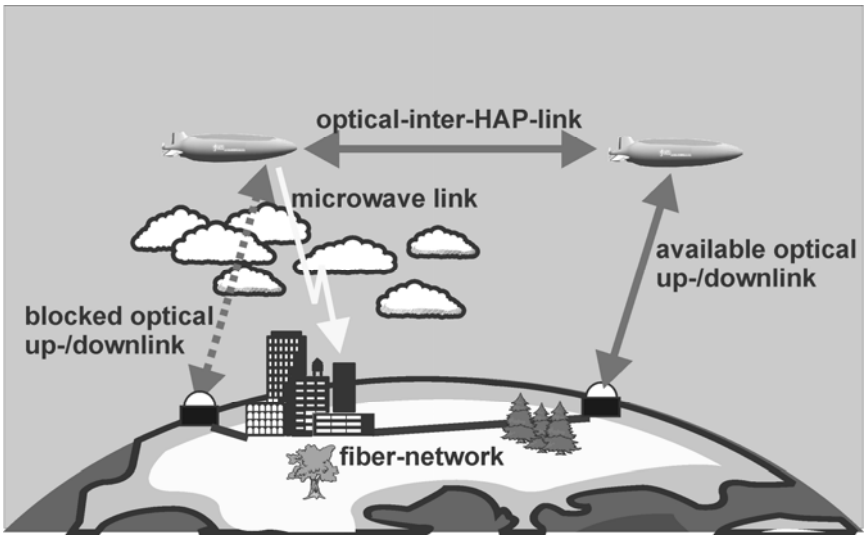

Figure 64: Ground station space diversity concept: Several HAPs are used as relay stations and if the optical downlink is blocked by clouds another ground station is used

Figure 65 shows the cloud cover structure in Europe on the 30. September 1999: occluded front system from Scotland to Normandy with low pressure centre above Faroe-Islands. The warm-front above Italy is more extended than the cold-front above France and the Pyrenees. HAPs are placed above congested areas (Sweden: Stockholm, Germany: Munich and Berlin, Italy: Rome, France: Paris, Great Britain: London, Spain: Madrid). The north-east distance is at least *700 km* (Munich - Paris) so that HAPs (with corresponding ground stations below them) can be found in regions with uncorrelated weather conditions. All HAPs are connected with inter-platform-links to a network. Maximum HAP-to-HAP distances can be from *300 km* up to *1000 km* depending on the platform altitude and the graze height [31].

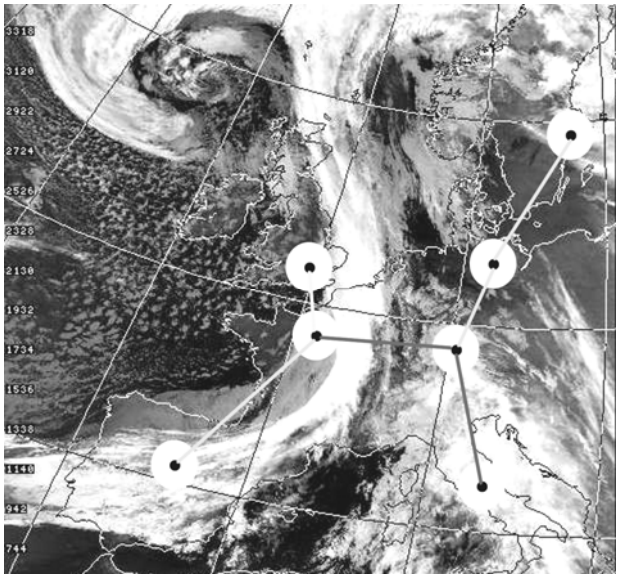

Figure 65: NOAA cloud cover satellite picture (30th September 1999) with HAPs above congested areas. At least one HAP in the network can be found with clear sky low attenuation downlink conditions

4.2.4.3 Availability

For some fraction of time p clear weather conditions are hold at a single ground station [44]. The attenuation under clear weather conditions a_0 is due to scattering and absorption by air molecules and thin cirrus-clouds. Further on q is the probability of not having clear weather. $w_1(a_0)$ is the fraction of weather conditions at any given single side for which the path attenuation is less then a_0. This result is also extended to obtain the joint weather probability, $w_k(a_0)$, that at least one of the k sites has an extinction loss $a<a_0$ for k independent sites.

$$p = 1 - q = w_1(a_0) \tag{44}$$

$w_k(a)$ is therefore the probability that at least one HAP-ground station link in the network has less than a *dB* path attenuation. That is equal to the availability of the up-/downlink system which can cope with maximum a *dB* attenuation.

$$w_k(a) = 1 - \left[q \cdot \exp\left(-0,23 b_S \left(a[dB] - a_0[dB] \right) \right) \right]^k \tag{45}$$

b_S is a scaling constant. For Germany b_s is found to be *0.22* (mean optical thickness *7 (a=30 dB)*, probability for clear sky *p=0.2* or *q=0.8*, a_0*=4.3 dB*, w_1*(a=30 dB)=0.8*). Re-arrangeing Eq. (45) gives:

$$a_{ges} = a_0 + \frac{1}{0,23 b_s \cdot k} \ln\left(\frac{q^k}{1 - w_k(a)} \right) \qquad \text{if } w_k(a) > p \tag{46}$$

The next figure (66) shows for two different probabilities of clear sky the expected path attenuation using *k=1, 2* or *3* diverse ground stations. It can be observed that for a clear sky probability of *0.2* and a maximum acceptable path attenuation of *15 dB* three ground stations are required for a demanded link availability of only *90%*. For enhanced clear sky conditions of *0.6* probability only two diverse ground stations are required for the same link availability.

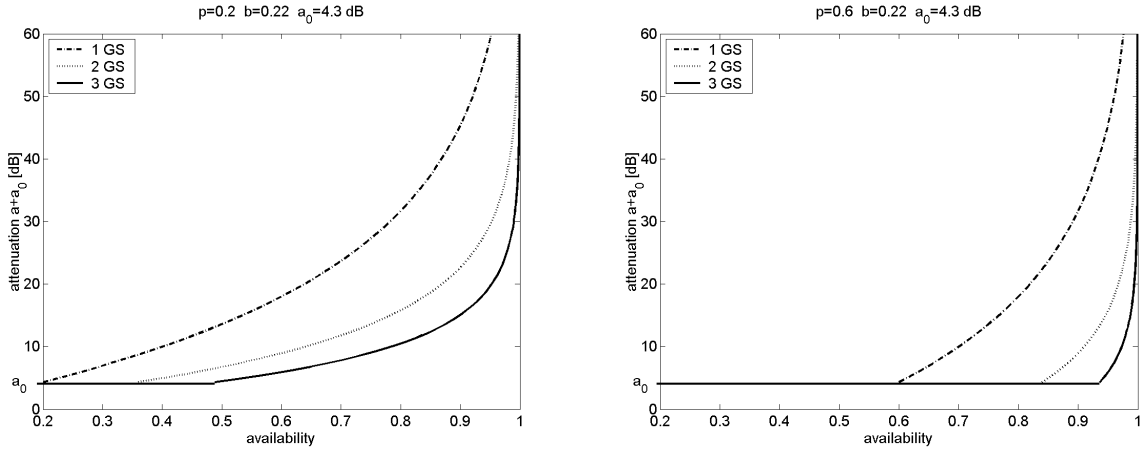

Figure 66: Path attenuation for 1, 2 or 3 diverse ground stations (GS) vs. link availability for clear sky probability of 0.2 (left) and 0.6 (right), b_S=0.22, a_0=4.3 dB

4.2.5 Simulation of models for special applications (UToV, Ca. Du. Be)

In this subsection, we discuss the simulation models developed and being currently used to investigate different characteristics of the Inter-satellite links.

4.2.5.1 LEO-GEO Motion simulations

In a GEO-LEO link it is possible to assume circular orbits in order to calculate some system parameters. Results from these formulas are, however, difficult to obtain for all kind of link since parameters variate with time. For this reason simulations are important to evaluate the performance, if the link is established. All graphics and results are obtained by means the AGI software Satellite Tool Kit (STK) and MATLAB. By STK it is possible to take into account pointing acquisition and tracking procedure as well, so that when the link is established the actual communication starts, if power requirements are satisfied. If all distances have been calculated with high accuracy, all the other parameters can be found from geometry properties of the link and from the way it changes.

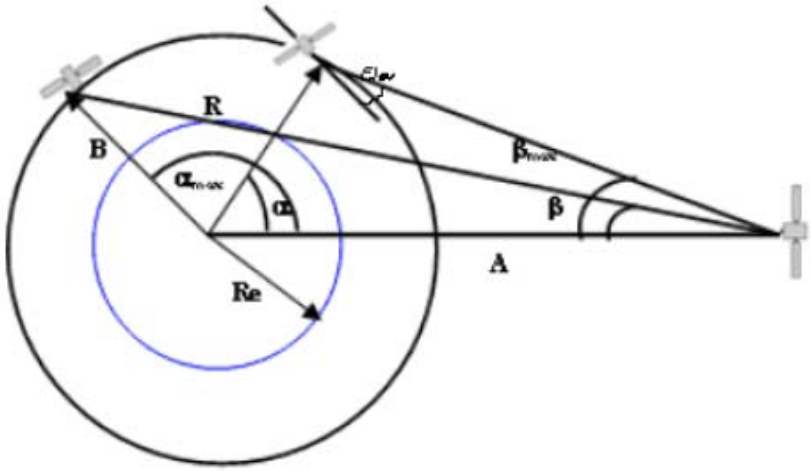

Figure 67: Link geometry

When the altitude of each satellite has been found, it is possible to calculate the link ranges by simplifying:

$$\begin{aligned} A &= R_e + h_{geo} \\ B &= R_e + h_{leo} \end{aligned} \tag{47}$$

The relation between the nadir, the elevation and the internal angles is given by:

$$\frac{\sin\beta}{B} = \frac{\sin(\varepsilon + \pi/2)}{A} = \frac{\sin\alpha}{R} \tag{48}$$

The distance between two satellites (R) can be found by the cosine law applied to the triangle described by the satellites and the Earth center:

$$R = \sqrt{A^2 + B^2 - 2AB\cos(\alpha)} \tag{49}$$

When a new access starts, often the range is too high to ensure a good quality of link. Since if the distance is too high, the link is more sensitive to pointing error and mechanical vibrations, the spot size is wider and the losses are higher.

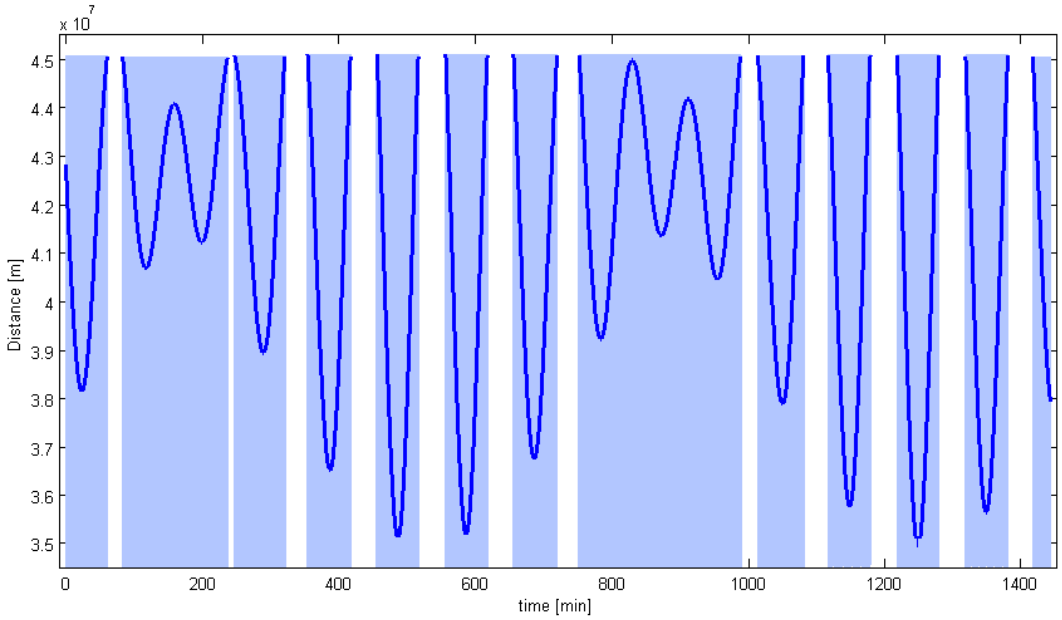

Figure 68: LEO-GEO distance in a day available links

The “contact” time between satellites is the 72.9% of the simulation time, meanwhile the access gaps are the 27.1% of the time. The knowledge of the access gap is important in order to evaluate the onboard memory requirements in case of storing information before to relay it.

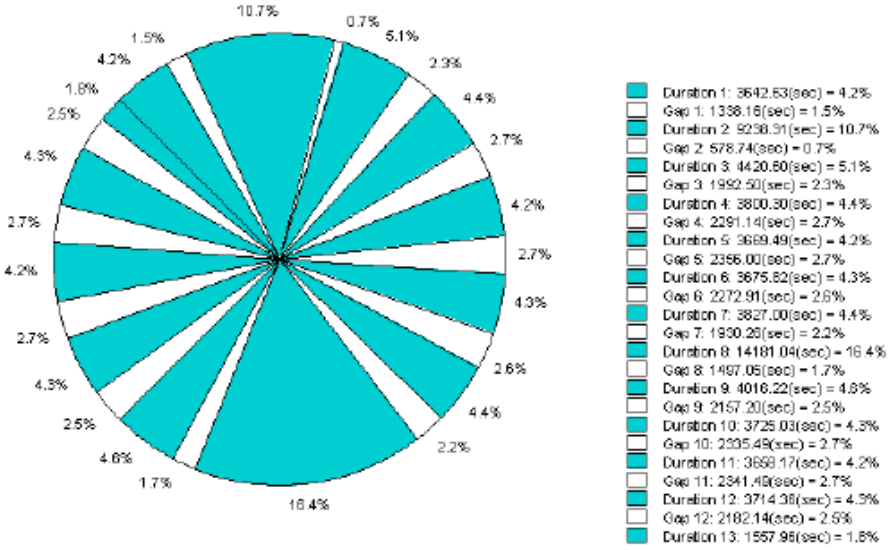

Figure 69: Access time and gap duration (in seconds and in percentage of the total time)

This wide range of distance leads to design a transmitter with a wide range of power level, in order to ensure the quality of service for the required time. By comparing figure 68 and figure 70, it is possible to see that ensuring to work under the maximum tolerable BER during the whole access could be very expensive for a 1Gbps OOK system.

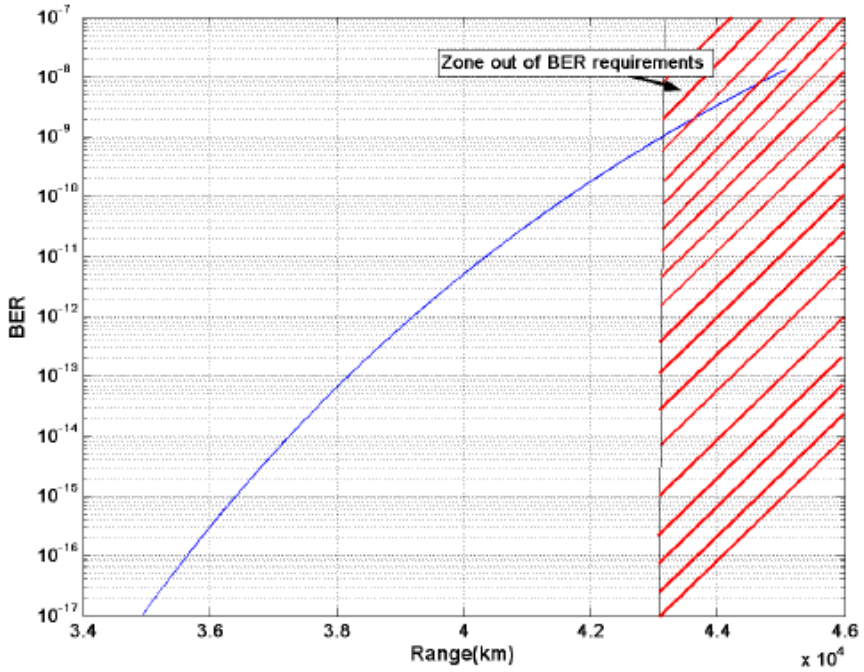

Figure 70: BER vs distance between satellite, with no adaptive power on transmission side

4.2.5.2 LEO-GEO Link: Chosing the modulation format

In order to overcome such power requirements, it is possible to follow to ways: the first approach is to consider the link as available in terms of QoS in a shorter time during a day; on the other side it is possible to implement different schemes of modulation.
For example by the use of a DPSK modulation format, it is possible to save up to half the power in terms of transmission consumption, if compared to an OOK modulation format, with the consequence of a longer available link if the same amount of power is transmitted. By the implementation of such a modulation format, the power adaptation becomes easier and less expansive. If the Doppler shift is avoided as shown in 4.1.3.5 paragraph, a possible receiver scheme for a DPSK-DD system is illustrated in figure 71 [50].

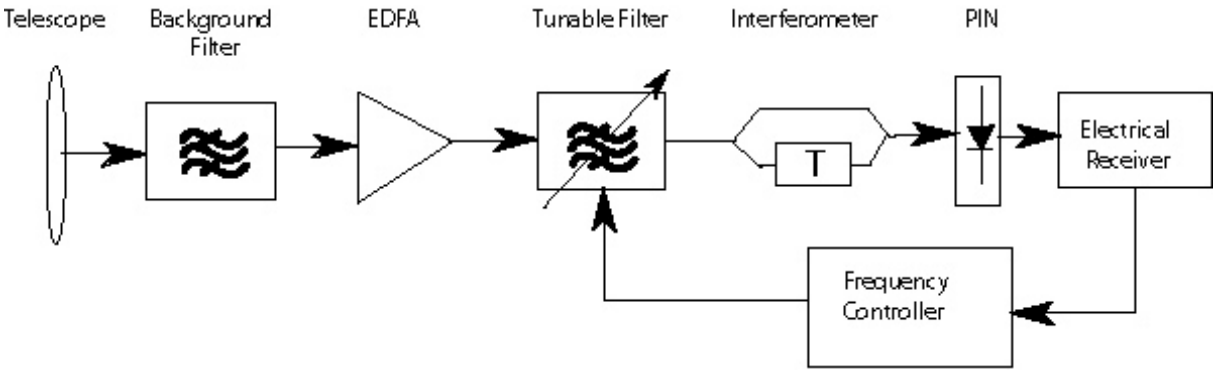

Figure 71: DPSK-DD pre-amplified receiver scheme with optical Doppler compensation

By simulations it is possible to evaluate the performance of such a system. The most important constraints are mechanical vibrations that are related to phase impairments on the receiver end. Since such phase errors affect the system, its performance can get worse in terms of BER. Anyway even if a phase error θ_e = 40° affects the system, the DPSK modulation format performs better than an OOK with the same transmitted power. This comparison it is shown in figure 72, the simulations have been carried out with a set of system parameters which values are reported in table 1.

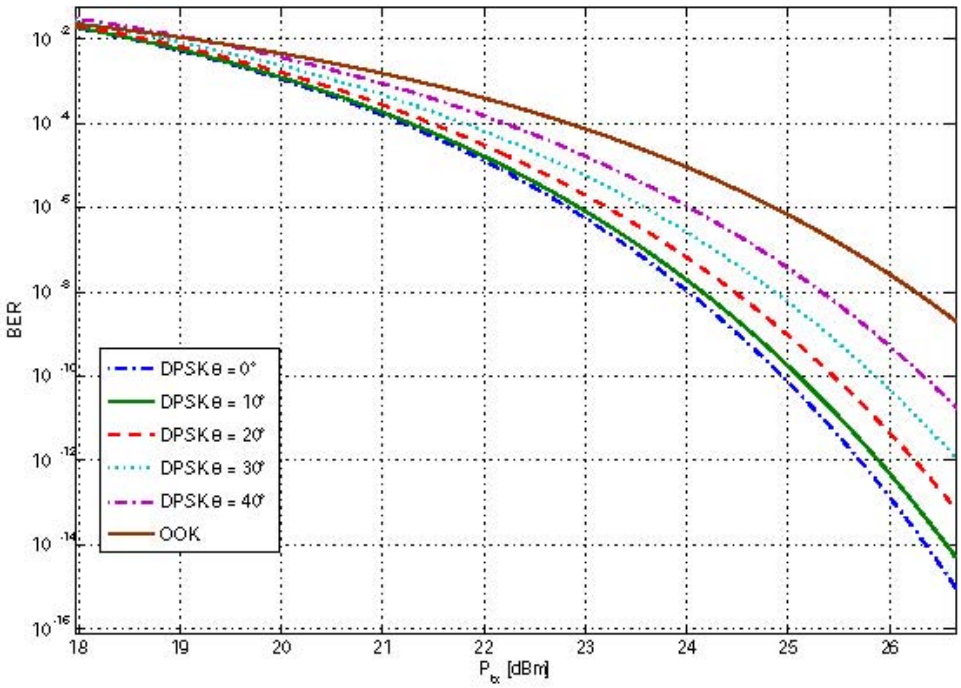

Figure 72: BER for DPSK with different phase errors and OOK, vs transmitted Power. A constant average distance of 40995 km has been considered

System wavelength	1550 nm
Transmitter output power	28 dBm
Average range	40995 km
Bit rate	2.5 Gbps
Coding gain	2.15 dB
Link margin	3dB
Pointing losses ($\sigma = 1\mu rad$)	3 dB
Insertion losses	3 dB
Tx/Rx antenna diameter	25 cm
Tx/Rx antenna efficiency	0.8
EDFA preamplifier gain	33 dB
EDFA preamplifier noise figure	3.3 dB
PIN bandwidth	9 GHz
PIN responsivity	0.8 A/W
PIN dark current	5 nA
Minimum received power	-37.62 dBm
Optical background irradiance	0.1 $W/m^2/\mu m$
RIN	-145 dB/Hz
B_{opt}	8 GHz
System temperature	500 K

Table 1: System parameter used in simulations

Since a DPSK modulation format, is a binary coding over a two bits interval, the two symbols can be written as:

$$
\begin{aligned}
s_1(t) &= \begin{cases} \sqrt{\frac{E_b}{2T_b}} cos(2\pi f_c t + \theta_e) & 0 \le t \le T_b, \\ \sqrt{\frac{E_b}{2T_b}} cos(2\pi f_c t + \theta_e) & T_b \le t \le 2T_b, \end{cases} \\
s_2(t) &= \begin{cases} \sqrt{\frac{E_b}{2T_b}} cos(2\pi f_c t + \theta_e) & 0 \le t \le T_b, \\ \sqrt{\frac{E_b}{2T_b}} cos(2\pi f_c t + \pi + \theta_e) & T_b \le t \le 2T_b, \end{cases}
\end{aligned} \tag{50}
$$

it can be easily proved that these symbols are orthogonal over the two bits interval if $\theta_e = 0$. For a differential detection of binary signals in a AWGN channel, it is possible to define the optimal demodulator that computes the decision variables, leading to the follow expression of the bit error probability as a function of the cross-correlation coefficient ρ [51].

$$
P_e = Q_1(a,b) - \frac{1}{2} e^{-\frac{(a^2+b^2)}{2}} \cdot I_0(ab) \qquad b > a > 0 \tag{51}
$$

where a(ρ) and b(ρ) are defined as follow, with γ the signal to noise ratio:

$$
\begin{aligned}
a &= \sqrt{\frac{\gamma}{2}(1 - \sqrt{1 - |\rho|^2})} \\
b &= \sqrt{\frac{\gamma}{2}(1 + \sqrt{1 - |\rho|^2})}
\end{aligned} \tag{52}
$$

The presence of a phase error on the received field leads to an increase of the minimum required power to ensure a given BER. It is possible to evaluate the penalty induced on the system performance in terms of sensitivity increase, if a non zero phase error affects the signal. If an average geometrical free space loss is taken into account, from the sensitivity penalty it is possible to evaluate the penalty in terms of transmitted power, as in figure 73. A margin of 1dB on the transmitter side must be taken into account at the time of design the system.

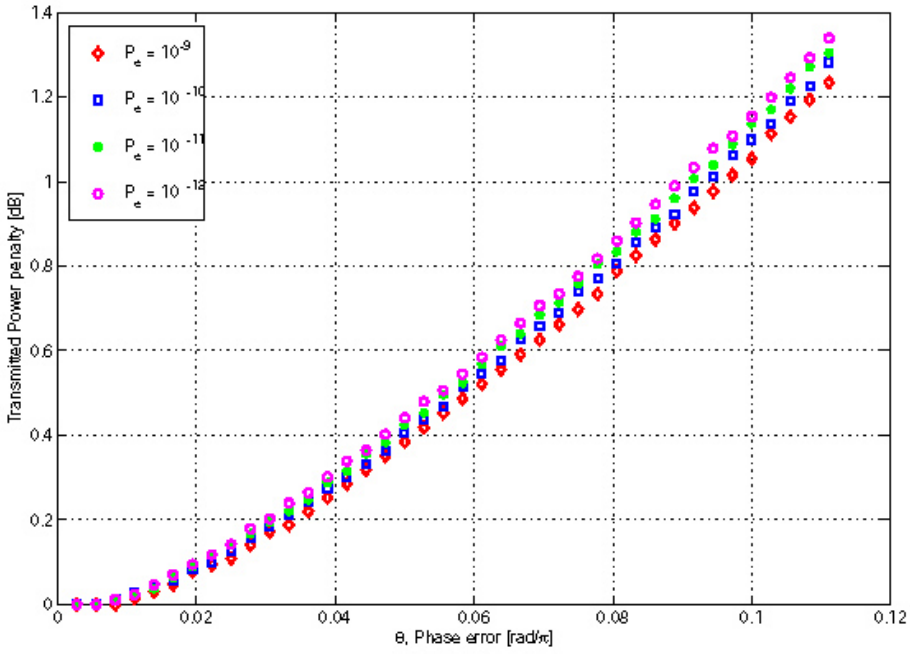

Figure 73: Penalty on the transmitter side, if a phase error affects the received field

There are many advantages in working at 1550 nm. First of all, the availability of EDFA amplifier leads to an increase of system performance if it is used as receiver preamplifier; then the system performs better in terms of Doppler effect and the background noise due to star field is lower than at other frequencies available for optical communications; at least an easy implementation of DPSK ensure to save up to 3 dB on transmitted power. By simulations it has been proved that such modulation scheme for satellites applications suffers phase errors induced by mechanical vibrations and interferometers error.

4.3 Coding- and networking techniques in Clear Sky Optics (TUG)

This section of the chapter will discuss the details of the modulation and channel coding, and the networking techniques being employed in terrestrial Free Space Optics links. The basic aim of this work is to enhance the performance of the existing terrestrial FSO links by introducing a well suited modulation and channel coding scheme. Selecting an appropriate modulation and coding scheme for the FSO systems requires thorough knowledge of the behavior of the FSO systems under different conditions and the objectives that need to be achieved out of the modulation mechanism. Since modulation for the FSO systems are primarily targeted at achieving higher average optical power, so that the penetration of the light waves through the adverse weather conditions can be increased. Thus, the power efficiency of the scheme remains the deciding criteria in the selection of the modulation format. The choice of the modulation and coding format has to be based on measurements and simulation of the performance of FSO systems under nonfavourable atmospheric conditions. An effort is also being made to simulate the atmospheric free space optical channel to get more insight into the problem. The current networking techniques (being employed to provide a possible solution to the “last mile” connectivity gap) are also discussed.

4.3.1 Coding and Modulation techniques for Terrestrial FSO (TUG, Sh. Le. Ch.)

Free space optical communications (FSO) has gained importance in recent times due to a variety of applications in the field of telecommunications. FSO applications span over a wide range from satellite links to robotics and generates interest for several distinct markets. FSO is becoming famous both as a preferable last mile solution and as a supplement to the more conventional RF links [52, 53]; and this has given rise to the need of investigations in mechanisms to enhance the performance of the systems.

The free-space, direct detection, optical intensity-modulated channel offers the modem designer interesting new challenges. Most practical FSO systems use light emitting diodes (LED) or laser diodes as transmitters and PIN photodiode or avalanche photodiodes (APD) as receivers forming a relevantly simple communication system. These devices modulate and detect solely the intensity of the carrier, not its phase, which implies that all transmitted signal intensities are non-negative. Furthermore, biological safety considerations (eye safety) constrain the average radiated optical power, thereby constraining the average signal amplitude. Conventional signal space models and coded modulation techniques for electrical channels cannot be directly applied to this channel [54].

Historically, optical intensity channels have been modeled as Poisson counting channels, and the model remains a valid assumption for basic investigations in FSO as well. The literature is replete with channel capacity results for the photon-counting channel. In the absence of background noise, the capacity of such channels is infinite [55, 56]; and M-ary Pulse Position Modulation (PPM) can achieve arbitrarily small probability of error for any transmission rate. McEliece demonstrated that schemes based on photon counting in discrete intervals require an exponential increase in bandwidth as a function of the rate (in nats per photon) for reliable communication [57]. The most prominent modulation formats for wireless optical links are binary level PPM and on-off keying (OOK). Shiu and Kahn developed lattice codes for free

space optical intensity channels by constructing higher dimensional modulation schemes from a series of one dimensional constituent OOK constellations [58].
In this part, we present the channel modeling effort for the terrestrial FSO channel based on photon counting and simulations of the channel. Section 4.3.1.2 provides the results of investigations in appropriate modulation schemes for FSO and the next section deals with the channel codes to be combined with the modulation format to provide better gains.

4.3.1.1 Channel Modelling for Modulation and Coding

To get more insight into the problem, a better understanding of the characteristics of terrestrial FSO channel is necessary. Modeling the channel for terrestrial FSO is a problem of considerable complexity due to the variety of impairments possible and the disagreement over the mathematical modeling of the various phenomena. FSO links are impaired by absorption and scattering of light by earth´s atmosphere. The atmosphere interacts with the light due to its composition, which normally consists of a variety of different molecular species and small suspended particles called aerosols. This interaction produces a variety of phenomena: frequency selective attenuation, absorption, scattering and scintillation. In addition, sunlight can affect FSO performance when the sun is co-linear with the free space optical link. An effort is being made to simulate these effects as accurately as possible so that the resultant channel model may later be used as a test-bed for the verification of the selected modulator and channel coder [59]. Investigations into the capacity of optical intensity channels have focussed on channels in which the dominant noise source is quantum in nature. In these channels, the transmitted optical intensity is constant in discrete time intervals and the received signal is modeled by a poisson-distributed count of the number of received photons in each discrete interval. In order, to understand the theoretical framework of optical channels, this photon counting channel has been utilized and the development of an efficient modulation and coding format has been based on the mathematical analysis of this channel model, and to bring the work nearer to reality the terrestrial free space optical channel has been simulated with an effort to keep it as close to the real environment as possible.

The Photon Counting Channel: We assume a photon counting communication system as the basic model for investigating the behavior of the channel. For this purpose, we built up a model in a way that the time interval during which communication takes place is divided into many sub-intervals ("slots"), each of duration t_0 seconds. The transmitter is a laser which is pulsed during each time slot; it may be pulsed with a different intensity in each slot. At the receiver is a photon counter which accurately counts the number of photons received during each time slot. We denoted by x_i the expected number of photons received during the *ith* time slot; x_i will be the *intensity* of the *ith* pulse. We assume that no noise photon exists and because of the poisson nature of photon arrivals, the probability that exactly k photons will be received during a slot in which the laser was pulsed with intensity x is $\frac{e^{-x}x^k}{k!}$, thus we can summarize this discrete memoryless channel by the conditional probability

$$P(k \mid x) = e^{-x}\frac{x^k}{k!} \tag{53}$$

The channel described by the above equation is called the *photon channel* and has been extensively used in research on optical communication channel design [57]. The photon channel is the appropriate model when applied to optical channels in which the receiver intensity is low, such as the fiber optic and the free space optical channel. Photons are detected by the photon counter with the probability of their detection depending

on the energy in the electric field. For a given electric field energy E, the probability of the number of photons detected over a given time T has a poisson distribution

$$P_r(j) = \frac{1}{j!} n^j e^{-n}, j = 0,1,2,.... \quad (54)$$

Here $n = n(E)$ is the mean number of photons detected in the counting time t. It is equal to the expected field energy in time t divided by hf. Note that

$$P_r(0) = e^{-n} \quad (55)$$

is the probability that no photons are detected. The number n is called the poisson parameter. In [56], Pierce argued that if one uses photon counting techniques for communication at optical frequencies, channel capacity is $\frac{hf}{kT}$ nats/photon where f is the photon center frequency and T is the noise temperature (h is Planck´s constant, k is Boltzmann´s constant). Later, it was also observed that techniques of linear amplification yield a capacity of 1 nat/photon. However, channel capacity is an absolute limit on performance and only tells us what is possible using arbitrarily complex encoding and decoding strategies [60].

The Terrestrial Free Space Optical Channel: The terrestrial free space optical channel represents one of the most challenging environments to model and simulate. A significant effort in this regard was made by M.Achour [61, 62]; but still much more is desired. A channel model has been developed to look more deeply into the issues of modulation and coding and at present this model simulates the major attenuators for the FSO links namely fog, rain and snow besides providing the flexibility to introduce different levels of turbulence based on the turbulence coefficient [59]. The simulation was tried to be setup in a way to keep as many parameters variable as possible, to give the model a very general outlook.

1) Fog Attenuation: The theoretical background of fog attenuation for light based on Mie Scattering can be found in detail in literature [5, 63]. Several models exist which allow to calculate specific attenuation for different optical wavelength based on visibility data. The two most widely used models are the Kim and the Kruse model, they have been implemented and the resultant attenuation curves are shown. At very high attenuations the Kim model is the better choice.

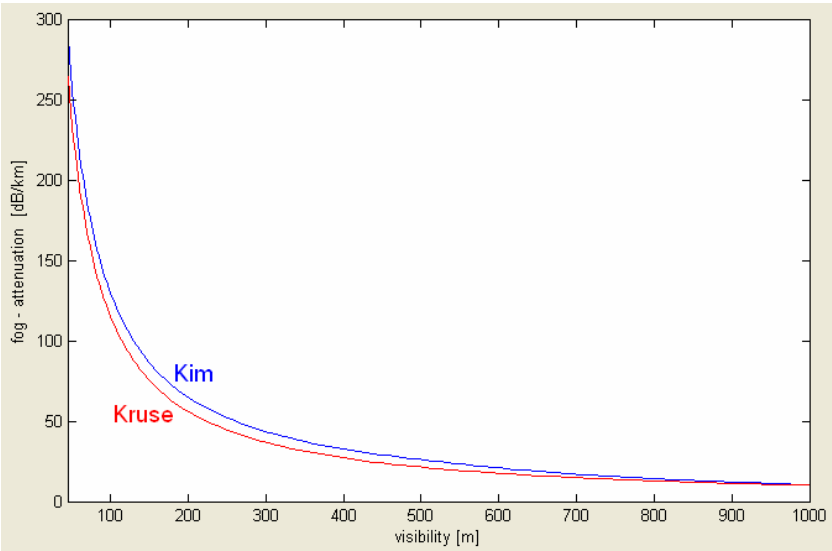

Figure 73: Fog Attenuation curves

2) Rain and Snow Attenuation: Rain is also an important attenuator for optical signals and has been modeled using the best known relations. The attenuation due to snow fall has been modeled based on dry and wet snow, the simulated attenuations are shown in Fig. 74b.

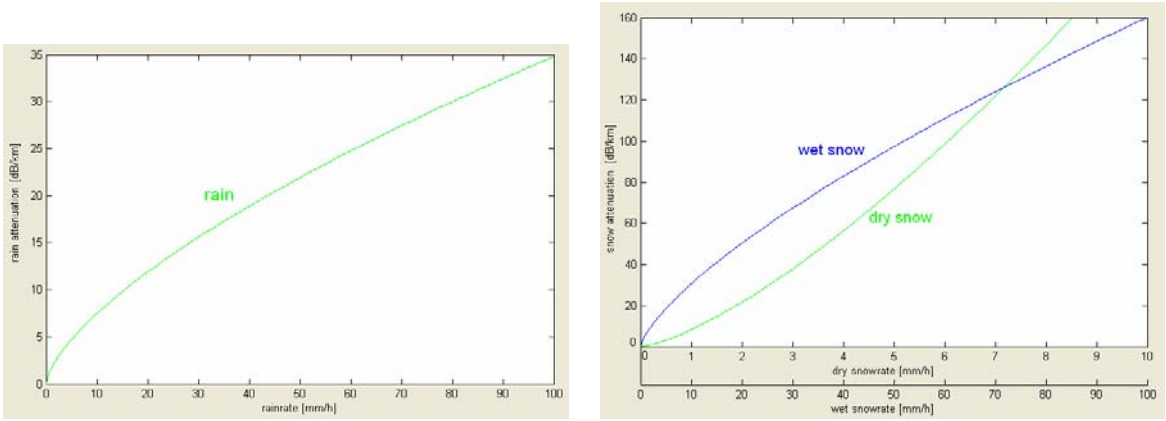

Figure 74: Attenuation due to rain (a) and dry and wet snow (b)

3) Scintillation: Randomly distributed cells are formed under the influence of thermal turbulence inside the propagation medium; the wave fronts vary causing the focussing and de-focusing of the beam. Such fluctuations of the signal are called scintillations. The intensity and speed of the fluctuations increase with wave frequency. Based on the refractive index structure parameter Cn^2, the scintillation losses have been modeled for low, medium and high turbulence and are depicted in Fig. 75.

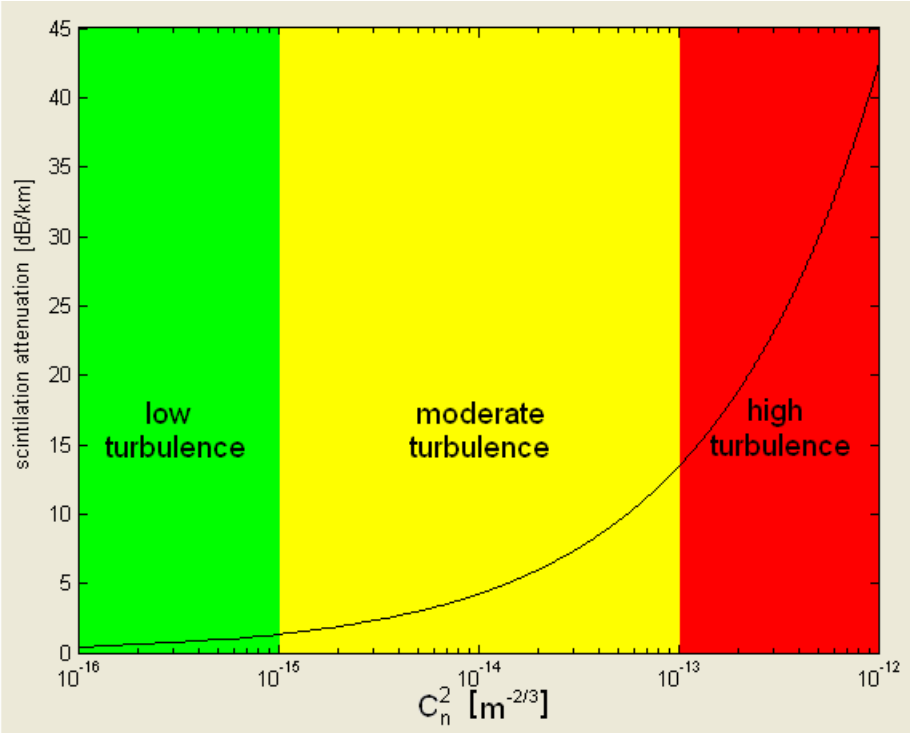

Figure 75: Scintillation losses

A Graphical User Interface for the channel model has been developed to provide the user the convenience of handling the simulation setup on his own. This channel model directly provides availability and reliability prediction for terrestrial FSO. In the next steps, it will be used to test the performance of the modulation and channel coding schemes mentioned in this chapter.

4.3.1.2 Modulation Schemes

Most of the FSO systems being currently used employ the intensity modulation with direct detection scheme (IM/DD), and the performance of the FSO systems is hampered by varying atmospheric conditions. Previous investigations [64] have shown that deep fog is the most severe deterrent, as the light penetration through fog reduces considerably, and thus intuitively it appears that the penetration of light can be improved by concentrating more power into lesser areas. This indicates towards the utilization of power efficient modulation schemes.
The transmission of information using optical intensity channels differs significantly from the conventional RF channel. Unlike the RF technologies, where the carrier amplitude and phase are varied, wireless infrared relies on the intensity modulation of a terahertz range optical signal. The response of the photodiode is the integration of tens of thousands of wavelength of incident light. Using incoherent, diffuse light sources (for eye safety reasons), only the intensity of the optical signal can be determined, which must remain positive [65].
Let $x(t)$ denote the intensity of the transmitted optical signal and let $ry(t)$ be the photodetector current at the receiver, where the constant r is the photodetector responsivity. When the intervening channel has impulse response $h(t)$, $y(t)$ is given by

$$y(t) = \int_{-\infty}^{+\infty} x(\tau)h(t-\tau)d(\tau) + n(t) \tag{56}$$

The input $x(t)$ represents power, not amplitude and this leads to two unusual constraints on the transmitted signal; firstly, $x(t)$ must be positive, and secondly, the average amplitude of $x(t)$ is limited. If the average of the transmitted light wave is constrained to a value which we denote by $\Re$, then the input $x(t)$ of the baseband channel must satisfy

$$x(t) \geq 0 \tag{57}$$

$$\lim_{T \longrightarrow \infty} \frac{1}{2T} \int_{-T}^{T} x(t)dt \leq \Re \tag{58}$$

The first constraint implies that any modulation scheme for an optical intensity channel must have a DC component which transmits no information but consumes energy [11].
These special requirements for the optical intensity channel prevents applying the wealth of modulation analysis available for the conventional channel to the FSO application. Different binary schemes like the on-off keying (OOK), two pulse-position modulation (2-PPM) and subcarrier binary phase shift keying (BPSK) have been compared, based on their power efficiency, measured by the average optical power required to achieve a given BER at a given bit rate. It has been noticed that 2-PPM has the same power requirements as OOK, whereas BPSK suffers a 1.5 dB optical power penalty [52]. For a given optical power P_t, the receiver SNR can be improved by transmitting a waveform $X(t)$ having a high peak-to-average ratio, such as L-PPM. We note that the optical path loss of the channel is $H(0) = \int_{-\infty}^{\infty} h(t)d(t)$, and the received optical power is $P = H(0)P_t$ [66].

Pulse Position Modulation: Most modulation schemes for data transmission on landline or wireless optical channels rely on binary levels to transmit data. Schemes such as on-off keying and pulse position modulation depend on the use of two levels to transmit data. Multilevel modulation schemes can provide better bandwidth and power efficiencies because of their more complex signal constellations. Schemes such as L-PAM and QAM achieve higher bandwidth efficiency at the expense of decreased power efficiency. L-level PPM is a

fundamentally different modulation scheme that achieves high power efficiency at the expense of reduced bandwidth efficiency [11]. Digital Pulse Position Modulation (PPM) is widely used in intensity-modulated optical communication systems, such as fibre optic and satellite systems, primarily because of its high average-power efficiency [56, 57]. The abundance of bandwidth in these applications makes the poor bandwidth efficiency of PPM of little concern, the FSO environment represents a very similar situation, and PPM with its significantly better power efficiency seems the appropriate choice.

Talking in terms of our photon communication channel, if we take a block of M counting times t and use pulse position modulation, we can find how large M can be so that the probability of error will still be low. We can have an error if there is a noise photon during one of the $M-1$ time intervals when the shutter is closed. There maybe no noise photons in these intervals, but we may fail to receive a signal photon when the shutter is open. This corresponds to an *erasure*, in which no photons at all are received. It is well known that, in an erasure channel, the erasure lowers the capacity in bits/second, but only by the probability of an erasure. So it is reasonable that we can ignore the probability of erasure in computing the capacity in *bits per photon*. This is assumed true and the capacity in bits per photon is then

$$C = log_2 M \tag{59}$$

Here M is the largest number of intervals for which the probability of receiving a noise photon in some interval during which the shutter was closed is small.
In a pulse-position modulation scheme, each symbol interval of duration

$$T = \log_2 \frac{L}{R_b} \tag{60}$$

is partitioned into L subintervals, or chips, each of duration $\frac{T}{L}$, and the transmitter sends an optical pulse during one and only one of these chips. PPM is similar to $L-ary$ FSK, in that all signals are orthogonal and have equal energy. PPM can be viewed as the $rate-\frac{\log_2 L}{L}$ block code consisting of all binary $L-tuples$ having unity hamming weight. A PPM signal can be written as

$$x(t) = LP\sum_{k=0}^{L-1} c_k p(t-\frac{kT}{L}) \tag{61}$$

where $[c_0, c_1, c_2, ..., c_{L-1}]$ is the PPM codeword, and where $p(t)$ is a regular pulse of duration $\frac{T}{L}$ and unity height. All of the signals are equidistant, with:

$$d_{min} = min_{i\neq j} \int (x_i(t) - x_j(t))^2 dt = 2LP^2 \log_2 \frac{L}{R_b} \tag{62}$$

therefore, the average power requirement is approximately:

$$P_{PPM}/P_{OOK} = d_{OOK}/d_{min} = \sqrt{\frac{2}{L\log_2 L}} \tag{63}$$

From the above equation, we say that, for any L greater than 2, PPM requires less optical power than OOK. In principle, the optical power requirement can be made arbitrarily small by making L suitably large, at the expense of bandwidth, the bandwidth required by PPM to achieve a bit rate of R_b is approximately the inverse of one chip duration, $B = L/T = L\frac{R_b}{\log_2 L}$ [67].

PPM is an orthogonal modulation technique and can be viewed as a simple nonlinear block code; specifically, the rate $\frac{\log_2 L}{L}$ block code consisting of the set of L-binary L-tuples with unity hamming weight [68]. It has been shown in [11] and can be seen through (63) that 2-PPM has same power efficiency as OOK but requires twice the bandwidth and 4-PPM requires 3.8 dB less optical power, and as L increases from 4 to 16, the bandwidth requirement doubles, while the sensitivity increases from 3 dB better than OOK to 7.5 dB better than OOK, and clearly increasing L improves the power efficiency for multilevel PPM.

4.3.1.3 Efficient Channel Codes

The channel capacity of the *photon channel* was discussed earlier, and it is a general rule that the closer one approaches channel capacity, the more complex and costly the needed coding strategies become. In the case of photon communication, however, coding problems seem to become more serious much sooner than usual, and for an unexpected reason. It is not the noise temperature, but the nature of the photon-counting process itself, that causes the most serious problems; so that even in the limiting case $T = 0$, when capacity is in principle infinite, it seems unlikely that a signalling efficiency of even 10 nats/photon can be achieved practically. This is because, as the signalling rate increases one encounters an explosive increase in bandwidth expansion.
In [56], Pierce suggested the use of Pulse Position Modulation (PPM) for optical communications. In PPM, a fixed integer $q \geq 2$ is selected, and the transmission interval is divided into consecutive blocks of q slots each. In each such block the laser is pulsed in exactly one of the q slots at a fixed intensity. Each of these q patterns can be regarded as a letter in the sender's alphabet. In coded PPM, the idea is to regard the $q-letter$ transmission alphabet as the input alphabet of a discrete memoryless channel with $q+1$ output letters, the $(q+1)st$ letter is regarded as the erasure symbol. In order to achieve better performance, appropriate channel codes need to be combined with PPM. Three strong possibilities for channel coding exists with PPM namely Reed Solomon codes [57], Turbo Codes [69, 70] and Trellis coded modulation [71].

Reed Solomon Codes: A PPM signalling scheme seems to lend itself naturally to a Reed Solomon code, whose alphabet size can be easily matched to the PPM order. This result in a one-to-one correspondence between RS code symbols and PPM symbols. Using a maximum count or threshold hard decision rule, a single PPM error translates directly into a single RS-code symbol error. Or, by using threshold or $\delta - max$ demodulation, an erasure may be declared based on the soft counts in a PPM symbol. This is sometimes referred to as soft decision RS coding. Since every RS code is a maximum distance code, it appears that no more powerful code could be found for this application.

Turbo Codes: There have been proposals for combining Turbo codes with PPM [69, 70] primarily because of their higher coding gains and their ability to utilize soft outputs, but for the FSO applications it is envisaged that the gains achieved by Turbo codes may not justify the increase in the complexity and the delay requirements inherent to them, and moreover, its always thought better to be utilizing hard decision demodulators in FSO applications. A relevantly innovative scheme is proposed where through the quantization of APD/PIN output voltage levels, soft decisions can be generated; which can then be used for the Turbo decoding and this will lead towards significant coding gains. However, its still an open question as to how Turbo codes may perform in combination with higher level PPM on a terrestrial FSO channel and only further investigations can prove with certainty their supremacy.

Trellis Coded Modulation: Since PPM is an orthogonal multipulse modulation scheme, the Euclidean distance between any pair of symbols is the same, and trellis coded modulation which is designed to maximize the minimum Euclidean distance between allowed signal sequences may provide performance enhancement on multipath intersymbol interference (ISI) effected channels [71] , but it will not be of much benefit in a FSO environment which does not suffer from multipath problems.
Thus, all in all, the choice is really between Reed Solomon Codes and Turbo Codes as the most suitable for FSO application and their combination with multilevel PPM should yield significant performance enhancement. Reed Solomon codes are well known channel codes and are extremely efficient at correcting erasures and well established encoding and decoding procedures exist for them. Similarly, Turbo codes have gained considerable importance due to their high coding gains and utilization of iterative decoding mechanism in them.
The optimal PPM order for FSO applications can be 256 and the $rate \frac{1}{2}$ (255,128) RS code can be a good choice to be combined with $256-ary$ PPM. Hence, one of the possible modulation and coding scheme to be utilized in FSO systems is believed as RS-coded PPM. Still an open question is the selection of the PPM order in combination with Turbo codes to yield desired results.

4.3.2 Networking in Free Space Optics (TUG, Ch. Le. Sh. Ge.)

Terrestrial Free Space Optics (FSO) links can be used to upgrade the “last mile” connectivity gap to a high speed backbone link at very low costs. The last mile resides between the individual subscriber and the network operator’s central office. Although state of the art FSO technology cannot compete with the high data rates of leased fiber cables and its network equipment, respectively, it can offer important applications for public and private use. The last mile connectivity with FSO is often used on campus sites where point-to-point or building-to-building data links are required. Another application scenario of FSO could be in connecting hardly reachable settlements with the central office, thus providing a possible “broadband for all”-solution.

4.3.2.1 FSO in Terrestrial Access Networks

But when independent carriers deploy their own fiber networks to the customer premises, each provider needs to deploy separate fiber cable to virtually every building and within every riser in each building. This results in a significant number of independent fiber cables, and hence road trenching, required to interconnect all the downtown buildings with the multitude of service providers. The other result is that many municipalities are declaring moratoria on digging up the roads by carriers who want to install new fiber cables. In addition, many cities are refusing to grant new construction permits for any road section that has been repaved or rebuilt within the last five years.
The set up of an access network requires considerations of economic, legal and technical questions in the field of services and applications, data distribution and customer issues. It is necessary to fit into the local situation, to fulfill the customers need, to take advantage of the providers existing knowledge and strength and to consider carefully already existing or planned competing services at the location. For this reason it seems to be essential to get an overview of all aspects to be able to find the best solution [73].
FSO Systems are available as protocol dependent units as well as protocol transparent ones. They differ in cost, range of use and speed, which nowadays reaches data rates from 10 Mbit/s up to 1 Gbit/s. It is possible to couple from FSO-systems directly in the optical domain or with optical / electrical conversion and regeneration to the network-fibre. Also coupling into a Wavelength Division Multiplex (WDM) is possible, by connecting different Optical Wireless Systems with a Wavelength Division Multiplexing unit to the WDM-fibre network.

Besides network access protocols like Token Ring, Local Talk or FDDI, the ATM and Ethernet protocol are by far the most widely used. Current transfer rates of ATM lies between 25 and 2488 Mbit/s whereas Ethernet reaches speeds up to 1250 Mbit/s.

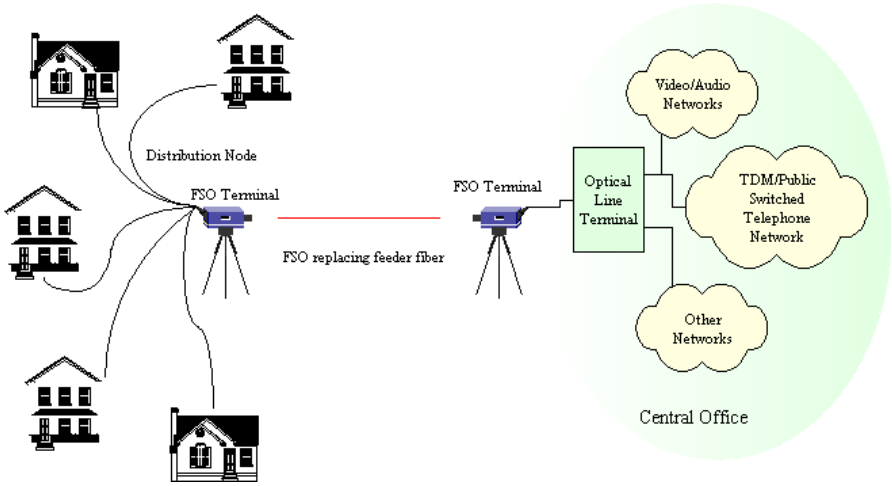

Figure 76: FSO connection between the central office and a settlement

At the time ATM technology was introduced, it offered data rates up to 155 Mbit/s and thus was 1.5 times faster than Fast Ethernet. Although ATM has higher bandwidth over a SDH/SONET net it can no longer compete in pure speed. Both technologies Gigabit Ethernet as well as ATM have their advantages and disadvantages and applications show that these protocols will also coexist in the future. For integrating ATM technology into Ethernet networks emulation services like LANE (LAN Emulation) and IPOA (IP over ATM) have been created. For providing Quality of Service in Ethernet networks special protocols like RSVP (Resource Reservation Protocol) and RTSP (Real Time Streaming Transport Protocol) have been realized. The main selling point for ATM is its well established Quality of Service standards, delivering real time applications like voice or video over a single line to the customer. But the wide deployment of Ethernet products makes it the most popular LAN technology. All Ethernet protocols are connectionless and have variable frame sizes. As a matter of fact, users in an ethernet network are sharing the bandwidth and the media. Gigabit Ethernet products are compatible to older standards like Ethernet or Fast Ethernet, which makes upgrading to state of the art technology more comfortable. ATM uses a connection-oriented technology like telephone lines, thus a path between host and client has to be established at first [72].

Benefit	Gigabit Ethernet	ATM
IP-Compatibility	yes	with LANE
Ethernet Packets	yes	with LANE or Routing
Real Time Applications	no	yes
Multimedia Applications	restricted	yes
Quality of Service	restricted, RSVP	yes
VLAN capable	yes	yes
Scalability	yes	yes
Reliability	Spanning tree	redundant nets

Table 2: Comparison of properties in ATM and Gigabit Ethernet networks

4.3.2.2 Available Services

Telephone service can be implemented by Voice-over-Internet-Protocol (VoIP) technology. Like for all real-time applications delay must be kept very small, actually the ITU recommends a total of less than 140 ms, to allow a talk without restrictions. On the other hand

the required data rate is rather small, in the order of 30 – 70 kbit/s typically for one link. For this reason usually no data compression is implemented, to avoid any further delay. Also for this reason the information should be transported in small size data packets through the network, because every higher layer network node has to receive the full packet before it is transmitted over the next segment and for short packets this is less time consuming. To avoid interrupts VoIP packets should be transported with priority, which refers to the Quality-of-Service (QoS) aspect of the net, and usually is no problem if the access network offers high data rates in excess of the actual need. A very high availability in the order of 99.999 % of time is another requirement which is explained with emergency calls mainly. For IP networks like for mobile phone networks this is a very hard challenge, which usually cannot be achieved. However, due to the good telephone copper cable infrastructure, which is already deployed in most regions, and the low costs for a call, VoIP service can rather be implemented as an additional attractive feature in the net, which allows to reduce the figure for availability. Even major telecom providers have chosen to reduce the very high network availability, because it makes the net very expensive and is not so important for other services actually.
Broadcast of TV or radio programmes has quite different aspects. Delay is not critical at all, so efficient data coding can be implemented to allow high quality by efficient use of transmission data rate.
MPEG-4 is a state of the art coding technology and approved for the broadcast television industry. In a test set up at TU Graz the delay due to encoding and decoding was in the order of 2 seconds, which allows to compensate even for occasional burst errors or lost packets without notice for the application. The required data rate for one TV cannel varied between 2 and 19 Mbit/s, depending on the content of the video signal.
Internet access is the main and original concept behind an IP based Ethernet access network. For this reason the network usually is best suited for this service. Typically a fixed uplink transmission line over the Wide Area Network (WAN) is used and unbundled to all customers in the central office of the access net. Many subsequent applications can be offered over Internet connection by Centralized Service Providers, and the whole structure is flexible and open to new services which may come up in future with an increasing number of customers with really broadband access.
External data store is an option currently used in expensive professional computer networks, today implemented in banks or major production companies, which is getting more and more interesting also for small and medium companies or even for private persons, because during the latest disasters people did get aware of the damage caused by data loss and the importance of a secure store. Backup copies in the same room are not helpful if fire or water damage appears. If a broadband data network exists, external data store can be an attractive service to many more customers than today if it can be offered at low costs. Availability and delay is not critical for this application, but high data rates and a secure transmission are very important.

4.3.2.3 The Distribution Network

To approve the proposed access network a demonstrational set up was made at TU Graz. The network consisting of a central office, the FSO distribution network and the customer home equipment was tried out for the different applications like Internet access, Voice-over-IP and Video distribution by IP streaming technology. Using new equipment from different manufacturers all applications could be demonstrated successfully over the net based on the Ethernet networking standard.
In general, the central office connects the distribution network to a larger Metropolitan (MAN) or Wide Area Network (WAN), or to other service networks. The management of the whole network takes place in a room, the network structure is maintained and function and data flow is controlled and logged there [72].

From the central office the information is distributed to every customer according to Ethernet networking standard over the distribution network. The feeder fiber which connects the customer with the central office is terminated there on equipment known as an optical line termination (OLT) unit. The central office OLT equipment can be designed to support various data link layer interface types and densities: 100 FX Fast Ethernet, SONET, ATM, and Gigabit Ethernet, among others. On the service provider side, the central office equipment has multi-service interfaces that connect to the public switched telephone network, IP routers/ATM switches or to core video networks. The customer premises equipment (CPE), also known as the optical network unit (ONU) has POTS (plain old telephone service) and 10/100 Base-T Ethernet interfaces and, optionally, an RF video interface [74].

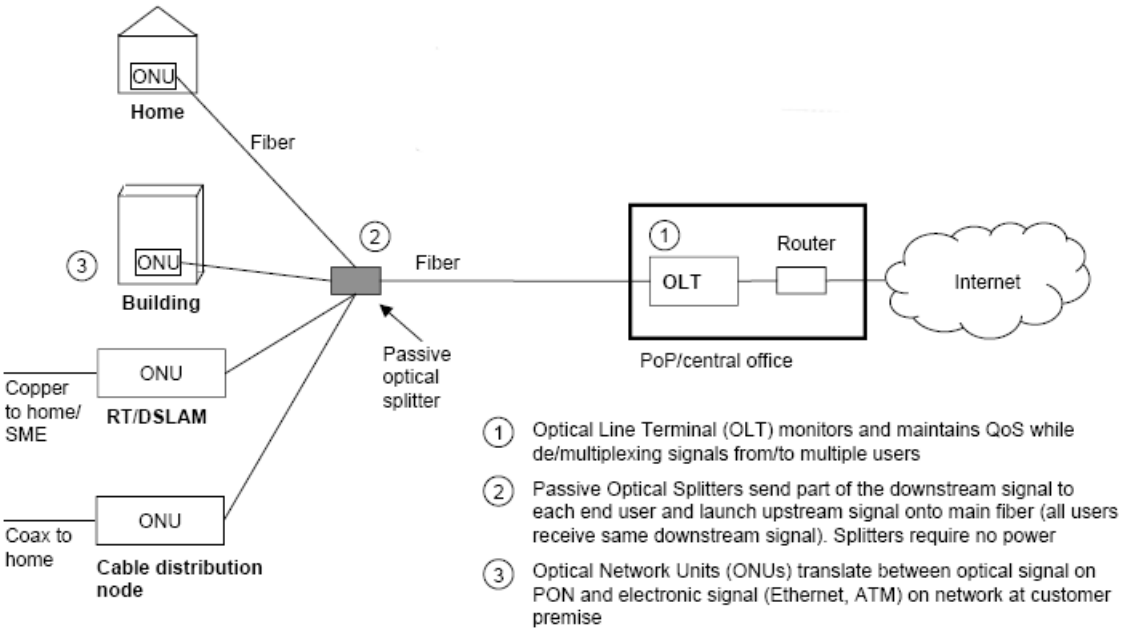

Figure 77: Typical Access Network [W5]

Depending on the size of the access network, a broadband cable connection to a few sub-nodes may exist, and the central office will also act as a node. From these locations the actual data distribution to the customer over dedicated FSO point-to-point connections starts. Deployment can be realized in different topologies such as a star, tree, ring or mesh network structure. It is important to consider these in regard to FSO properties and the local situation.
The physical parts at the customer consist of the mounted FSO system, a lead-in of the data line and a network termination box, which can be extended by a set top box for TV reception or other networking parts. Depending on the organisation form of the network, it may be important to define a specific place for the indoor equipment similar to the electricity meter board, which is easy to access for the provider in case of service or maintenance and clearly defines the limit of legal responsibility for the provider. The network termination box is the last and active part of the access network in the customers room and the interface between the responsibility of provider and customer. For network monitoring in the central office the termination box should allow active control of the settings to every port. Further it should allow Virtual LAN technology and port truncing. This means that every port can be separately addressed by a data stream for TV applications, IP telephony and data services. These data streams are available separately for the customer, even though they are transmitted over one broadband serial FSO connection. With these features implemented it is even possible to upload new system software to the boxes at the customer, to allow additional services and to extend or to reduce the data transmission rate without a personal visit to every customer.

Figure 78: “Lead-in” housing, Network termination box, MPEG-2 conversion box for TV reception

A star network is a very clear and simple concept, every customer has his own connection line which simplifies installation and service and the full data rate is dedicated to one customer. But FSO connections require a free line-of-sight, so it must be assured that the distribution node can reach every potential customer. High availability, depending on local climate, is a strong function of distance, but the distance to different customers will be different. To assure high availability, all customers connected to a distribution node must be within a limited radius of a few hundred meters, depending on the FSO equipment and local climate. This requires more sub-distribution nodes for an area and a certain number of possible customers around a distribution node, similar to the situation of high capacity cellular phone systems, but it is more comfortable for the provider to maintain the net after installation. Some manufacturers already offer point-to-multipoint equipment which is designed for this strategy.
A Free Space Optic tree topology can be very interesting because it fits well to the system properties and can be based on typical point-to-point technology. The idea is to start from the distribution node a connection to the first customer, and from this location to connect a second customer with another conventional point-to-point link. This allows to connect customers even without direct line-of-sight to the distribution node. And it takes advantage of the fact that it is comparatively easy to implement a higher data rate in FSO but it is very difficult and expensive to extend the distance for highest availability. Using the Ethernet protocol for transmission, data packets of different customers can be transported over the same connection and are identified by their address fields. Like in fiber optic links virtual LAN technology allows to implement virtual parallel connections of specified capacity for every customer and even for every interface plug of the customer equipment, so interference problems can be excluded. Assuming three customers on one line and a typical distance of 200 m, an area of more than one kilometer between two fiber connected distribution nodes can be connected with high availability and with moderate equipment costs. However, the strategy requires a certain customer density in the area, and a clear agreement for network maintenance must be handled out with every customer. This makes it attractive especially for association structures between the customers.
A ring topology simplifies the distribution node, because only two conventional point-to-point FSO systems are necessary equal to every customer location for one ring. This is easy to implement at locations like companies with broadband fiber access. Customers can be quite distant to the distribution node, if only a certain customer density and a line-of-sight from one customer to the next is present. In a ring one broken link does not cause a failure, because a redundant connection over the other direction in the ring is already installed. This redundancy can be interesting also for business customers with an existing fiber access, because of the very different failure conditions of wired and wireless connections, both offering the same transmission quality.

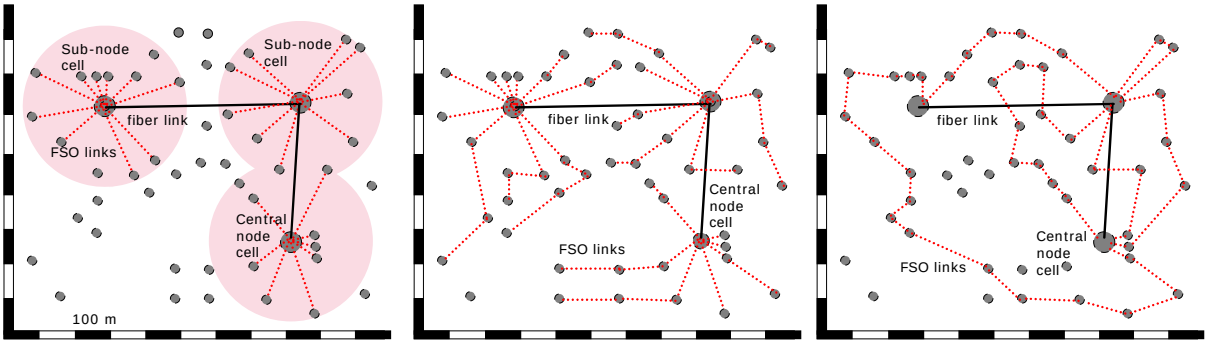

Figure 79: Star-, Tree- and Ring topologies in principle

In practice network evolution may initially start with a star network at the central node, being extended to a tree and then to several rings over a wider area, and finally result in a meshed topology offering the most redundancy for high availability.

4.4 Summary/Conclusions (TUG, DLR, UToV)

Optical Wireless is an excellent broadband solution for connecting end users to the backbone (Last-Mile-Access). This technology should be seen as supplement to conventional radio links and Fibre Optics. The use of low cost FSO-systems for short distances makes this technology interesting for private users.

At the moment the main work in this field is to increase reliability and availability (shown in 4.1). Those two parameters of the FSO-link are mainly determined by the local atmospheric conditions. Good reliability and availability can be achieved by using the Free Space Optics for short distances, by calculating enough link-budget and by using the optimal network architecture for each FSO application.

The optimal solution for FSO configurations is a meshed architecture. This network architecture combines shorter distances and high reliability, because of the location of the Optical Multipoint Unit in the centre of the network. For increasing the reliability and availability it is also necessary to perform field-tests with FSO-systems regarding the local atmospheric conditions. Models for propagation and for predicting link availability in different climate zones could improve the installation of this technology.

The combination of FSO- and microwave-links is also a further possibility for increasing reliability and availability, because terrestrial FSO is most effected by fog, whereas the microwave propagation is mainly influenced by rain. Within parallel studies, wireless hybrid (optical / microwave) links have been evaluated at the Department of Communications and Wave Propagation [1, 11]. First results show a reliability of 99.9991 % for hybrid systems.

Although terrestrial FSO has been in practice widely developed and has provided direct applications, other types of atmospheric scenarios are possible (see 4.2). Always more effort is put on optical up- and downlinks. To avoid cloud coverage for these scenarios, ground terminals are placed at astronomical sites. High-data-rate links between aircrafts in the troposphere are also conceivable provided the link is relatively short and that no clouds obstruct the line of sight. Terminals supported by high-altitude platforms above the cloud ceiling (~ 13 km) can provide a wide range of link scenarios. However, also above the cloud ceiling, atmospheric effects are significant: aerosol attenuation, wind, turbulence. These effects must be studied in order to be overcome. For scenarios in the upper atmosphere, an essential difference compared to terrestrial FSO is the terminal mobility. The aircraft motions and vibrations become a serious issue for the PAT systems which are supposed to make the terminals look in the right directions.

Section 4.3 summarizes the preliminary research results for providing a suitable modulation and channel coding format for the FSO systems. This is the first of its kind attempt to introduce the well established principles of power efficient modulation and channel coding in the FSO environment; and these investigations indicate that the use of these schemes will eventually lead to better systems with substantial coding gains to combat fog and other attenuators which limit the performance of the technology. We are now, in the process of developing hardware and software modules to test the performance of these ideas on a real world environment and the results will be published in due course of time.

REFERENCES

[1] E. Leitgeb, J. Bregenzer, M. Gebhart, P. Fasser, A. Merdonig, „Free-space optics: Broadband wireless supplement to fiber networks“, Proceedings SPIE, Vol. 4975-07 (2003), January 2003, San Jose, USA

[2] E. Leitgeb, M. Gebhart, P. Fasser, J. Bregenzer, J. Tanczos, „Impact of atmospheric effects in free-space optics transmission sytems“, Proceedings SPIE, Vol. 4976-28 (2003), January 2003, San Jose, USA

[3] I. Kim, B. McArthur, E. Korevaar, „Comparison of laser beam prop. at 785 nm and 1550 nm in fog and haze for optical wireless communications“, Proceedings SPIE, Vol. 4214, pp. 26-37 (2001)

[4] F. David, D. Giggenbach et al., „Preliminary results of a 61 km Ground-to-Ground Optical IM/DD Data Tramsmission Experiment“, Proceedings SPIE, Vol. 4635 (2002)

[5] M. Gebhart, E. Leitgeb, S. Sheikh Muhammad, B. Flecker, Ch. Chlestil, M. Al Naboulsi, H. Sizun, F. de Fornel, “Measurement of Light attenuation in dense fog conditions for Optical Wireless Links”, Proceedings SPIE's Optics & Photonics conference, August 2005, San Diego (USA)

[6] E. Leitgeb, S. Sheikh Muhammad, Ch. Chlestil, M. Gebhart, U. Birnbacher, „Reliability of FSO Links in Next Generation Optical Networks”, Proceedings of the IEEE-conference ICTON 2005, July 2005, Barcelona

[7] P. J. Winzer et al. “Optimum filter bandwidths for optically preamplified NRZ receivers”, Journal of lightwave technology, September 2001

[8] G. Hyde, B.I. Edelson “Laser Satellite Communications: current status and directions”, Space Policy, 1997

[9] E. Leitgeb, J. Bregenzer, P. Fasser, M. Gebhart, “Free Space Optics – Extension to Fibre-Networks for the „Last Mile“, Proceedings of the 15th Annual IEEE / LEOS-Meeting Nov. 2002, Glasgow

[10] H. Willebrand, B. S. Ghuman, „Free Space Optics“, ISBN 0-672-32248-X, SAMS (2001)

[11] E. Leitgeb, M. Gebhart, U. Birnbacher, W. Kogler, P. Schrotter, „High availability of hybrid wireless networks“, Proceedings SPIE's International Symposium Photonics Europe, Vol. 5465, pp. 238-249, April 26th - 30th 2004, Strasbourg

[12] L. Bartelt-Berger, F. Heine, U. Hildebrandt et al. “1W laser transmitter for intersatellite links”, in Proc. ECOC, 26th European Conference on Optical Communication

[13] J. R. Barry, „Wireless Infrared Communications“, ISBN 0-7923-9476-3, Kluwer Academic Publishers, (1994)

[14] S. Betti, G. De Marchis, E. Iannone “Multifrequency Modulation for High Sensitivity Coherent Optical Systems”, IEEE Journal of Lightwave Technology, LT11 , Vol.11, pp. 1839-1844, 1993

[15] S. Betti, G. De Marchis, E. Iannone “Coherent Optical Communications Systems”, John Wiley and Sons Inc. 1995

[16] S. Arnon and N.S. Kopeika, “Performance limitation of freespace optical communication satellite networks due to vibrations: direct detection digital mode”, IEEE Optical Engineering Nov. 1997

[17] G.C. Baister and P.V. Gatenby, “Pointing, acquisition and tracking for optical space communications”, Electronics and Communications Engineering Journal, pp. 271-280, Dec. 1994

[18] G.C. Baister and P.V. Gatenby, “Why optical communication links are needed for future satellite constellations”, IEEE 1996

[19] S. Betti, M. Giaconi “Comunicazioni ottiche”, Aracne 2003

[20] S. Betti, V. Carrozzo, E. Duca, A.B. Lopez Zamarreño, “Performance analysis of a 1550 nm optical intersatellite link”, European workshop in the framework of NEFERTITI IST-2001-3276, Network of excellence on broadband fiber radio techniques and its integration technologies, Rome March 2005

[21] S.G. Lambert and W.L. Casey, “Laser communications in space”, Artech House Publishers, 1995

[22] G.D. Fletcher, T.R. Hicks, B. Laurent “The SILEX optical interorbit link”, IEEE Electronic and Communication Engineering Journal, December 1991

[23] “WTEC Panel Report on Global Satellite Communications Technology and Systems”, International Technology Research Institute, 1998

[24] G. Planche, B. Laurent, and J. C. Guillen “SILEX final ground testing and inflight performance assessment," in Proc. SPIE, Free-Space Laser Communication Technologies XI, Vol. 3615, pp. 64, 1999

[25] S. Coletto, “Forward Error Correction at Transport Layer for Satellite Applications”, Master Thesis, Universitá di Bologna, March 2005

[26] F. David, “Scintillation loss in free-space optic IM/DD systems”, LASE 2004, San José, California,January 24-29, 2004, SPIE - The International Society for Optical Engineering, Proceedings of SPIE 2004, (2004)

[27] B. Mayer, S. Shabdanov, D. Giggenbach, "Electronic Database of atmospheric absorption coefficients", DLR-internal report by DLR-IPA and DLR-IKN-DN-OCG, DLR-Oberpfaffenhofen, December 2002, based on the atmospheric constituents profiles according to "G.P. Anderson, et al: AFGL Atmospheric Constituent Profiles (0-120km), AFGL-TR-86-0110, Hanscom Air Force Base, MA 01736, 1986"

[28] D.L. Knepp, “Multiple phase-screen calculation of the temporal behavior of stochastic waves”, Proc. IEEE 71, p. 722-737, 1983

[29] N. Gasso, H. Ernst, “Transport Layer Protocols for the Land Mobile Satellite Broadband Channel”, European mobile & personal Satellite Communications Workshop, 2004

[30] D. Giggenbach, F. David, et al, "Measurements at a 61 km near-ground optical transmission channel", Proceedings of the SPIE, Vol. 4635, 2002

[31] D. Giggenbach, R. Purvinskis, M. Werner, M. Holzbock, "Stratospheric Optical Inter-Platform Links for High Altitude Platforms", AIAA - Proceedings of the 20th Int. Communications Satellite Systems Conference (ICSSC), Mai 2002

[32] D. Giggenbach, "Optimierung der optischen Freiraumkommunikation durch die turbulente Atmosphäre", Shaker-Verlag, 2005

[33] H. Henniger, F. David, D. Giggenbach, C. Rapp, “Evaluation of FEC for the Atmospheric Optical IM/DD Channel”, Proc. SPIE, vol. 4975, January 2003

[34] H. Henniger, D. Giggenbach, C. Rapp, “Evaluation of optical up- and downlinks from high-altitude platforms using IM/DD”, LASE 2005, San Jose, California, SPIE - The International Society for Optical Engineering, Conference on Free Space Laser Communication Technologies XVII, 2005

[35] R. Jüngling, “Simulation gerichteter Ausbreitung optischer Wellen in turbulenter Atmosphäre“, diploma thesis, Münster, 2001

[36] S. Karp, R. M. Gagliardi, S. E. Moran und L. B. Stotts, „Optical Channels“, Plenum Press, 1988

[37] M. Kästner and K. T. Kriebel, “Alpine cloud climatology using long-term NOAA-AVHRR satellite data”, German Aerospace Center (DLR), Institute of Atmospheric Physics, Report No. 140, 2000

[38] R. F. Lutomorski and H. T. Yura, “Propagation of a finite optical beam in an inhomogeneous medium,” Appl. Opt. 10, 1652-1658 (1971)

[39] C. Macaskill, T.E. Ewart, ”Computer Simulation of Two-dimensional Random Wave-Propagation”, IMA J. Appl. Math. 33(1), 1-15, 1984

[40] J.M. Martin, S.M. Flatté, “Intensity images and statistics from numerical simulation of wave propagation in 3-D random media”, Applied Optics 27(11), S. 2111-2126, 1988

[41] N. Perlot, D. Fritzsche, “Aperture-Averaging - Theory and Measurements”, LASE 2004, San Jose, California, Proceedings of SPIE, 2004

[42] J.A. Rubio, A. Belmonte, A. Comeron, “Numerical simulation of long-path spherical wave propagation in three-dimensional random media”, Optical Engineering 38, 1462-1469, 1999

[43] L. Sartorello, “Low-Density Parity-Check Codes. An Application to the Binary Erasure Channel”, Master Thesis, Universitá degli Studi di Ferrara, June 2004

[44] K. S. Shaik, “A Preliminary Weather Model for Optical Communications through the Atmosphere”, JPL, TDA Progress Report 42-95, 1988

[45] V. I. Tatarski, “Wave propagation in a turbulent medium”, McGraw-Hill, New York, 1961

[46] T. Weigel, K. Kudielka, B. Thieme, H. Mannstein, R. Meyer, C. Werner, V. Banakh, W. Holota and S. Manhart, „Optical Groud Station“, ESA-Study, ESA Contr. No.: 14231/00/NL/WK, 2001

[47] V. E. Zuev, “Propagation of visible and infrared radiation in the atmosphere”, John Wiley & Sons, New York, 1974

[48] L. C. Andrews, "An analytical model for the refractive-index power spectrum and its application to optical scintillations in the atmosphere", J. Mod. Opt. **39**, 1849-1853 (1992)

[49] L. Andrews, R. Phillips, “Laser Beam Propagation through Random Media”, SPIE Press, Bellingham, 1998

[50] S. Betti, V. Carrozzo, E. Duca, “Optical Intersatellite System based on DPSK modulation”, IWSSC05, Siena September, 7-9 2005

[51] S. Haykin, “Communication Systems”, 4th Ed., John Wiley & Sons, 2001

[52] S. Sheikh Muhammad, C. Chlestil, E. Leitgeb, M. Gebhart, „Reliable terrestrial FSO systems for higher bit rates”, Proceedings at 8th International Conference on Telecommunications ConTEL, Zagreb, Croatia, 2005

[53] E. Leitgeb, S. Sheikh Muhammad, O. Koudelka, G. Kandus et al., “Hybrid wireless networks combining WLAN, FSO and satellite technology for disaster recovery”, Proceedings at IST Mobile and Wireless Communications Summit, Dresden, Germany, 2005

[54] F. R. Kschischang, S. Harnilovic, „Optical intensity-modulated direct detection channels: Signal space and lattice codes”, IEEE transactions on Information Theory, 49:1385–1399, 2003

[55] J. P. Gordon, “Quantum effects in communication systems”, Proceedings IRE, 50:1898–1908, 1962

[56] J. R. Pierce, “Optical channels: Practical limits with photon counting”, IEEE transcations on Communications, 26:1819–1821, 1978

[57] R. J. McEliece, “Practical codes for photon communications”, IEEE transactions on Information Theory, IT-27:393–398, 1981

[58] J. M. Kahn, D. Shiu, “Shaping and nonequiprobable signalling for intensity modulated signals”, IEEE transactions on Information Theory, 45:2661–2668, 1999

[59] S. Sheikh Muhammad, E. Leitgeb, P. Köhldorfer, „Channel modelling for free space optical links”, Proceedings at 7th International Conference on Transparent Optical Networks ICTON, Barcelona, Spain, 2005

[60] E. R. Rodemich, J. R. Pierce, E. C. Posner, “The capacity of the photon counting channel”, IEEE transactions on Information Theory, 27:61–77, 1981

[61] M. Achour, “Simulating atmospheric free-space optical propagation: Part I, rainfall attenuation”, SPIE proceedings, Volume 3635, 2002

[62] M. Achour, “Simulating atmospheric free-space optical propagation: Part II, haze, fog and low clouds attenuations”, SPIE proceedings, Volume 4873, 2002

[63] F. de Fornel, M. Al Naboulsi, H. Sizun, “Fog attenuation prediction for optical and infrared waves”, Journal SPIE, 2003

[64] P. Fasser, E. Leitgeb, M. Gebhart, “Reliability of free space laser communications: Investigations at Technical University Graz”, Proceedings at the Annual WCA Technical Symposium, San Jose, CA, USA, 2002

[65] D. A. Johns, S. Harnilovic, “A multilevel modulation scheme for high speed wireless infrared communications”, IEEE proceedings, 1999

[66] J. R. Barry, M. D. Audeh, J. M. Kahn, “Performance of pulse position modulation on measured non-directed indoor infrared channels”, IEEE transactions on Communications, 44, 1996

[67] J. Barry, H. Park, “Modulation analysis for wireless infrared communications”, IEEE International Conference on Communications, pages 1182–1185, 1995

[68] J. M. Kahn, D. C. Lee, “Coding and equalisation for PPM on wireless infrared channels”, IEEE transactions on Communications, 47, 1997

[69] J. Hamkins, “Performance of binary turbo-coded 256-ary pulse position modulation”, TMO Progress Report, JPL, 1999

[70] M. Srinivasan, J.Hamkins, “Turbo codes for APD-detected PPM”, JPL Progress Report, 1999

[71] M. D. Audeh, D. C. Lee, J. M. Kahn, “Trellis coded pulse position modulation for indoor wireless infrared communications”, IEEE transactions on Communications, 45:1080–1807, 1997

[72] H. Orlamünder, “High-Speed-Netze”, Hüthig Verlag Heidelberg, 2000

[73] M. Gebhart, E. Leitgeb, U. Birnbacher, P. Schrotter, „Ethernet access network based on free-space optic deployment technology”, Proceedings at SPIE‘s Photonics West, Laser and Applications in Science and Engineering (LASE 2004) Symposium, Vol. 5338, pp. 131-142, January 24th – 29th 2004, San Jose, USA

[74] I. Chlamtac, A. Gumaste, C. A. Szabo, “Broadband Services – Business Models and Technologies for Community Networks”, John Wiley and Sons, 2005

WEB-SITES

[W1] Webpage ESA http://www.esa.int/export/esaCP/ESASGBZ84UC_index_0.html (Dec. 22nd 2003)

[W2] Webpage OGS (Dec. 22nd 2003) http://www.iac.es/gabinete/oteide/ogs/2ogs.html and http://www.iac.es/gabinete/iacnoticias/1-2001/47.pdf

[W3] Webpage ISCCP International Satellite Cloud Climatology Project (ISCCP) http://isccp.giss.nasa.gov/

[W4] Webpage: C. Neumann, V. Roca, J. Labouré, and Z. Khallouf, *MCLv3 an open source gnu/gpl Implementation of Low-Density Parity Check (LDPC) Large Block FEC Code*, URL: http://www.inrialpes.fr/planete/people/roca/mcl/mcl.htm

[W5] Webpage FCC: http://www.fcc.gov/oet/tac/april26-02-docs/BB-Access-Tech.pdf, Broadband Access Platforms, Tutorial FCC

Abbreviations

APD	Avalanche Photo Diode
CAPANINA	Communications from Aerial Platform Networks delivering Broadband for All
DD	Direct-Detection
DLR	Deutsches Zentrum für Luft- und Raumfahrt
DLR-OCG	DLR- Optical Communications Group, part of DLR-IKN (Institute for Communications and Navigation) at DLR-site Oberpfaffenhofen, near Munich
FELT	Free-space optical Link Terminal
FSO	Free Space Optics
GEO	Geostationary Earth Orbit satellite
HAP	High Altitude Platform
IM	Intensity-Modulation
IM/DD	Intensity-Modulation / Direct-Detection
JPL	Jet Propulsion Lab
LAN	Local Area Network
LCT	Laser Communications Terminal
LEO	Low Earth Orbit satellite
LOLA	Liaison Optic en Laser Aeroporté
HALE	High-Altitude Long Endurance aircraft
MALE	Mid-Altitude Long Endurance aircraft
MAN	Metropolitan Area Network
MEO	Mid Earth Orbit satellite
OGS	Optical Ground Station
OOK	On-Off-Keying
OPALE	Optical Payload for Inter Satellite Link Experiment
OICETS	Optical Inter-orbit Communications engineering Test Satellite
OISL	Optical Inter-Satellite Link
PPM	Pulse Position Modulation
RS	Reed Solomon Codes
SatNEx	Satellite Communications Network of Excellence
SROIL	terminal for Short Range Optical Inter-satellite Links
STREP	Specific Targeted Research Project, one type of EU-project
STROPEX	Stratospheric Optical Link Experiment
TUG	University of Technology Graz
UAV	Unmanned Aerial Vehicle
UToV	University Tor Vergata Rome
WLAN	Wireless Local Area Network